Order Number 9315471

Theoretical molecular orbital modeling of organic free radical reactions and the polarized pi-frontier molecular orbitals method for predicting diastereofacial selectivities

Huang, Xiao Ling, Ph.D.

City University of New York, 1993

U·M·I
300 N. Zeeb Rd.
Ann Arbor, MI 48106

THEORETICAL MOLECULAR ORBITAL MODELING

OF

ORGANIC FREE RADICAL REACTIONS

AND

THE POLARIZED Pi-FRONTIER MOLECULAR

ORBITALS METHOD FOR PREDICTING

DIASTEREOFACIAL SELECTIVITIES

By

XIAO LING HUANG

A dissertation submitted to the Graduate Faculty in Chemistry in partial fulfillment of the requirements for the degree of Doctor of Philosophy, The City University of New York

1993

This Manuscript has been read and accepted for the Graduate Faculty in Chemistry in satisfaction of the dissertation requirement for the degree of Doctor of Philosophy.

30 Dec 1992
Date

Chair of Examining Committee

4 Jan 1993
Date

Executive Officer

Supervisory Committee

The City University of New York

ABSTRACT

THEORETICAL MOLECULAR ORBITAL MODELING OF ORGANIC FREE RADICAL REACTIONS AND THE POLARIZED Pi-FRONTIER MOLECULAR ORBITALS METHOD FOR PREDICTING DIASTEREOFACIAL SELECTIVITIES

By

Xiao Ling Huang

Adviser: Professor Joseph J. Dannenberg

AM1/CI calculations on the reactions paths for the coupling of organic free radicals are presented. The calculations are in good agreement with previously reported experimental results for benzyl radical coupling. Selectivities for combinations of methyl radicals with allyl azaallyl, benzyl, and variously cyano-substituted benzyl radicals, the coupling reactions of two tri-substituted methyl radicals, as well as seven different coupling reactions of two benzyl radicals are reported. Analyses of the results suggest the existence of an intrinsic barrier about 25 kcal/mol for the coupling of carbon-centered free radicals.

The AM1 molecular orbital method was used to compute

the activation enthalpies for H-transfer between carbons as a function of C-H-C angle and size of the cyclic transition state for intramolecular H-transfer. In the case of intramolecular H-transfer, reactions of a primary radical site with primary, secondary, and tertiary C-H's were considered for H-shifts to C_1 from C_3-C_8. The activation enthalpies are insensitive to C-H-C angle in the range 145-180°. Activation enthalpies are lowest for intramolecular H-transfers involving 1-5 and 1-6 H-shifts. The higher activation enthalpies for the other internal H-transfers are attributed to C-H-C strain for 1-3 and 1-4 transfers only, and conformational effects other than C-H-C angle in the transition states.

A new method (polarized π-frontier molecular orbitals, PPFMO) is presented for predicting the electronic component of π-diastereofacial selectivities. The effects of the various substitutents adjacent to carbon π-systems cannot be categorized completely in terms of electron-withdrawing and electron-donation effects. The substitutent effects on the polarization of FMO's are shown to be quite different from those on their energies. The PPFMO theory is adapted to include both effects. A comparison of PPFMO theory with earlier proposals made by Anh and Cieplak are discussed in terms of the predicted effects on FMO's.

The polarized π-frontier molecular orbital (PPFMO) is used to analyze several experimental observations that have

been previously discussed in terms of other theoretical models for predicting the electronic components of π-diastereofacial selectivities. In particular, the reductions of propanal, fluoroethanal, and R-fluoropropanal as a function of rotational angle are compared with other high level calculations. The reductions of many (>40 cases) substituted cyclohexanones, methoxydioxanes, 1,3-dioxin-4-ones, norbornanones and adamantanones are compared with other calculations and experimental data. The PPFMO polarizations are in qualitative agreement with the experimental results in all cases. Comparison with *ab initio* transition states leads to only one discrepancy, where an unusual repulsive factor in the TS seems to be responsible.

ACKNOWLEDGEMENT

First of all, I would especially like to express my deep sincerity and appreciation to my thesis adviser, Prof. Joseph J. Dannenberg. During the entire period of my Ph.D. study, he has spent much his precious time freely and generously giving me valuable advice and sharing his insights with me, from which I have benefited a lot in my research. His patience, understanding, guidance and encouragement, made my successful completion of this work possible.

I would like to thank my committee members, Prof. Jerome M. Schulman, Prof. Max Diem and Prof. Richard W. Franck for their time, help and encouragement.

I would also like to thank Waldemar Cieniewicz for his assistance in computer facilities throughout the years. Thanks to all the other members of the department who offered their assistance.

Finally, I am deeply indebted to my parents and my mother-in-law whose love and confidence in me have always be my sources of encouragement and support. And most of all, from bottom of my heart, I especially thank my husband, Johnny Wong, for his love, patience, understanding and supporting during these years.

Dedicated to

My parents

and

My husband

TABLE OF CONTENTS

LIST OF TABLES

LIST OF FIGURES

CHAPTER 1

1. INTRODUCTION

Theoretical models, based on molecular orbital theory, have become increasingly useful tools. They are used not only to explain or rationalize known experimental results, but also in a predictive manner. This thesis addresses two different subjects:

A) The molecular orbital modeling for the reactions of organic free radical recombination and of intramolecular hydrogen atom transfer.

B) The Polarized π-Frontier Molecular Orbital (PPFMO) method studies for predicting diastereofacial selectivities of various reactions.

To fulfill the first subject of the thesis, we confront the necessity of making a choice among the modeling methods based upon the particular problem studied and computer expense. Many different methods of doing molecular orbital calculations are now available. These methods can be divided into two major categories, they are the *ab initio* MO and semiempirical MO approaches. The following chapter will discuss the similarities and differences between them.

In the second part of this thesis, the development of a new method called polarized π-frontier molecular orbitals (PPFMO) is described. The applications of the PPFMO method is applied to several individual problems. Some analyses of experimental result are discussed.

CHAPTER 2

2. THEORETICAL BACKGROUND

The LCAO Approximation To The Self-Consistent Field Molecular Orbital Theory

The purpose of the self-consistent field molecular orbital theory is to consider electron repulsion correctly for antisymmetrization of the wave function. If it is not complete, at least to some extent it allows all the electrons to find the distribution of lowest energy while subject to each others' repulsion.

In the self-consistent field theory, the wave function Ψ for a closed-shell molecule of 2N electrons is written as a normalized Slater determinant (Equation 2.1)

$$\Psi = (2N)!^{-\frac{1}{2}} \begin{vmatrix} \psi_1(1)\alpha(1) & \psi_1(2)\alpha(2) & \dots & \psi_1(2N)\alpha(2N) \\ \psi_1(1)\beta(1) & \psi_1(2)\beta(2) & \dots & \psi_1(2N)\beta(2N) \\ \psi_2(1)\alpha(1) & \psi_2(2)\alpha(2) & \dots & \psi_2(2N)\alpha(2N) \\ \vdots & \vdots & \vdots & \vdots \\ \psi_N(1)\beta(1) & \psi_N(2)\beta(2) & \dots & \psi_N(2N)\beta(2N) \end{vmatrix}, \quad (2.1)$$

where the ψ_i is a molecular orbital, α or β is a spin function. The energy for the many-electron wave function Ψ is the expectation value E of the total Hamiltonian H:

$$E = \int \Psi^* \, \mathrm{H} \, \Psi \, d\tau_1 \ldots d\tau_{2N} \, , \qquad (2.2)$$

where the total Hamiltonian operator H is given in

$$\mathrm{H} = \sum_i h(i) + \sum_i \sum_{<j} \frac{e^2}{r_{ij}} \, , \qquad (2.3)$$

where h(i) is the one-electron part of the Hamiltonian for electron i. In the atomic units, in which the charge and mass of the electron and $\hbar$ are all taken as unity, h(i) has the form

$$h(i) = -\sum_i \frac{1}{2} \nabla_i^2 + \sum_A V_A \, . \qquad (2.4)$$

Where,

$$\nabla^2 = \frac{\partial^2}{\partial x^2} + \frac{\partial^2}{\partial y^2} + \frac{\partial^2}{\partial z^2} \, , \qquad (2.5)$$

V_A is the nuclear-electron potential energy equal to $-Z_A e^2/r_A$ (Z_A being the nuclear charge). It is immediately clear that a wave function such as Equation 2.1 cannot lead to the exact energy, because the sum of products of one-electron

terms can never be the solution of a Schrödinger equation with a Hamiltonian involves two-electron repulsion potentials $\Sigma\Sigma_{i<j}(e^2/r_{ij})$.[1] However, the calculation of the energy by Equation 2.2 when the total Hamiltonian is used, leads, by the usual variational procedure, to a set of one-electron equations, the "Hartree-Fock equations,"

$$F(1)\psi_i(1) = \epsilon_i\psi_i(1) \ , \qquad (2.6)$$

where F is the effective Hamiltonian or the Hartree-Fock operator for an electron in ψ_i. It depends on the position of all the other electrons through their average Coulomb and exchange field. The set of Equations 2.6 must therefore be solved simultaneously for all the molecular orbitals, the solution being reached when self-consistency is attained.

The SCF molecular orbitals are taken to be eigenfunctions of the operator F and if the LCAO expansion Equation 2.7 is adopted,

$$\psi_i = \sum_\nu \phi_\nu C_{\nu i} \ , \qquad (2.7)$$

where ϕ_ν is an atomic orbital. Then the coefficients and energies are determined by the Roothaan[2]-Hall[3] equations,

$$\sum_{\nu} C_{\nu} (F_{\mu\nu} - ES_{\mu\nu}) = 0 \ , \qquad (2.8)$$

$$| F_{\mu\nu} - ES_{\mu\nu} | = 0 \ , \qquad (2.9)$$

$$F_{\mu\nu} = \int \phi_{\mu}^{*} \, F \, \phi_{\nu} \, d\tau \ . \qquad (2.10)$$

However, F matrix elements, $F_{\mu\nu}$, are given by expressions first derived by Lannard-Jones,[4] Hall[3] and Roothaan.[5]

$$F_{\mu\nu} = H_{\mu\nu} + \sum_{\rho} \sum_{\sigma} P_{\rho\sigma} \left[(\mu\nu|\rho\sigma) - \frac{1}{2} (\mu\rho|\nu\sigma) \right] \qquad (2.11)$$

The $H_{\mu\nu}$ is the Hamiltonian for an electron. It consists of the kinetic energy operator for an electron and the potential energy between an electron and all atomic cores of the molecule.

The remaining terms in Equation 2.11 give the effect of the electron interaction, two-electron repulsion integrals. It is defined as,

$$(\mu\nu|\rho\sigma) = \int\int \phi_\mu(1)\phi_\nu(1)\left(\frac{e^2}{r_{12}}\right)\phi_\rho(2)\phi_\sigma(2)\, d\tau_1 d\tau_2 . \quad (2.12)$$

The final term to be defined in Equation 2.11 is the bond order $P_{\rho\sigma}$ which is written,

$$P_{\rho\sigma} = 2 \sum_k C_{k\rho}\, C_{k\sigma} , \quad (2.13)$$

the summation extending over all occupied molecular orbitals ψ_k.

The Equation 2.11 only applies to closed-shell electron configurations that is when all occupied molecular orbitals contain two electrons. It therefore applies to the ground states of most molecules. For radicals, or most excited electronic states, slightly different equations are required.[2]

The total electronic energy of the molecule is given by Equation 2.14. Upon addition of Equation 2.15,

$$E_{elec} = \frac{1}{2} \sum_{\mu,\nu} P_{\mu\nu}(H_{\mu\nu} + F_{\mu\nu}) , \quad (2.14)$$

which accounts for the core-core repulsions, (where Z_A and Z_B are the atomic number of atoms A and B, and R_{AB} is the

their separation),

$$E_{nr} = \sum\sum_{A<B} \frac{Z_A Z_B}{R_{AB}} , \qquad (2.15)$$

one obtains an expression for the total energy of the molecule (Equation 2.16).

$$E_{total} = E_{elec} + E_{nr} . \qquad (2.16)$$

The Roothaan-Hall Equations 2.8 are not linear since the Fock matrix, itself, depends on the molecular orbital coefficients, $c_{\mu i}$, through the density matrix expression (Equation 2.13). So the solution of the Roothaan-Hall equations necessarily involves an iterative process. The technique is called the self-consistent-field (SCF) method.

Two main-streams of computational techniques branch out from different treatments of the expression (Equation 2.11). There are *ab initio* molecular orbital methods and semiempirical molecular orbital methods.

2.1 Semiempirical MO Methods

To reduce the computational time of the

calculations, it is necessary to simplify the Roothaan-Hall treatment by reducing the number of integrals. The various semiempirical methods differ in the approximations that are made concerning repulsion integrals between electrons in different orbitals. In the semiempirical methods, the various terms in the Fock matrix, especially the one and two-electron integrals, and the core repulsions, E_{ss}, are not evaluated analytically. They are determined either from experimental data or from semiempirical expressions that contain numerical parameters that can be adjusted to fit experimental data.

The earlier semiempirical MO methods to be applied extensively to organic molecules included the Extended Hückel Theory (EHT),[6] CNDO[7] (Complete Neglect of Differential Overlap), INDO[8] (Intermediate Neglect of Differential Overlap), and NDDO[8,9] (Neglect of Diatomic Differential Overlap).

More recent semiempirical methods are MINDO/3[10] and MNDO[11] and AM1[12] (These acronyms refer to semidescriptive titles of the calculation method, specifically "Modified Intermediate Neglect of Differential Overlap," and "Modified Neglect of Differential Overlap."). The MNDO and AM1 methods are based on the NDDO approximations. In the NDDO approximation, the repulsion integrals $(\mu\mu|\nu\nu)$ between any AO ϕ_μ of atom A and any AO ϕ_ν of atom B are not assumed to be equal. Moreover, in NDDO there are a number of

additional bicentric integrals to be considered, which involve one-center differential overlap. In the AM1 method, Dewar and coworkers have developed an alternative and more reasonable procedure for estimating the NDDO repulsion integrals. They have used it in a complete reparametrization of NDDO for hydrogen, carbon, nitrogen and oxygen.

In the AM1 method one starts with the complete expression for the elements, $F_{\mu\nu}$, which is the sum of a one electron part $H_{\mu\nu}$ (core Hamiltonian) and a two-electron part, $G_{\mu\nu}$. We assume that the AO's ϕ_μ and ϕ_ν are centered at atom A and the AO's ϕ_λ and ϕ_σ at atom B ($A \neq B$). In this notation, the AM1 Fock matrix elements are:

$$F_{\mu\mu} = U_{\mu\mu} + \sum_B V_{\mu\mu,B} + \sum_{\nu}^{A} P_{\nu\nu}\left[(\mu\mu,\nu\nu) - \frac{1}{2}(\mu\nu,\mu\nu)\right] + \sum_{B}\sum_{\lambda\sigma}^{B} P_{\lambda\sigma}(\mu\mu,\lambda\sigma) \tag{2.17}$$

$$F_{\mu\nu} = \sum_B V_{\mu\nu,B} + \frac{1}{2}P_{\mu\nu}\left[3(\mu\nu,\mu\nu) - (\mu\mu,\nu\nu)\right] + \sum_{B}\sum_{\lambda\sigma}^{B} P_{\lambda\sigma}(\mu\nu,\lambda\sigma), \tag{2.18}$$

$$F_{\mu\lambda} = \beta_{\mu\lambda} - \frac{1}{2}\sum_{\nu}^{A}\sum_{\sigma}^{B} P_{\nu\sigma}(\mu\nu,\lambda\sigma). \tag{2.19}$$

The following terms appear in the Fock matrix:

(a) One-center one-electron energies, $U_{\mu\mu}$, which represent the sum of the kinetic energy of an electron in AO ϕ_λ at atom A and its potential energy due to the attraction by the core of atom A.

(b) One-center two-electron repulsion integrals, i.e., Coulomb integrals $(\lambda\lambda|\mu\mu)=g_{\lambda\mu}$ and exchange integrals $(\lambda\mu|\lambda\mu)=h_{\lambda\mu}$.

(c) Two-center one-electron core resonance integrals, $\beta_{\mu\lambda}$.

(d) Two-center one-electron attractions $V_{\mu\nu,B}$ between an electron in the distribution $\phi_\mu\phi_\nu$ at atom A and the core of atom B.

(e) Two-center two-electron repulsion integrals $(\mu\nu|\lambda\sigma)$.

The total energy E_{tot}^{mol} of the molecule is the sum of the electronic energy E_{el} and the repulsions E_{AB}^{core} between the cores of atoms A and B (Equation 2.20).

$$E_{tot}^{mol} = E_{el} + \sum_{A<B}\sum E_{AB}^{core} \qquad (2.20)$$

The heat of formation ΔH_f^{mol} of the molecule is obtained from its total energy by subtracting the electronic energies E_{el}^A and adding the experimental heats of formation ΔH_f^A of the atoms in the molecule (Equation 2.21).

$$\Delta H_f^{mol} = E_{tot}^{mol} - \sum_A E_{el}^A + \sum_A \Delta H_f^A \qquad (2.21)$$

In the AM1 treatment, the various terms in the Fock matrix and the core-core repulsions E_{AB}^{core} are not evaluated analytically. They are determined either from experimental data or from semiempirical expressions that contain numerical parameters that can be adjusted to fit experimental data. The introduced adjustable parameters will compensate both for the basic deficiencies of the single-determinantal MO approach (i.e. neglect of electronic correlation) and for the additional errors due to the simplifying assumptions of the NDDO scheme. The different treatments for the terms are outlined as following:

The one-center terms $U_{\mu\mu}$ are taken as variable parameters but to retain Oleari's values[13] for the one-center repulsion integrals $g_{\mu\nu}$ and $h_{\mu\nu}$. The semiempirical values for the one-electron repulsion integrals $g_{\mu\nu}$ and $h_{\mu\nu}$ are much smaller than the corresponding analytical values. This reduction is attributed to the Coulombic correlation between the motions of the electrons that tends to keep them apart at every moment and to decrease their repulsion. By deriving the one-electron repulsion integrals from experimental data, some allowance for the correlation effects that are formally neglected in the MO approach was

made.

In the case for calculating two-electron repulsion integrals, they are expanded[14] in terms of semiempirical multipole-multipole interactions. The semiempirical multipole-multipole interactions insure the proper behavior of each semiempirical repulsion integral in the limits $R_{AB} \rightarrow \infty$ and $R_{AB} \rightarrow 0$. Dewar and Thiel have compared the semiempirical and analytical integrals. They have shown that both are very similar at large interatomic distances ($R_{AB} > 3\text{Å}$). At small and medium distances, the semiempirical integrals are appreciably smaller, due to inclusion of correlation effects in the semiempirical integrals.

For the core-electron attractions, $V_{\mu\nu}$, and the core-core repulsions, E_{AB}^{core}, parametric functions were used to keep the balance between the attractions and repulsions in the molecule.

The remaining quantities in the AM1 method are the one-electron resonance integrals, $\beta_{\mu\lambda}$, they are assumed to be proportional to the corresponding overlap integrals, $S_{\mu\lambda}$,

$$\beta_{(\mu\lambda)} = \frac{1}{2}\left(\beta_{\mu}^{A} + \beta_{\lambda}^{B} \right) S_{(\mu\lambda)} \qquad (2.22)$$

where β_{μ}^{A} is an adjustable atomic parameter. This completes the short description of the approximations and parametric functions used in the AM1 method.

2.2 *Ab initio* Methods

The term *ab initio* implies a rigorous, nonparametrized molecular orbital treatment. This is not completely true. There are several simplifying assumptions in *ab initio* theory, but the calculations are more complete, and therefore more expensive, than those of the semiempirical methods.

Ab initio methods are also based on self-consistent-field molecular orbital (SCF-MO) theory. Electron-electron repulsion is specifically taken into account. Normally, calculations are approached by the Hartree-Fock closed-shell approximation, which treats a simple electron at a time interacting with an aggregate of all the other electrons. In the ab initio calculations, atomic basis sets are first assigned to each nucleus with standard set of coefficients and exponents that define the orbitals. Then the various one- two-electron integrals (often hundreds of thousands of them) are analytically evaluated. Self-consistency is achieved by a procedure in which a set of orbitals is assumed, and the density matrix elements are calculated. These are then used to calculate a new set of orbitals, which in turn are used to calculate a new density matrix. The process is continued until convergence occurs and self-consistency is achieved.

Two types of atomic basis functions have received

widespread use in an *ab initio* calculation. Slater-type atomic orbital (STO) have exponential radial parts ($\exp(-\xi r)$). They are labeled like hydrogen atomic orbitals, 1s,2s,2px,$\cdots$. The second type of basis consists of gaussian-type atomic functions. These are powers of x,y,z multiplied by $\exp(-\alpha r^2)$. Most modern ab initio calculations employ Gaussian-type orbital (GTO) basis set. These bases, in which each atomic orbital is made up of several Gaussian functions, have considerable advantages over other types of basis set for evaluation of one- two-electron integrals. They are therefore much faster computationally than, for instance, equivalent Slater orbitals.

2.3 Comparison Between *Ab initio* And Semiempirical Methods.

Both *ab initio* and semiempirical calculations treat the combination of orbitals by iterative computations which establish a self-consistent-field and minimize the energy of the system.

A fundamental difference between *ab initio* methods and the semiempirical methods is the absence of parameters to adjust the results toward specified points of agreement with other calculations or experimental data in the former ones. In particular, in the Fock matrix elements of the AM1 method, $U_{\mu\mu}$, $g_{\mu\nu}$, $h_{\mu\nu}$, $V_{\mu\nu}$, $\beta_{\mu\nu}$, and $(\mu\nu|\lambda\sigma)$ terms are determined either from atomic spectroscopic values or from

semiempirical expressions that contain parameters that can be adjusted to fit experimental data. The *ab initio* calculations usually make fewer assumptions and then calculate the one- two-center integrals analytically in the Fock matrix elements.

In contrast with the semiempirical methods, however, there are many different possible choices of atomic orbitals (basis set). Most modern ab initio calculations employ Gaussian type orbital (GTO) basis set. The simplest of the optimal basis set in gaussion programs is the STO-nG bases. The STO-nG basis set means that each Slater-type atomic orbital consists of n Gaussian functions. Other basis sets are 3-21G, 4-31G and 6-21G etc. For example, in the 3-21G basis set, each inner shell is represented by a single basis function taken as a sum of three Gaussians, and each valence orbital is split into inner and outer parts described by two and one Gaussian, respectively.

The difference, in respect of electron correlation, is that ab initio calculations at Hartree-Fock limit neglect the electronic correlation effects. Although configuration interaction (CI) and the Møller-Plesset perturbation theories account for partial electron correlation in a molecule, they are often limited by the computer time and disk space needed for the calculations of a large molecule. The semiempirical methods, like MNDO and

AM1, are parametrized at the SCF level to fit experimental results, which already reflect correlation. Therefore any calculation using these methods may give more realistic heats of formation, because the correlation energy has been included via the parametrization.

In the AM1 approximation, one-center Coulomb terms are set from the following expression first given by Pariser[15]

$$\gamma_{\mu\nu} = (\mu\mu|\nu\nu) = I - A \ . \qquad (2.23)$$

Pariser reasoned that the difference between the ionization potential and electron affinity of a carbon atom in a valence state should be equal to the repulsion of two electrons in that valence state. The value of $\gamma_{\mu\nu}$ calculated from *ab initio* method is 16.93 eV,[16] but estimated of I-A is around 10 Ev for a carbon.

Comparison of the semiempirical and analytical integrals of the one-center Coulomb terms shows that the correlation energies are not given correctly by the Hartree-Fock model. In the AM1 method, by choosing an empirical value of $\gamma_{\mu\nu}$, a correction can be made for the neglect of these terms in a molecular calculation.

We turn now to the other time-consuming aspect of calculations. The time required for a single SCF

calculation, using the STO-3G basis set, is two orders of magnitude greater than using MNDO, or AM1. The time required by 6-31G* (polarization functions only on heavy atoms) is two orders of magnitude greater again.[17] As Dewar[17] shows, the results from MNDO or AM1 calculations are generally comparable with those from ab initio methods that require much at least 1000 times more computing time[12]. The data and statistics provided in the Dewar and Thiel paper[11] shows that the MNDO and AM1 values for the heats of formation, molecular geometries, ionization potentials and dipole moments are quite close to experimental values.

2.4 Methods of Modeling Radical Recombination Reactions

Theoretical calculations of bond dissociation or radical recombination reactions require consideration of several important features. First, a calculational method has to produce the product radical pairs rather than ions. Second, a calculational method must describe the bond dissociation reaction path at all distances between the dissociating species properly. Third, a calculation has to include the electron correlation effects.

The Restricted Hartree-Fock (RHF) calculations normally used for ground state calculations do not correctly produce the first feature. As they limit the electrons to pairwise occupation of the molecular orbitals,

they lead to ionic rather than the desired homolytic cleavage. Therefore, they lead to an energy curve that deviates considerably from that of the radical recombination reactions.

The solution to the problem lies in mixing the two electronic configurations to obtain a good description of the bond breaking process. This can be achieved either by considering more than one configuration from the start, as in generalized valence bond or multiconfiguration self consistent field (MCSCF) calculations; or by mixing excited states into the single-determinant wave function, as in configuration interaction (CI) calculations. So the Unrestricted Hartree-Fock (UHF), or Restricted Hartree-Fock calculations (RHF) coupled with electron correlation must be used. The geometries of the species must be carefully optimized along each point of the reaction path if small activation barriers are to be determined.

The energy difference between the experimental and the Hartree-Fock limit values, called the correlation energy, arises from the instantaneous interactions between the electrons. The SCF-MO method is also known as Hartree-Fock or single-determinant theory. As discussed before, the main deficiency of Hartree-Fock theory is its incomplete description of the correlation between the electrons. As is widely recognized, Hartree-Fock theory with any basis set gives poor results for direct calculation of the energy of

a homolytic dissociation process A-B → A + B. Nevertheless the correlation energy correction for the electrons forming the bond is a significant fraction of the total bond energy. If correlation is omitted, this error will be greater for bonded system A-B than for separated A and B, and calculated dissociation energies will be too small.

One way to apply some sort of correction for electron correlation to the SCF method is to us Rayleigh-Schrödinger many-body perturbation theory. This has been applied to molecular system by Møller and Plesset[18] and implemented by Pople and his coworkers.[19] These methods, which can be terminated at second (MP2), third (MP3), or fourth order (MP4), are based on perturbation theory. Like many methods for calculating the correlation energy, they rely on a good description of the virtual orbitals in the original SCF wave function. Another approach is called the configuration interaction (CI) method.

The *ab initio* calculations with the electron correlation may be possible for studying the dissociation paths of small molecules.[20] Calculating bond dissociation surface for large organic molecules accurately is beyond the range of ab initio methods. Simple Hartree-Fock procedures do not adequately account for the correlation of electron motion. MCSCF or Hartree-Fock with Møller-Plesset (MP) calculations give some correlation energy, but the calculations would be much too involved and too time

consuming to be practical. The cost of calculations for large organic molecules with complete geometrical optimization precludes their use in this area.

As a result, empirical methods, often based upon approximations originally made by Gorin[21] and later reviewed by Benson,[22] are often used to estimate the reaction parameters of fast radical reactions.

The electron correlation error is much less a problem for semiempirical calculations such as MNDO or AM1 methods. An important point to notice is that the semiempirical methods, MNDO[11] and AM1,[12] are parametrized at the SCF level to fit experimental results, which already reflect correlation. Moreover, care has to be taken when calculating interaction energies from some types of correlated wavefunctions. Some methods of treating electron correlation must be used to give results that are size consistent.

However, the semiempirical methods, like MNDO[11] and its successor AM1[17] with 3 X 3 CI using the half-electron method[23] calculations, have been shown to give good results in several reaction paths involving radicals,[24] biradicals[25] and complex molecules.[26] The calculations produce the bond dissociation curves for small molecules[27] and show fair agreement with experiment and ab initio calculations.

AM1 versus MNDO Methods

The most serious defects of MNDO are its failure to reproduce hydrogen bonds,[28,29] energies that are too positive for crowded molecules, too negative for those containing four-membered rings, and activation energies that tend to be too large. Overestimated repulsions between atoms at their van der Waals distance is a main cause resulting in those errors.

The way to correct this was to modify the core repulsion function in MNDO, which was done in the AM1 method developed by Dewar in 1985.[17] The AM1 is a new parametric quantum mechanical molecular mode. The Dewar paper[12] clearly indicates that there has been a major improvement in the treatment of crowded molecules by examining 58 hydrocarbons and 80 molecules containing nitrogen and/or oxygen from both MNDO and AM1 calculations. It turns out that repulsions between atoms will be described more properly by AM1 than MNDO. The main gains are the ability of AM1 to reproduce hydrogen bonds and the promise of better estimation of activation energies.

Upon comparing the AM1 and MNDO methods, MNDO/CI predicts some small barriers to radical recombination where they are not expected. For example 2.4 kcal/mole is the predicted barrier for methyl radical combination. This could result from the exaggeration of repulsion of

hydrogens, the 1,4-repulsion in ethane. This apparent barrier disappears in the AM1 calculation. In addition, the AM1 could provide a reaction surface that looks more like the multiconfiguration SCF (MCSCF) surface than the comparable MNDO calculation. In chapter 3, the radical recombination reactions involving methyl with allylic and benzylic couplings, dibenzyl couplings, dicyanobenzyl couplings, and ditrimethyl couplings use AM1/CI method throughout.

For the calculation of radical combination reaction paths within AM1/CI bound, 3 x 3 CI was adopted. When one uses 3 X 3 CI, the ΔH_f's of the separated radicals are almost identical to the ΔH_f's of the individual radicals. Therefore, the size consistency is achieved.

The 3 X 3 procedure in the AM1 program uses an open shell excited singlet state for the basic SCF calculation, then adds two other states. One is the doubly excited state by promoting an electron from the excited singlet state. The other one is the ground state by demoting an electron from the excited singlet state. Both radicals and the open shell excited singlet states are calculated using the half-electron method.

The half-electron method has the advantage that it is on the same energy scale as RHF calculations for closed-shell molecules. This means that the relative energies of singlet and triplet states can be compared directly if the

singlet is calculated with the RHF and the triplet with the half-electron method. Thus, all the results are size consistent by this method.

The simpler 2 x 2 CI also gave a smooth dissociation curve. However, the calculated energy at large bond separation of the radicals did not approach the sum of the individual radical energies calculated by the half electron method.[23] The 3 x 3 CI procedure does not have this problem. The 2 x 2 procedure is adequate for diatomic molecules, like F_2 and Cl_2.[27]

RHF Half-electron versus UHF

In the open-shell SCF-MO treatment (UHF), the symmetry of the orbital occupation is broken, one orbital is unsymmetrically occupied by an electron that has either α or β spin. In the closed-shell SCF-MO (RHF) treatment, each MO is either empty, or symmetrically occupied by two electrons of opposite spin. If we are to treat radicals by the closed-shell method, we must therefore get rid of this asymmetry. The half-electron method is one kind of approach in formal manner. Instead of using the two-configuration function (α or β), one could represent the radical symmetrically by a single determinant if one replaced the unpaired electron in it by two "half-electrons" of opposite spin. A "half-electron" in

this sense would be defined as an imaginary particle with half the charge of an electron, the orbital energy of such a particle, occupying the MO, being Eu/2 (Eu is the ordinary orbital energy). This implies that the orbital is occupied by half an electron of α spin and half an electron of β spin.

RHF AM1 with 3 x 3 calculation using the half-electron method for the radical recombination reaction paths might be the proper and easier way to obtaining the correct curvature of the radical recombination curve. This conclusion could be demonstrated by the calculations done in this thesis.

CHAPTER 3

3. BIRADICAL COMBINATION REACTIONS

3.1 Introduction

The recombination of two free radicals to form a single covalent bond is often thought to occur without activation. This conception is probably due to analogy with the combination of two atoms, such as H, to form a covalent molecule, such as H_2. Exceptions to this idea are usually attributed to steric interactions alone. Nevertheless, experimental observations that have long been in the literature suggest that other effects, presumably electronic in nature, also might cause barriers to combination of radicals.

In fact, the first free radical characterized, triphenylmethyl, has long been known to be in equilibrium with its dimer, which has been shown to have structure 1, rather than the originally expected hexaphenylethane.[1] Also

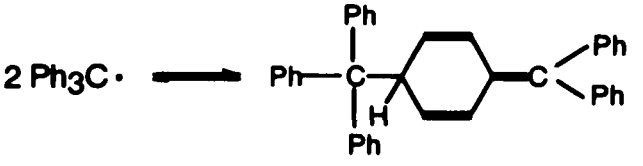

1

prominent among the experimental observations that support

this idea, are the observed selectivities for attacking at radicals that can, in principle, react at more than one site. Thus, allyl radical reacts at the terminal positions, rather than the central carbon (to give cyclopropyl products), and benzyl radicals couple dominantly at the α-carbons, rather than at the ring carbons. A particularly striking example involves the coupling of triphenylimidizoyl radicals, which couple to form two different products, one kinetically and the other thermodynamically favored.[2] The kinetically favored product, 2, is clearly more sterically hindered than the thermodynamic product, 3.

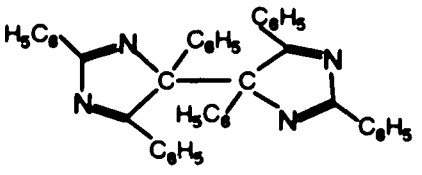

2

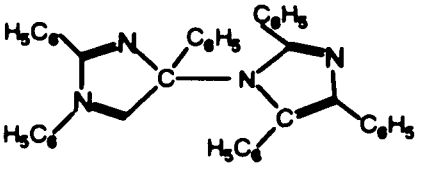

3

Theoretical calculations suggest that barriers to radical recombination might exist in certain situations. MNDO/CI calculations have suggested that 1-azaallyl radical be preferentially attacked at the carbon, rather than the nitrogen,[3] and there be a barrier to the recombination of ethyl and ethyldiazenyl radicals.[4] *Ab initio* and

semiempirical calculations both suggest that barriers to the combination of the diamino and dihydroxylaminyl radicals should exist.[5]

3.2 Method

Upon discussing the methods used to study homolytic bond dissociation paths before, We use AM1 with 3 x 3 CI. The geometries of all species discussed were completely optimized in all internal degrees of freedom. Each of the transition states was characterized by calculating its force constants. One, and only one, force constant was found to be negative in each case.[6]

3.3 Results and Discussion

3.3.1 Methyl with Allyl and 1-Azaallyl Radical Couplings

In this part of the chapter, we present results of calculations for bimolecular reactions of allyl with methyl radicals (reaction I-III, Table 3.1). The calculated activation enthalpies for the attack of methyl radical on allyl and 1-azaallyl radical are collected in Table 3.2. The previously published MNDO/CI values by Dannenberg[7] are included for comparison. The activation energy for methyl radical attack upon allyl radical (reaction I) is predicted

Table 3.1

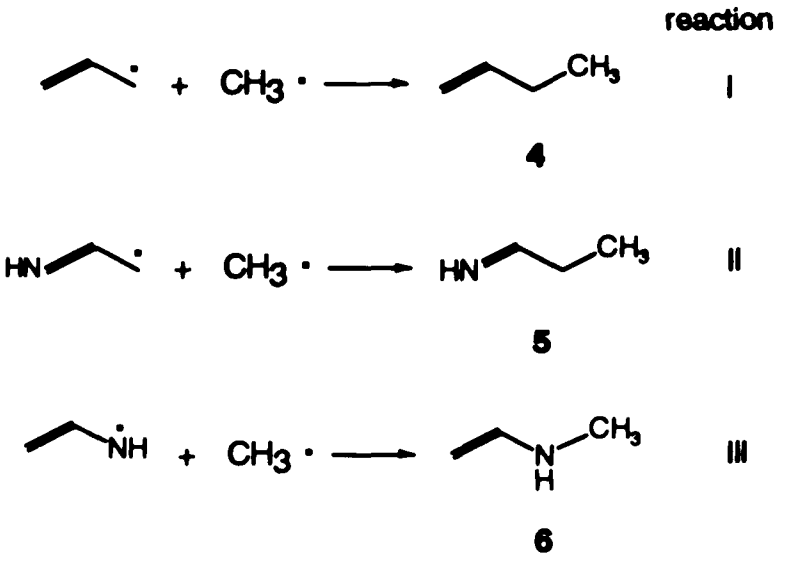

Table 3.2 Activation Energies for Recombination Reactions of Allyl, 1-Azaallyl and Benzyl with Methyl Radicals.

Reaction	Radical site	ΔH_{act} (kcal/mol)	
		MNDO	AM1
I		5.5	0.3
II	C	3.9	0.2
III	N	11.0	2.8
IVa	C_{alpha}	3.0	0.7
Va	C_{ortho}	14.0	2.4
VIa	C_{para}	10.0	1.6

to be 0.3 kcal/mol by AM1/CI, rather than the 5.5 kcal/mol predicted by MNDO/CI. Similarly, the activation energies for attack at the carbon and nitrogen termini of the 1-azaallyl radical (reaction II,III) decrease to 0.2 and 2.8 kcal/mol from the previously reported MNDO/CI values of 3.9 and 11.0 kcal/mol. While the quantitative results are different, and improved for AM1/CI, the trends remain the same. In particular, attack upon the carbon terminus of 1-azaallyl is favored by both sets of calculations. AM1 removes the apparently anomalous overestimation of the activation barriers in these cases, as it did for the combinations of methyl radicals and aminyl radical with hydrogen.

3.3.2 Methyl with Benzyl Radical Couplings

The activation enthalpies for the combination of methyl and benzyl radicals to form products 7a, 8a, and, 9a (reaction IV_a-VI_a , Table 3.3) are collected in Table 3.4. The reaction is favored at the alpha, rather than ortho or para, positions on the benzyl radical. From these results, as well as those previously discussed for the combination of methyl and the allylic radicals, one might suspect that the relative ease of reaction at a particular position might be related to the spin density at that position.

To test that hypothesis, we located the transition

Table 3.3

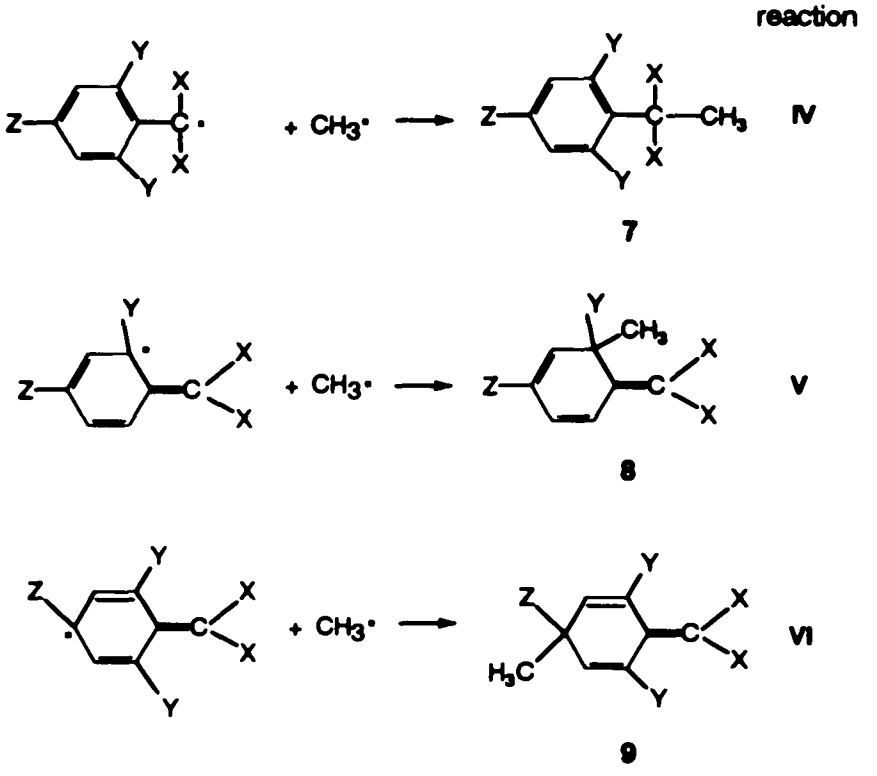

	X	Y	Z
a	H	H	H
b	H	H	CN
c	H	CN	H
d	H	CN	CN
e	CN	H	H

states for the reaction of methyl radical with benzyl radicals that have been variously substituted with cyano groups to form products 7b-e, 8b-e and, 9b-e (reaction IV_{b-e}-VI_{b-e}, Table 3.3). The cyano groups were used to perturb the spin densities of the parent benzyl radical. The

calculated activation barriers and spin densities are also collected in Table 3.4. The Figure 3.1 shows a plot of the calculated enthalpies of activation versus the spin densities for the appropriate positions of the

Table 3.4 AM1 Energies for the Recombination Reactions of Methyl with Substituted Benzyl Radicals in Kcal/mol.

Reaction	Radical position	ΔH_{act}	Spin density
IVa	alpha	0.7	0.48
Va	ortho	2.4	0.17
VIa	para	1.6	0.19
IVb	alpha	0.3	0.42
Vb	ortho	1.0	0.16
VIb	para	2.1	0.21
IVc	alpha	0.2	0.40
Vc	ortho	2.9	0.17
VIc	para	0.4	0.18
IVd	alpha	0.4	0.36
Vd	ortho	2.6	0.17
VId	para	1.9	0.20
IVe	alpha	1.1	0.46
Ve	ortho	2.6	0.11
VIe	para	1.2	0.12

corresponding radicals. The correlation is clearly quite poor. The obvious conclusion is that polarization of the spin of the reacting radical must be a reasonably facile process. As such, it contributes little to the activation energy.

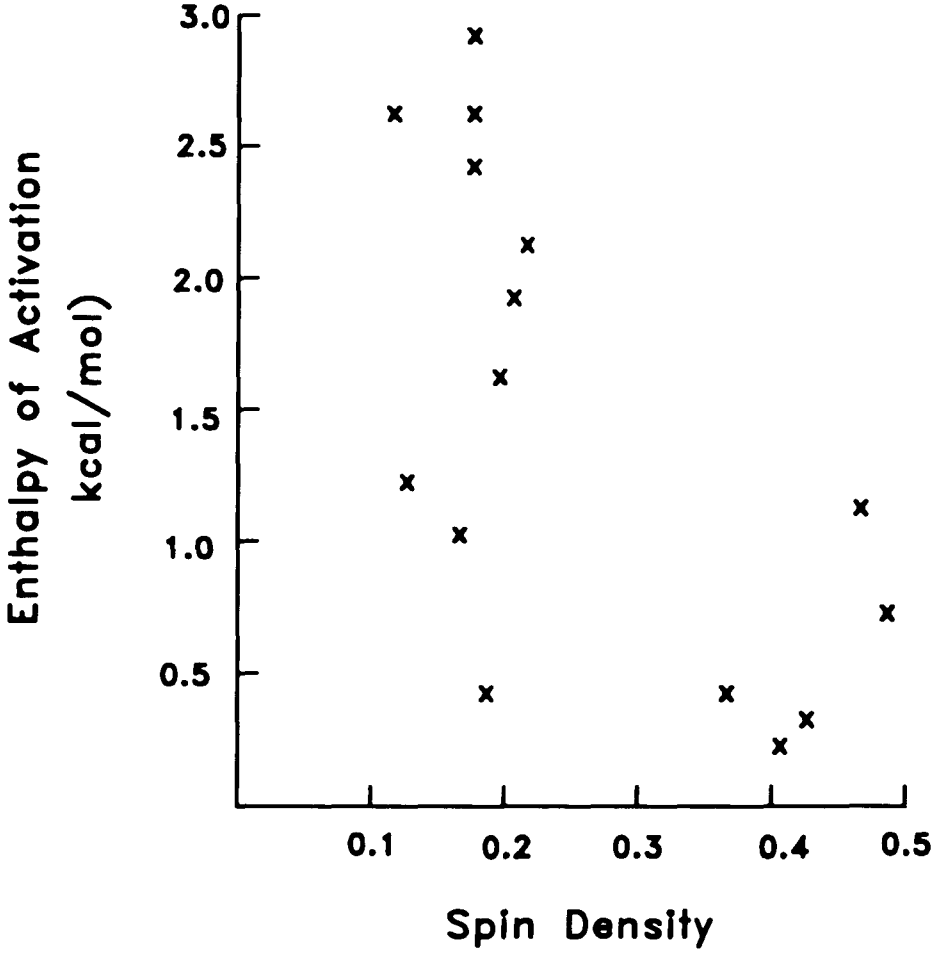

Figure 3.1 Plot of calculated enthalpies of activation versus spin densities on the position of the benzyl radical being attacked for the combination reactions of methyl and cyano substituted benzyl radicals.

3.3.3 Bibenzyl Radical Couplings

Table 3.5

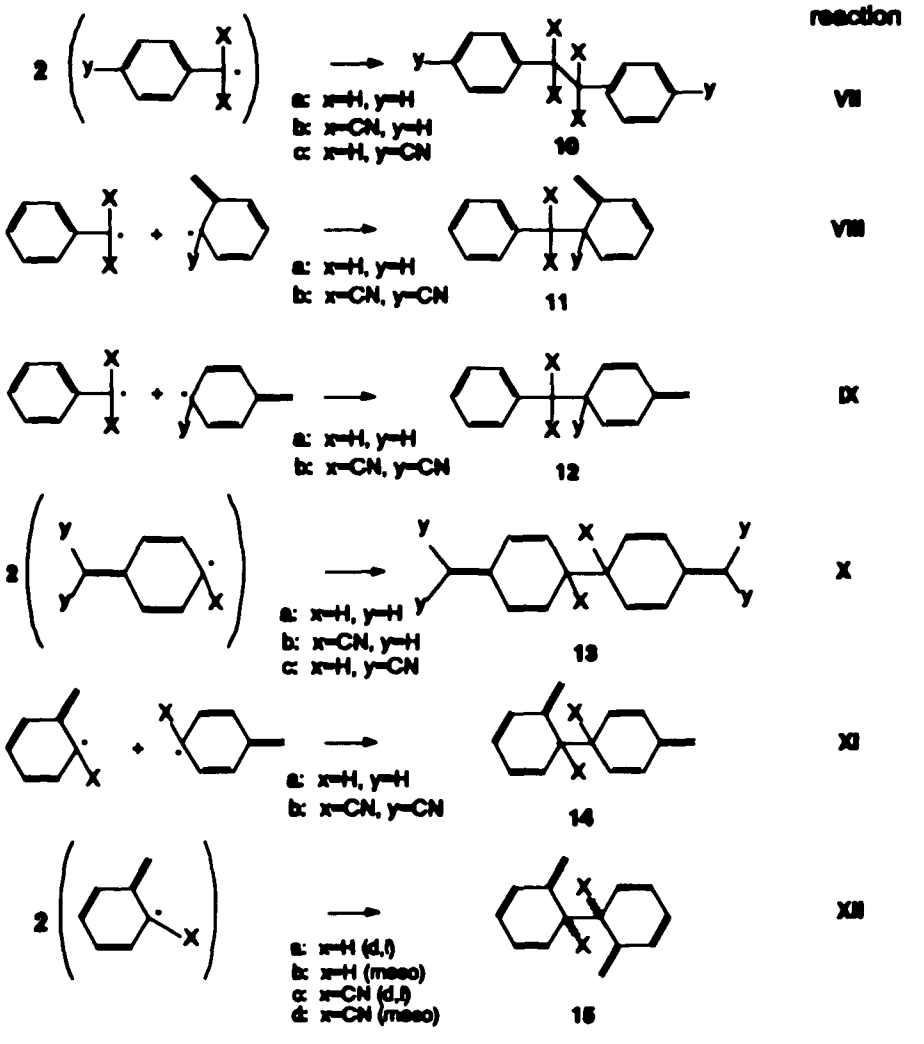

Calculations of the combination of pairs of benzyl radicals at various positions (reaction VII-XII, Table 3.5) give the activation enthalpies collected in Table 3.6. The favored combination to form 1,2-diphenylethane, 10a, has no enthalpic barrier. However, the calculations predict small, but significant barriers of 3.7 and 3.1 kcal/mol, respectively for the attacks of the α-carbon of one benzyl radical upon the ortho or para position of the other to form 11a and 12a. Couplings at the ortho or para position of both rings have barriers between 16.7 and 18.7 kcal/mol.

Table 3.6 AM1 Energies in Kcal/mol and C-C Bond Lengths for the Dimerization of Benzyl Radicals.

Reaction	Product	ΔH_f(TS)	ΔH_{act}(AM1)	$\Delta H°$(AM1)	C-C bond (Å)
VIIa	10a	-	0.0	-68.0	-
VIIIa	11a	107.9	3.7	-39.3	2.33
IXa	12a	107.2	3.2	-40.8	2.33
Xa	13a	120.7	16.7	-14.7	2.07
XIa	14a	122.3	18.3	-13.0	2.10
XIIa	15a(d,l)	121.7	17.7	-12.9	2.09
XIIb	15b(meso)	122.6	18.7	-10.7	2.10

Table 3.7 The Experimental Ratio of Different Coupling Products of Benzyl Radicals at Various Temperatures.[a]

T (°C)	αp/αα	αo/αα	αo/αp
-18	0.061	0.048	0.79
-9	0.088	0.071	0.81
+2	0.095	0.086	0.90
+12	0.102	0.099	0.97
+20	0.102	0.098	0.96
+28	0.103	0.107	1.04
+36	0.095	0.105	1.10
+45	0.086	0.104	1.21
+54	0.077	0.102	1.33
+62	0.071	0.109	1.54

[a]ref. 8

There are seven possible products (excluding attack at the meta-carbons): α-α, 10a; α-ortho, 11a; α-para, 12a; para-para, 13a; ortho-para, 14a; and two diastereomers of ortho-ortho, 15a-b. Significantly, the calculated activation enthalpies predict face selectivity in the formation of the ortho-ortho coupling product, 12a-b. Fischer and Lenghals[8] have reported experimental product ratios for the coupling of benzyl radicals to form three products: 10a (α-α coupling), 11a (α-ortho coupling) and 12a (α-para

coupling). The products of ortho-ortho, ortho-para, and para-para coupling, 13a, 14a, and 15a,b were not observed. The experimental results (see Table 3.7) cover ten different temperatures over a range of 100 degrees.

To evaluate the AM1 results presented above, we correlated the calculated and experimental results in the manner described below. It was not possible to calculate predicted product ratios simply based upon enthalpies of activation since that value is zero for α-α coupling. Thus, the entropy must contribute significantly to the free energy of activation. Instead, we compared the theoretical and all of the experimental results using Equation (3.1),

$$\frac{f_1}{f_2} = \frac{g_1}{g_2} e^{-\frac{(\Delta\Delta H_{act} - T\Delta\Delta S_{act})}{RT}}, \qquad (3.1)$$

where f_2/f_1 is the ratio between two products, g_2 and g_1 are the appropriate statistical weighing factors, $\Delta\Delta H_{act}$ and $\Delta\Delta S_{act}$ the differential enthalpies and entropies of activation. The experimental product ratios, and the theoretical enthalpies of activation are assumed to be correct. A least squares fit of the data accumulates all the errors into the differential entropies of activation. The differential entropies of activation are then corrected because the α-α transition state has one two-fold rotational

Table 3.8 Calculated Selectivities of Benzyl Radical Couplings.

Couplings	$\Delta\Delta H_{act}$ (kcal/mol)	$\Delta\Delta S_{act}$ (e.u.)	$\Delta\Delta S_{act}$(corr.) (e.u.)	g (Statistical factor)
αp/αα	3.1	3.8	2.4	2
αo/αα	3.8	4.8	3.4	4
αo/αp	0.7	1.0	1.0	2

axis, while the other transition states have none. If these differential entropies of activation are small, the correspondence between theory and experiment is good. The total range of (corrected) differential entropies of activation is 3.4 e.u., which corresponds to 1.0 kcal/mol at 300 K. Thus, the calculated and experimental values seem to be in mutual agreement (see Table 3.8).

3.3.4 Bicyanobenzyl Radical Couplings

The relatively high activation energies and low bond energies calculated for the o-o , o-p, and p-p couplings of benzyl radicals suggest the possibility of making kinetically stable compounds containing a C-C bond whose BDE is negative. Dannenberg et al. have previously

Table 3.9 AM1 Energies and C-C Bond Lengths for the Cyanobenzyl Radical Couplings.

Product	Radical Position	ΔH_{act} (kcal/mol)	BDE (kcal/mol)	C-C bond (Å)
10b	α-α	17.4	19.3	2.59
10c	α-α	0.0	68.5	-
11b	α-ortho	14.9	9.2	2.23
12b	α-para	13.9	12.1	2.24
13b	para-para	27.3	-1.7	2.09
13c	para-para	23.9	6.5	2.01
14b	ortho-para	26.7	-4.2	2.08
15c(d,l)	ortho-ortho	28.5	-7.3	2.09
15d(meso)	ortho-ortho	29.6	-8.5	2.09

discussed compounds with N-N and C-N bonds that have negative BDE's.[5b] For this reason we calculated the BDE's and activation energies for coupling and dissociation for several dimers of cyanobenzyl radicals, 10b-c, 11b, 12b, 13b-c, 14b, 15c-d (see Table 3.5). As the cyano group generally stabilized unsaturated and radical centers relative to saturated centers, we hoped that the products that would result from the coupling of cyanobenzyl radicals at their substituted positions would result in compounds that contained a C-C bond with a negative BDE. The relevant

data are collected in Table 3.9. As anticipated, the p,p-dimer of the p-cyanobenzyl radical, 13b, the o-p dimer of the o-cyano- and p-cyanobenzyl radicals, 14b, and the o,o-dimers of the o-cyanobenzyl radical, 15c-d have negative bond energies, yet are predicted to be kinetically stable species. In principle, compounds of this type could be prepared in the laboratory (using other preparatory procedures than coupling). Measurement of the ΔH_{act} and BDE's of these species would provide convincing evidence concerning our suggestions regarding barriers for radical coupling reactions.

Intrinsic Barrier

The results presented in this chapter strongly suggest the existence of an intrinsic or natural barrier for the coupling of two carbon centered radicals. We define such a barrier as the activation energy required to form (or break) a C-C bond whose BDE is zero. One can evaluate the magnitude of such a barrier in several manners. We have chosen the Marcus equation[9] and a linear equation after Leffler and Grunwald.[10]

Marcus and Linear Regression Equations

The Marcus equation[11] was originally developed to

explain electron transfer reactions. It has been extended to other organic reactions.[12] This subject has been thoroughly discussed by Murdoch et al.[13] A useful application of the Marcus equation involves calculating the intrinsic barrier from the theoretically determined activation enthalpies and heats of reaction using the Marcus equation in the form shown in Equation 3.2. In this

$$\Delta H_{act} = \Delta H^{i}_{act} + (\Delta H^{o})^{2} + \frac{(\Delta H^{o})^{2}}{16\ \Delta H^{i}_{act}} \quad . \qquad (3.2)$$

formulation, the enthalpy of reaction, ΔH^{o}, enthalpy of activation, ΔH_{act}, and the intrinsic enthalpic barrier, $\Delta H_{act}{}^{i}$, are related as indicated. Any of the variables can be calculated if the other two are known. By applying this equation, one can calculate the intrinsic barrier for each reaction by substituting the appropriate values for the calculated activation energies and heat of reaction in the Equation (3.2). If the individual reactions have a common mechanism, one might expect the intrinsic barriers calculated from them to be similar in magnitude. The intrinsic barriers calculated in this manner are present in Table 3.10.

Another useful application of Marcus theory is to recalculate the activation energies using the intrinsic

Table 3.10 Activation Enthalpies of Benzyl Radical Couplings from the Marcus Equation (3.2) in Kcal/mol.

Product	$\Delta H_{act}{}^{i}$	ΔH_{act}	ΔH_{act}(Marcus)
10a	-	0.0	1.1
11a	18.0	3.7	6.6
12a	17.6	3.1	6.2
13a	23.5	16.7	15.1
14a	24.4	18.3	15.8
15a(d,l)	23.7	17.7	15.8
15b(meso)	23.7	18.7	16.8
average	21.8		

barrier and the experimental heats of reaction. This allows the modeling procedure to overcome the errors due to the incorrect description of the heats of formation of the radicals and consequent erroneous heats of reaction. Complete optimization of the reaction paths and transition states may be extremely costly for many reaction processes. If one can establish that the Marcus equation works properly within a reasonable sample of reactions that presumably follow similar reaction paths, one can use the intrinsic barrier extracted from these calculations with simple thermochemical data for the additional reactions in question to calculate their activation parameters. The

thermochemical data may be obtained in whatever manner is most appropriate or available, either experimentally or theoretically. Dannenberg et al. have previously used this application in a theoretical study of hydrogen-atom abstraction by methyl radicals. The results calculated are also presented in Table 3.10.

Following Leffler and Grunwald,[11] we have also fitted the data to a linear Equation 3.3, where BDE is the

$$\Delta H_{act} = 24.51 - 0.052 \times BDE \,, \qquad (3.3)$$

bond dissociation energy. For this purpose, we have used all the data for bonds with BDE's < 48 kcal/mol. Bonds with BDE's > 48 kcal/mol would all give negative predicted barriers using this linear relationship. These results are included in Table 3.11.

Using Marcus theory, the intrinsic barrier calculated from the average of the couplings between the ring carbons is 23.8 kcal/mol, while that calculated from the average of the α-ring carbon couplings are 17.8 kcal/mole (the α-α coupling has no barrier). The overall average is 21.8 kcal/mol. The three higher barrier reactions are much less exothermic than the couplings involving the α-carbons. They also involve the loss of aromaticity in two rings rather than one (in the case of α-ring coupling) or none (in the case of α-α coupling). It is

Table 3.11 Comparison of Enthalpies of Activation Calculated Using AM1, the Marcus Equation and Linear Regression in Kcal/mol.

		Enthalpies of Activation		
Reaction	Product	AM1	Marcus	Linear Regression
IVa	7a	0.7	0.5	0.0
IVb	7b	0.3	0.4	0.0
IVc	7c	0.2	0.5	0.0
IVd	7d	0.4	0.5	0.0
IVe	7e	1.1	2.4	0.0
Va	8a	2.4	4.4	0.0
Vb	8b	1.0	4.3	0.0
Vc	8c	2.9	5.8	2.6
Vd	8d	2.6	5.8	2.5
Ve	8e	2.6	5.4	1.8
VIa	9a	1.6	4.2	0.0
VIb	9b	2.1	5.5	2.0
VIc	9c	0.4	4.3	0.0
VId	9d	1.9	5.7	2.4
VIe	9e	1.2	4.9	0.8
VIIa	10a	0.0	1.1	0.0
VIIb	10b	17.4	13.2	14.5
VIIc	10c	0.0	1.0	0.0

Table 3.11 Continued

Reaction	Product	Enthalpies of Activation		
		AM1	Marcus	Linear Regression
VIIIa	11a	3.7	6.6	4.1
VIIIb	11b	14.9	17.4	19.7
IXa	12a	3.1	6.2	3.3
IXb	12b	13.9	16.2	18.2
Xa	13a	16.7	15.1	16.8
Xb	13b	27.3	22.7	25.4
Xc	13c	23.9	18.7	21.2
XIa	14a	18.3	15.8	17.8
XIb	14b	26.7	23.9	26.7
XIIa(d,l)	15a	17.7	15.8	17.8
XIIb(meso)	15b	18.7	16.8	19.0
XIIc(d,l)	15c	28.6	25.6	28.3
XIId(meso)	15d	29.6	26.3	28.9

possible that the ΔH_{act}^{i} for the ring-ring couplings should differ from that for the ring-α coupling, which, in turn, would differ from that for α-α coupling. The activation barriers for all the reactions were recalculated using the overall average value of 21.8 kcal/mole for ΔH_{act}^{i}, with the results indicated in Table 3.10. As can be seen, the

agreement is reasonably good, even with the combinations involving α-carbons.

However, the use of the Marcus equation may not be entirely appropriate for bond dissociation/recombination surfaces, as it is predicated on the assumption of overlapping wells on the potential energy surface. One of the consequences of this formulation is the inverted effect described by Closs.[14] Clearly, there is no well-defined minimum on the potential surface for the separated radicals, so the model may not apply here. We believe that the apparent inconsistency of the intrinsic barriers calculated from the benzyl-benzyl data with the methyl-allyl and methyl-benzyl data is due to this problem.

The Leffler-Grunwald treatment could give a better fit to the data. In contrast with the Marcus treatment, this equation is reasonably general for all the cases studied. For example, one can assume the intrinsic barrier for coupling is the sum of two intrinsic half barriers, one for each radical. Using only the benzyl-benzyl data, the intrinsic barrier is calculated to be 24.5 kcal/mol. By symmetry, the half barrier for benzyl is half the intrinsic barrier or 12.3 kcal/mol. If one uses this value for the benzyl half barrier to calculate the methyl half barrier from only the benzyl-methyl data and the same slope, one obtains 12.8 kcal/mol, hardly different from the benzyl-benzyl half barrier. Thus, the data imply that there be one

intrinsic barrier for carbon-carbon bond dissociation or recombination (without steric or other specific complications).

The implications of this result are that the intrinsic barrier for the coupling of carbon radicals may be as high as about 24-25 kcal/mol. The low (often zero) ΔH_{act} values often encountered are due primarily to the large exothermicities of most observed combination reactions (Equation 3.3 predicts no barrier for combinations to form bonds stronger than 48 kcal/mol).

One should note that the intrinsic barrier has been calculated to be 21.5 kcal/mol for the coupling of substituted aminyl radicals,[15] in agreement with ab initio calculations,[5a] and in reasonably good agreement with the results we obtained.

Conclusion

AM1/CI calculations provide a reasonably accurate manner for calculating the reaction paths involved in the coupling of carbon-centered free radicals. These calculations are in good agreement with the experimentally observed selectivities for the combination of benzyl radicals. An intrinsic barrier of about 22 kcal/mol was obtained using Marcus equation and 25 kcal/mol using a best fit to a linear equation following Leffler and Grunwald.

These results suggest that organic compounds containing C-C bonds that have zero or negative BDE's might be synthesized and isolated; and that selectivities in radical recombinations can be understood and exploited.

3.3.5 Trisubstituted Methyl Radical Couplings

We have concluded that activation energies might be anticipated for the combination reactions of methyl with allyl, azallyl, and benzyl radicals, cyano substituted benzyl radicals. In this part, we study the recombination reactions of polysubstituted methyl radicals (Table 3.12). In particular, we were able to reinvestigate the importance of the effects contributing to the activation barriers when two radicals recombine. In addition, we wish to predict the diastereofacial selectivity of bimolecular radical reactions, and possible structures for synthetically accessible molecules, when they are substituted so that methyl carbons are stereogentic (reactions XIV-XX, Table 3.12).

As before, this work was done using the AM1 approximation to molecular orbital theory. The half electron method was used in these calculations as it is thought to give better heats of formation than the UHF procedure. The reaction path for each reaction was obtained using the distance between two carbon centers as the

Table 3.12

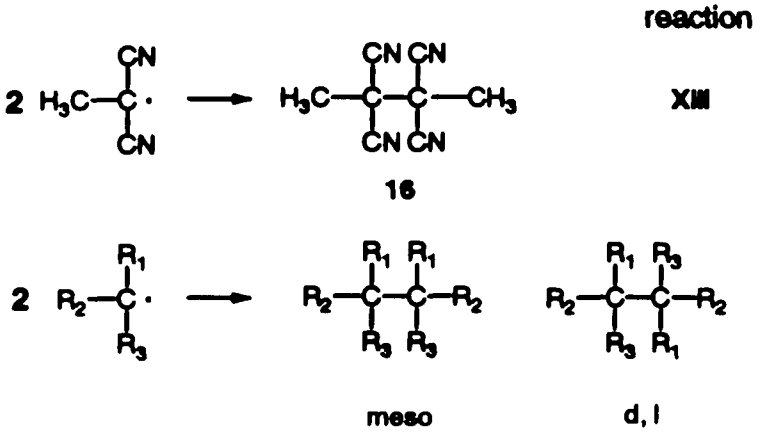

reaction XIII

16

meso d,l

R_1	R_2	R_3					reaction
CH_3	CN	NH_2	→	17	+	18	XIV
CH_3	CN	OH	→	19	+	20	XV
CH_3	CN	OCH_3	→	21	+	22	XVI
CH_3	Ph	OH	→	23	+	24	XVII
CH_3	Ph	OCH_3	→	25	+	26	XVIII
CN	Ph	OH	→	27	+	28	XIX
CN	Ph	OCH_3	→	29	+	30	XX

reaction coordinate. The geometrical parameters were optimized for each stepped value of the reaction coordinate. All possible rotamers about the central carbon-carbon bond were considered. After a good approximation to the transition state was obtained by this

procedure, the transition states were directly and completely optimized.

The results of the calculations are presented in Table 3.13 - 3.14. The dihedral angle, ϕ, between two -OR or $-NH_2$ groups is defined in Figure 3.2. Activation

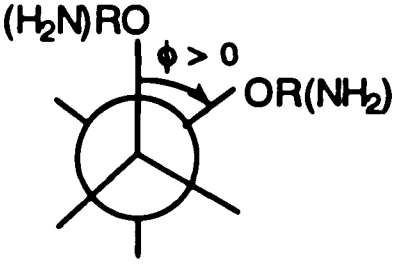

ϕ is a dihedral angle between two -OR or NH_2 groups

Figure 3.2 The Definition of the Dihedral Angle ϕ Used in Table 3.13.

enthalpies for the reactions in AM1 range between 0.93 - 9.95 kcal/mol (see Table 3.13). The facial selectivities of the dimerization are shown in Table 3.14. For the reactions of XV, XVII and XIX, the transition states of the products have one or two distinct hydrogen bonds between two hydroxy groups. The hydrogen bonding distances are in the range of 2.15 - 3.24 Å. In reactions of XVI, XIII and XX, we substituted two $-OCH_3$ groups for the two -OH groups to

eliminate the hydrogen bonding interaction. As expected, the activation barriers for these reactions are all higher than corresponded reactions with -OH group. The activation barrier difference is in the range of 2.6 - 7.2 kcal/mol.

Table 3.13 Geometric and Energetic Parameters for the Best Transition States for the Reactions of XIV-XX.[a]

reaction	product	ΔH_{act}	ΔH_f	bond length	ϕ
XIV	17	3.72	-14.14	2.47	-175.11
XIV	18	3.71	-16.03	2.48	-70.57
XV	19	2.00	-33.41	2.69	-66.91
XV	20	0.93	-33.07	2.69	-4.02
XVI	21	4.11	-30.41	2.65	72.79
XVI	22	3.82	-28.96	2.65	-161.20
XVII	23	3.38	-31.81	2.53	63.53
XVII	24	3.62	-31.54	2.58	173.47
XVIII	25	9.95	-23.95	2.51	69.70
XVIII	26	8.88	-24.25	2.55	77.68
XIX	27	2.41	-29.92	2.59	-57.04
XIX	28	2.79	-29.83	2.56	-2.91
XX	29	8.29	-20.65	2.57	70.93
XX	30	9.95	-19.94	2.54	-71.43

[a]Energy in kcal/mol, distance in Å, dihedral in degree.

Table 3.14 Comparison of Selectivities for Recombination Reactions of Trisubstituted Methyl Radicals[a].

reaction	$\Delta\Delta H_{act}^{a}$ (kcal/mol)
XIV	0.01
XV	1.07
XVI	0.29
XVII	-0.24
XVIII	1.07
XIX	-0.38
XX	-1.66

[a] $\Delta\Delta H_{act}$ is defines as $\Delta H_{act}^{meso} - \Delta H_{act}^{(d,l)}$.

The hydrogen bonding interactions presented in the transition state in above three cases tend to favor certain recombination reactions, hence, reduce their activation barriers.

In the case of reaction XIV, usual transition state conformations are obtained (see Figure 3.3). The calculations predict no diasteroselectivity for that reaction. Comparing the best meso with d,l form of the transition states for all the reactions from XV to XX, the diastereofacial selectivity appears to be due to a combination of steric and donor-acceptor polar effects

illustrated in the Newman projection of the best conformation of the transition states in both meso and d,l forms (see Figure 3.3).

In the reactions XV and XVI, one should note that the structure of the favored transition state of reaction XV leads to an eclipsed conformation. This moves the hydroxy groups to close to each other allowing extensive hydrogen bonding interaction to occur. The facial selectivity is for d,l product, suggesting that stabilizing hydrogen bonding interactions and polar-polar interactions (see Figure 3.3) are dominant in the formation of the diastereomers. It is also apparent that, in the reaction XVI, where two -OH groups are replaced by $-OCH_3$, eliminating the hydrogen bonding interaction results in raising the activation barriers about 3.54 and 2.57 kcal/mol respectively for meso and d,l forms (see Figure 3.3). Furthermore, the best conformations of the transition states assume the more usual staggered conformations (also see Figure 3.3). Once again, the stabilizing polar-polar interaction results in the preference of the d,l, rather than, meso product.

Comparing the reactions XVII and XVIII, reducing the H-Bonding, the activation barriers increase upon about by 6.57 and 5.26 kcal/mol for the meso and d,l products, respectively. Corresponding increases of about 5.88 and 7.16 kcal/mol occur for reactions XIX and XX, due to

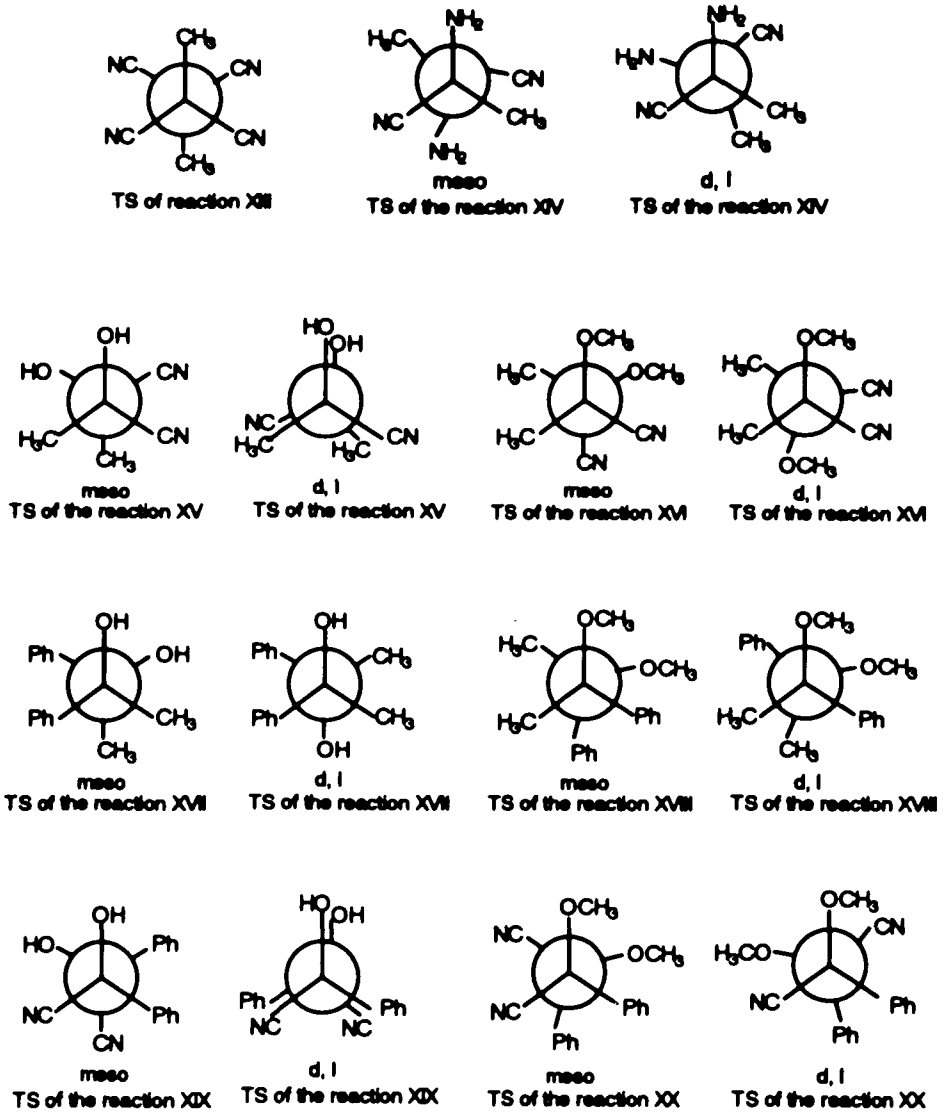

Figure 3.3 Newman Projections for the Structures of Transition States of the Reactions XIII-XX.

hydrogen bonding interactions. Significantly, the diastereofacial selectivity appears to be due to a combination of steric, polar and hydrogen bonding effects.

3.4 Energy Distribution

We can analyze the contributions to the activation energy in terms of the distortion and interaction energies (Equation 3.4 - 3.6). The activation energy is the energy difference between the transition state and the relaxed radical pair for each reaction studied. The distortion energy for each radical is defined as the energy difference between that radical frozen in the geometry it assumes in the transition state and its fully relaxed geometry. The total distortion energy is the sum of the individual distortion energies. The interaction energy is defined as the energy difference between the activation and distortion energies.

$$E_{act} - E_{TS} - \sum E_{rad.\,(relax)} \qquad (3.4)$$

$$E_{dist} - \sum E_{rad.\,at\ TS} - \sum E_{rad.\,(relax)} \qquad (3.5)$$

$$E_{act} - E_{dist} + E_{interact} \qquad (3.6)$$

Where, E_{act} is the activation energy of reaction, E_{TS} is the energy of reaction at transition state, $E_{rad.(rex)}$ is the energy of each individual radical, E_{dist} is the distortion energy of two radicals during the reaction, $E_{rad.at\ TS}$ is the energy of the distorted radical at transition state, and $E_{interact}$ is the interaction energy of two radicals during reaction.

The calculated results for all the radical reactions are included in Tables 3.15 - 3.17, and plotted in Figures 3.4 - 3.9. In all three cases, dominant contributions come from the interaction energies when methyl radical approaches the allyl, benzyl or cyano-benzyl radicals to form product (see Table 3.15). That is reasonable because methyl is too simple to involve much distortion upon interaction with other radicals. The correlations between the activation energy and distortion energy, or the activation energy with interaction energy are quite good for the reaction between methyl with allyl or benzyl radicals, but not for the reactions between methyl with cyano-benzyl radicals (see Figures 3.4 - 3.5).

For the coupling reactions of benzyl or cyanobenzyl radicals, again the major contribution to the activation energy is the distortion energy (see Table 3.16). The correlation of activation with distortion energies shown in Figure 3.13 is very good. This is not true for the interaction energies. Table 3.17 presents the energy partition

Table 3.15 Energy Partition for the Couplings of Allyl, Benzyl and Cyanobenzyl with Methyl Radicals in Kcal/mol.

reaction	product	ΔH_{act}	ΔH_{dist}	ΔH_{int}
I	4	0.29	0.01	0.28
II	5	0.19	0.01	0.19
III	6	2.83	1.53	1.30
IVa	7a	0.73	0.41	0.32
Va	8a	2.38	0.97	1.41
VIa	9a	1.60	0.50	1.10
IVb	7b	0.29	0.03	0.26
IVc	7c	0.22	0.06	0.16
IVd	7d	0.37	0.06	0.31
IVe	7e	1.14	0.12	1.02
Vb	8b	0.96	0.11	0.85
Vc	8c	2.94	1.76	1.18
Vd	8d	2.57	1.61	0.96
Ve	8e	2.64	1.41	1.23
VIb	9b	2.06	0.25	1.81
VIc	9c	0.36	0.02	0.34
VIe	9d	1.85	0.21	1.64
VIe	9e	1.24	0.17	1.07

for the coupling reactions of the trisubstitutedmethyl radicals. The distortion energy is also a major contributor to the activation energy. It seems that the activation energy for C-C radical combination reactions should be zero or very small except when both of the radicals in the pair are distorted significantly. The correlation of activation with distortion is much better than that with interaction in all cases (see Figures 3.4 - 3.9).

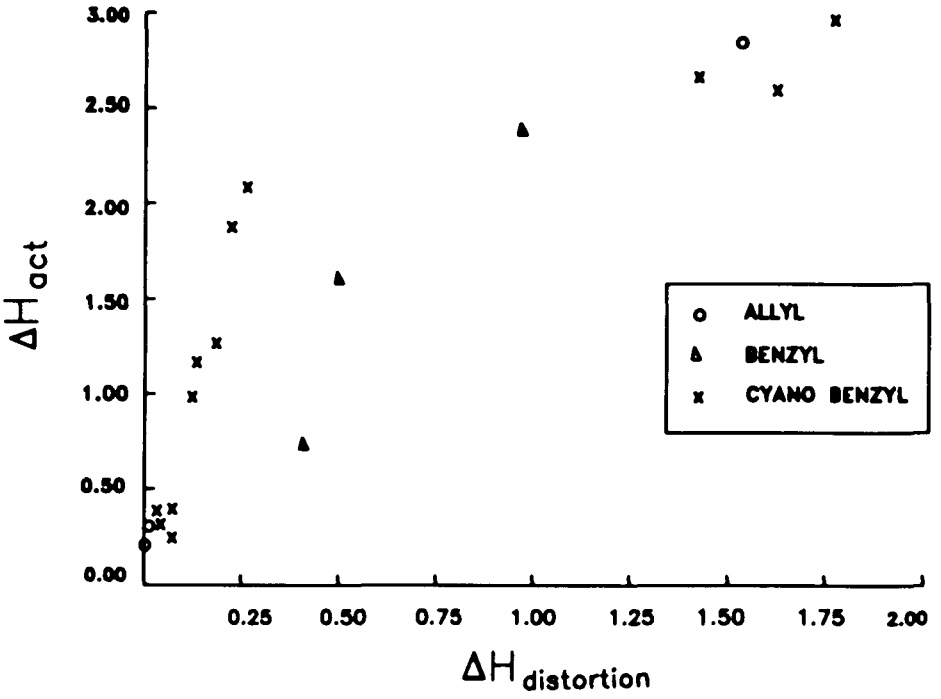

Figure 3.4 Activation Energy versus Distortion Energy for the Couplings of Allyl, Benzyl and Cyanobenzyl with Methyl Radicals in Kcal/mol.

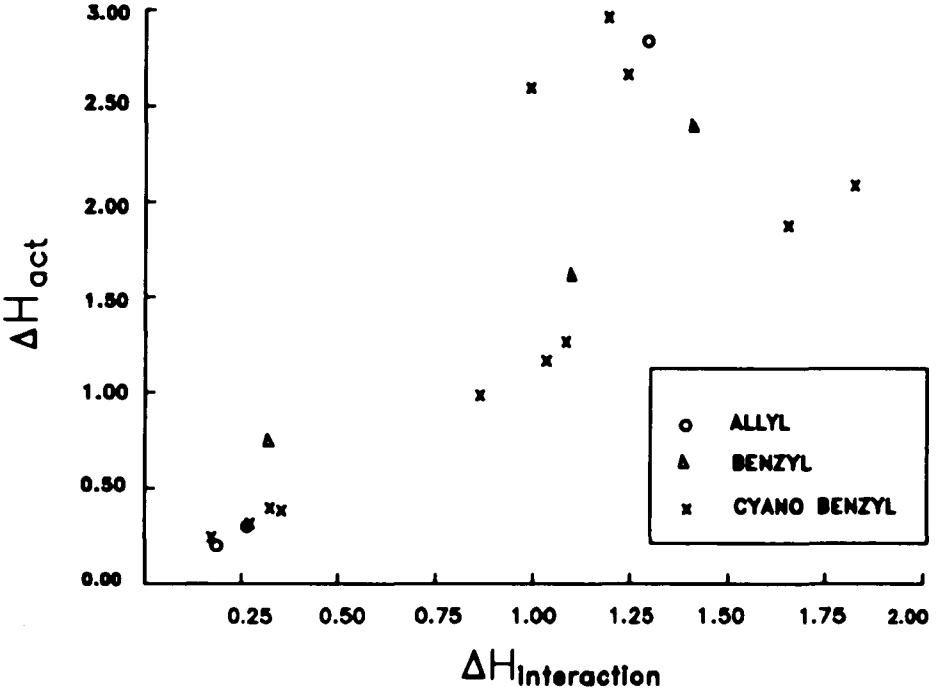

Figure 3.5 Activation Energy versus Interaction Energy for the Couplings of Allyl, Benzyl and Cyanobenzyl with Methyl Radicals in Kcal/mol.

Table 3.16 Energy Partition for the Couplings of Benzyl and Cyanobenzyl Radicals in Kcal/mol.

reaction	product	ΔH_{act}	$\Delta H_{dist.}$	$\Delta H_{int.}$
VII	10a	0.00	0.00	0.00
VII	10b	17.42	12.40	5.02
VII	10c	0.0	0.0	0.0
VIII	11a	3.72	3.89	-0.17
VIII	11b	14.88	13.88	1.00
IX	12a	3.11	3.46	-0.35
IX	12b	13.94	12.45	1.49
X	13a	16.68	16.24	0.44
X	13b	23.90	21.51	2.39
X	13c	27.26	22.63	4.63
XI	14a	18.33	16.83	1.50
XI	14b	26.70	24.45	2.25
XII	15a	17.67	16.94	0.73
XII	15b	18.73	17.25	1.48
XII	15c	28.54	25.93	2.61
XII	15d	29.58	28.24	1.34

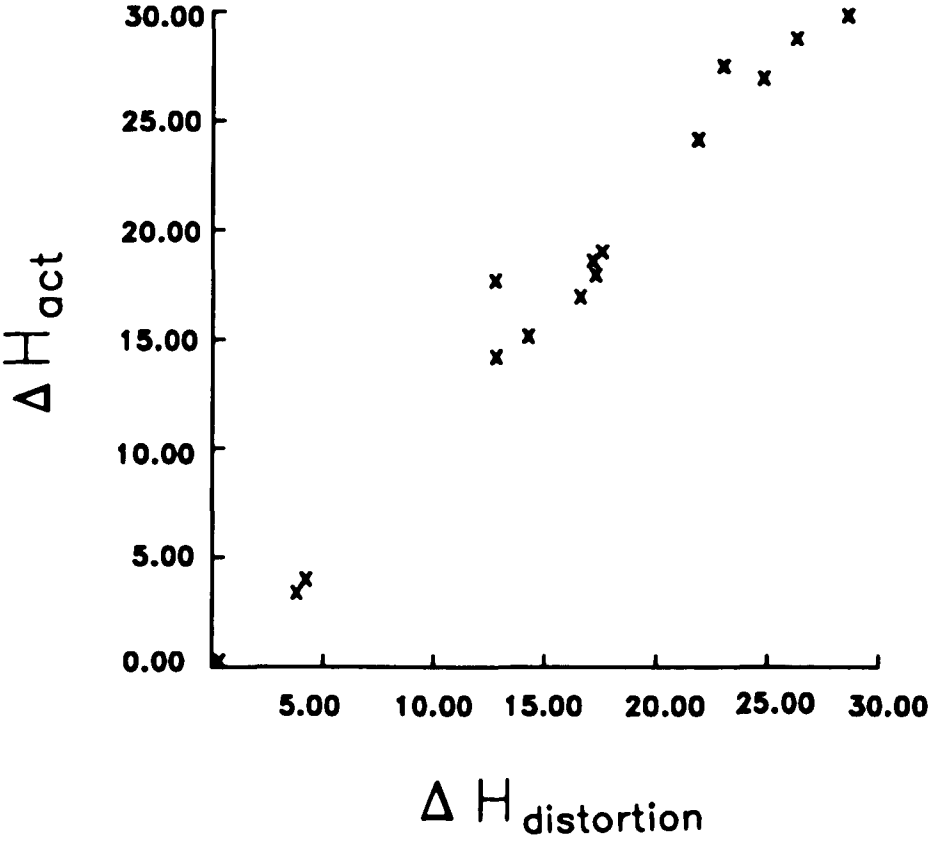

Figure 3.6 Activation Energy versus Distortion Energy for the Couplings of Benzyl and Cyanobenzyl Radicals in Kcal/mol.

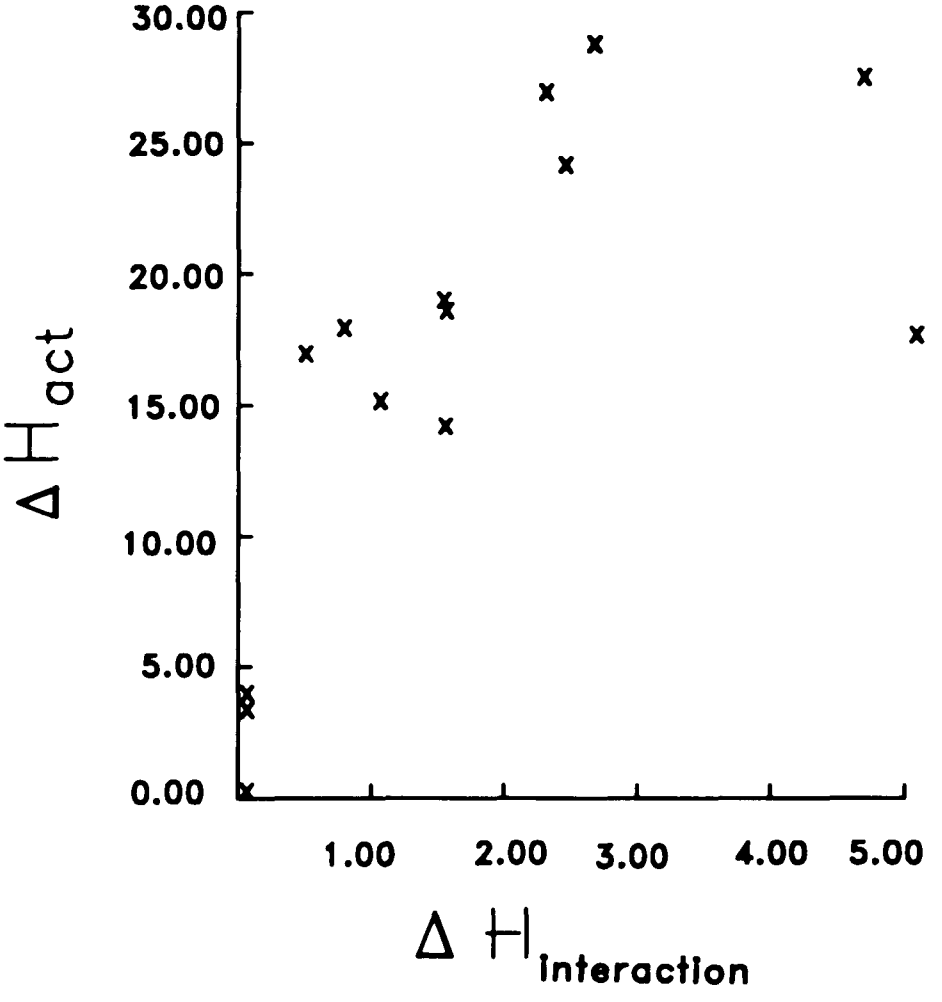

Figure 3.7 Activation Energy versus Interaction Energy for the Couplings of Benzyl and Cyanobenzyl Radicals in Kcal/mol.

Table 3.17 Energy Partition for the Couplings of Trisubstituted Methyl Radicals in Kcal/mol.

reaction	product	ΔH_{act}	$\Delta H_{dist.}$	$\Delta H_{int.}$
XIII	16	4.94	1.53	3.41
XIV	17	3.72	3.00	0.72
XIV	18	3.71	2.66	1.05
XV	19	2.00	1.72	0.28
XV	20	0.93	1.77	-0.84
XVI	21	4.11	2.67	1.44
XVI	22	3.82	2.38	1.44
XVII	23	3.38	3.72	-0.34
XVII	24	3.62	3.17	0.45
XVIII	25	9.95	9.22	0.73
XVIII	26	8.88	8.21	0.67
XIX	27	2.41	0.95	1.46
XIX	28	2.79	3.50	-0.71
XX	29	8.29	5.23	3.06
XX	30	9.95	8.07	1.88

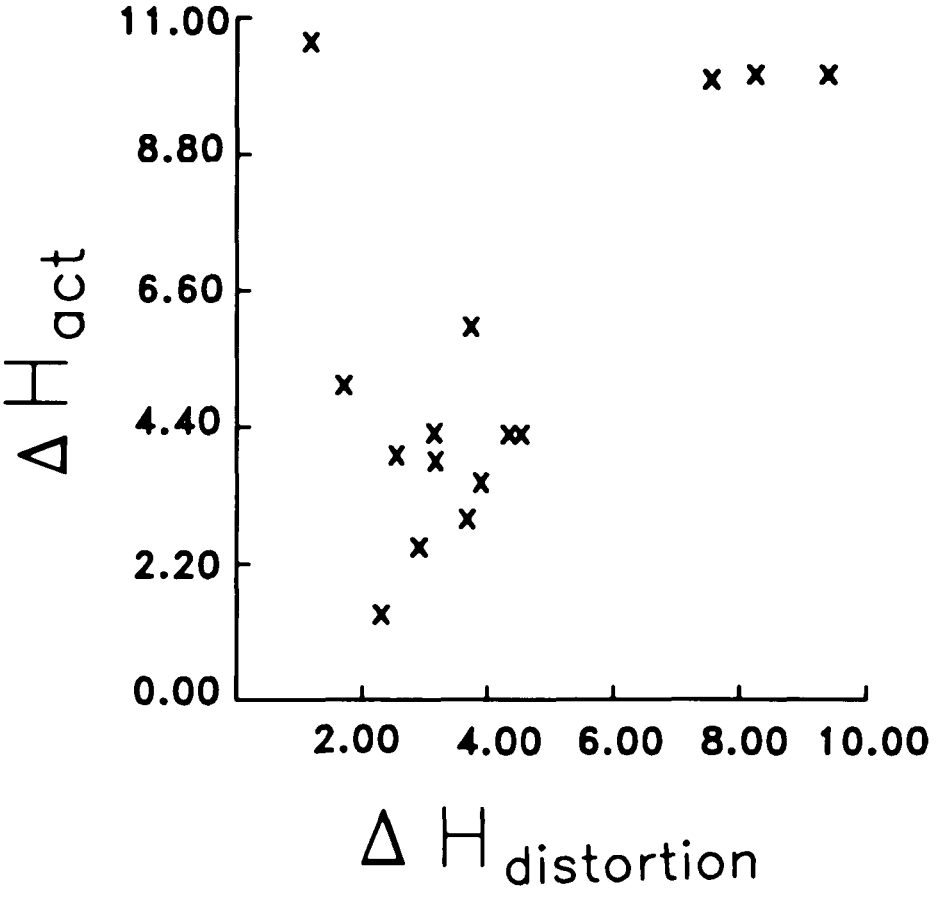

Figure 3.8 Activation Energy versus Distortion Energy for the Couplings of Trisubstituted Methyl Radicals in Kcal/mol.

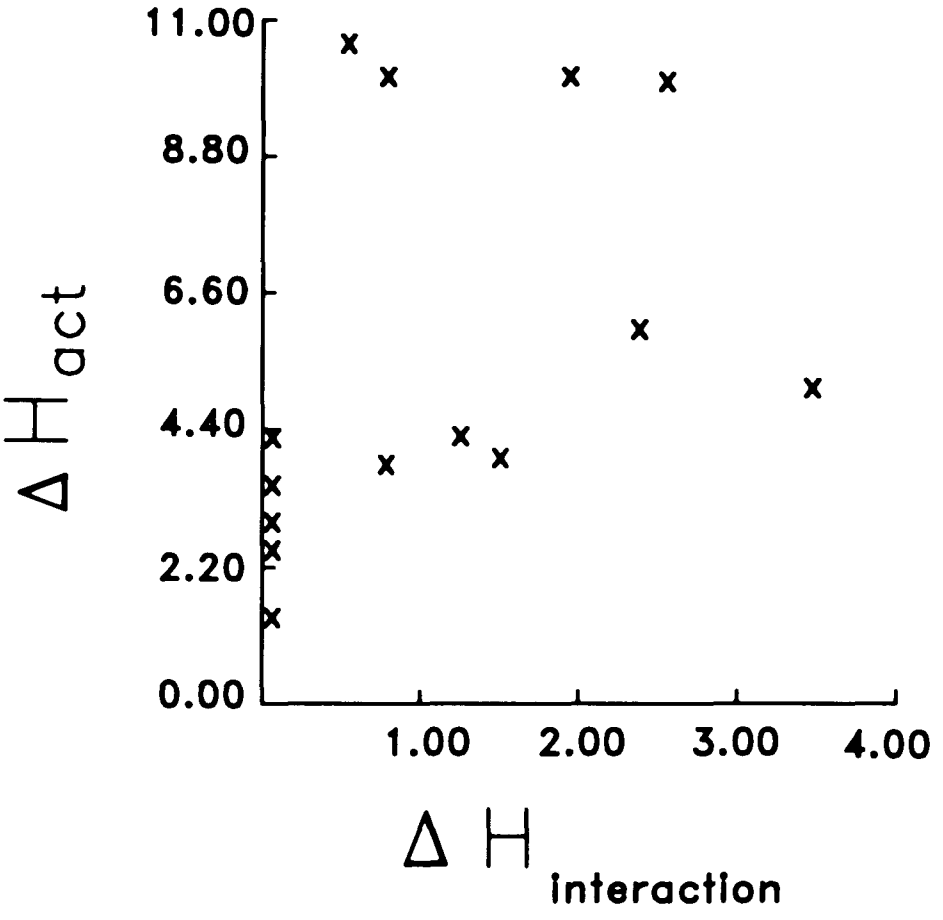

Figure 3.9 Activation Energy versus Interaction Energy for the Couplings of Trisubstituted Methyl Radicals in Kcal/mol.

CHAPTER 4

4. INTRAMOLECULAR H-ATOM TRANSFER REACTIONS

4.1 Introduction

An important recent development in synthetic organic chemistry is the use of free radical cyclizations for the synthesis of various natural products. In particular, the cyclization of the 1-hexenyl radical[1] has become a useful synthetic reaction[2].

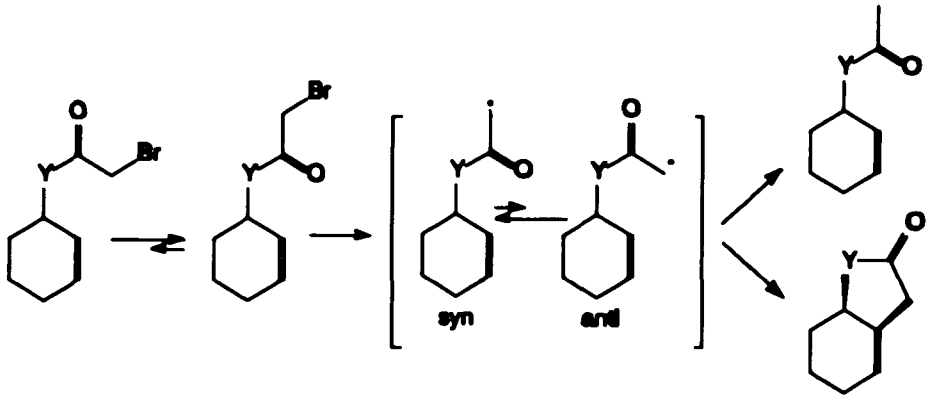

Figure 4.1

The Stork group has developed a more direct route to syntheses of allylic haloacetamides in the control of regio- and stereochemistry[3] (Figure 4.1). They found that the corresponding bromoacetamides (Y=NR in Figure 4.1) can

give good yields of addition products, if they have a large enough groups (R). An efficient radical cyclization route to cis-fused pyrroldone and piperidones is interesting because of the widespread occurrence of related systems in natural products.[4] For instance, treatment of bromoacetamide gave protected lactam (77%), with a trace of reduction product (2%). As a further sample of the generality of the method, they show that it is also useful for the construction of six-membered lactams[3] (see Figure 4.2).

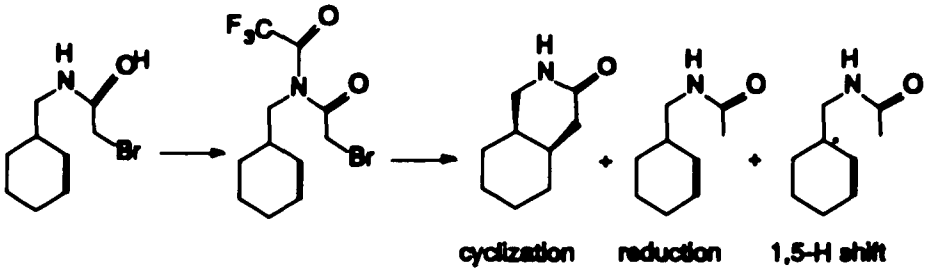

Figure 4.2

These applications occur with complete or high regio- and stereo-specificities.[5] However, cyclizations of this type[6] often have to compete with intramolecular hydrogen transfer or simple reduction pathways when the reactant contains appropriately situated hydrogen.[3,7] Clearly, the synthetic chemist needs to have a reasonable measure of when to expect a hydrogen atom transfer to

compete with a cyclization.

In view of the interest in this problem we have performed a molecular orbital study of the effects of C-H-C angle and ring size on intramolecular H-transfer. We have chosen to study the effect of C-H-C angle by calculating the transition states for H-transfer between two methyl groups as a function of C-H-C angle. The effects of ring size on the transition states for intramolecular H-transfer was studied for transfer of a hydrogen atom from primary, secondary and tertiary carbons to a primary radical center in cases involving three to eight carbons in the cyclic part of the transition states (Figure 4.3). There have been

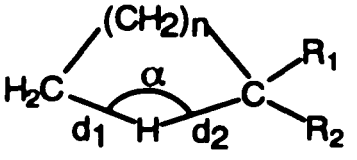

	R_1	R_2	n
a	H	H	1 - 6
b	H	$CH_3(CH_2)_{6-n}$	1 - 6
c	CH_3	$CH_3(CH_2)_{6-n}$	1 - 6

Figure 4.3 General Structures of the Transition States for the Cyclic Intramolecular Primary (type a), Secondary (type b), and Tertiary (type c) H-transfer Reactions.

no reports of applications of the molecular orbital approach to H-atom transfer reactions, other than ab initio study of intermolecular abstraction of a terminal hydrogen by n-butoxyl radical by Houk,[8] which is similar to the 1-5 shifts studied here except that abstraction is by oxygen.

4.2 Method

In this chapter, we directly calculated the transition states for the intramolecular hydrogen transfer by the AM1[9] half electron[10] method. This method has been previously shown to provide accurate results for H-transfer netween carbons.[11] Several conformations of the large ring were individually optimized with respect to all internal degrees of freedom that includes the effect of exchanging the alkyl groups (R_1 and R_2 in Figure 4.3). In each case considered, all the transition states were optimized in all of their internal coordinates. The transition states were fully characterized by calculating the force constants, only one of which was negative in each case studied. For determining the ring size effect, we modeled the transition states for transfer of a hydrogen between primary centers from the terminal carbon of the n-propyl, propyl, butyl, pentyl, hexyl, heptyl and octyl radicals to C_1. The transfers of H-atoms from secondary to a primary centers were modeled using the various transition states derived

from transfers of H's from carbons C_{3-8} to C_1 in the n-nonyl radical. The analogous transfers of H's from tertiary positions were modeled using transition states derived from the methylnonyl radicals, where the methyl group is attached to the carbon from which the H is being transferred.

The activation energies upon C-H-C angle for hydrogen transfer between two methyl groups were calculated in an analogous manner except that the C-H-C angle was fixed at each 5 degree interval from 100 to 180 degree while all other internal coordinates were varied. Since these are not true saddle points on the potential surface, force constants were not calculated for these structures.

4.3 Results and Discussion

The results of calculations are summarized in Table 4.1 - 4.4. In all three cases, intramolecular transfer from either C_5 or C_6 to C_1 have the lowest ΔH_{act}'s and are roughly equivalent. The 1-3 H-transfer is calculated to be particularly disfavored. The relative destabilizations for the 1-4, 1-7, and 1-8 H-transfers fall in the range of 2-5 kcal/mol, enough to kinetically disfavor their occurrences when 1-5 or 1-6 H-transfer is possible. Entropic factors should disfavor larger cyclic transition states as more rotations will be frozen. This effect should cause the 1-5

shift to be most favored at normal reaction temperatures. The amount of distortion from the 180 degree ideal transition state decreases slightly upon changing from transfer of primary to secondary to tertiary hydrogens. The C-H distances become more unsymmetrical as the transition state becomes earlier, as expected.

The data obtained from the H-transfer between methyls as a function of C-H-C angle is presented in Table 4.4 and in Figure 4.4. The effect of distorting the angle up to 35 degrees from linearity has less than a 1 kcal/mol effect upon ΔH_{act}. Examination of Tables 4.1-4.3 show that the C-H-C angle is never less than 145 degrees for all cases with 5 or more ring carbons in the transition state.

For the 1-3 H-transfers the C-H-C angles vary from 98.5 to 99.4 degrees, corresponding to an increased activation of about 19 kcal/mol based upon Table 4.4. The calculated ΔH_{act}'s are 21.6, 21.5 and 22.0 kcal/mol above that for 1-5 H-transfer for the cases of primary, secondary and tertiary H's, respectively. Thus, most of the additional activation can be attributed to strain in this angle. For the 1-4 H-transfers the C-H-C angles vary from 125.2 to 126.3 degrees. From the information in Table 4.4, we expect an increase in activation of about 5 kcal/mol for a transition state constrained to a C-H-C angle of 125 degrees. The calculated ΔH_{act}'s are 6.6, 6.4, and 6.3 kcal/mol above that for 1-5 H-transfers from primary

secondary and tertiary carbons, respectively. For the latter, the C-H-C angles vary from 144.5 to 147.3 degrees, corresponding to an expected destabilization of about 1 kcal/mol. Roughly two thirds of the additional barrier for 1-4 H-transfer is due to the C-H-C strain. The rest is apparently due to other conformational factors.

Table 4.1 AM1 Activation Enthalpies and Geometric Parameters for the Transition States of n-Alkyl Radical Primary Hydrogen Transfer Reactions*.

H-shift	ΔH_{act} (kcal/mol)	d_1 (Å)	d_2 (Å)	α (degree)	charge
1-3	42.5	1.41	1.41	98.5	0.157
1-4	27.5	1.35	1.35	125.2	0.153
1-5	20.9	1.32	1.32	144.5	0.168
1-6	21.0	1.31	1.31	158.0	0.165
1-7	23.0	1.30	1.31	163.6	0.163
1-8	24.9	1.31	1.31	178.1	0.163

*structures of type a in Figure 4.3.

Table 4.2 AM1 Activation Enthalpies and Geometric Parameters for the Transition States of Internal Secondary H-transfers in n-Nonyl Radicals*.

H-Shift	ΔH_{act} (kcal/mol)	d_1 (Å)	d_2 (Å)	α degree	charge
1-3	41.1	1.42	1.40	98.9	0.158
1-4	26.0	1.37	1.34	125.6	0.156
1-5	19.6	1.34	1.31	145.8	0.171
1-6	19.5	1.33	1.29	162.3	0.166
1-7	21.9	1.33	1.30	162.3	0.166
1-8	23.3	1.34	1.30	174.8	0.166

*structures of type b in Figure 4.3.

Table 4.3 AM1 Activation Enthalpies and Geometric Parameters for the Transition States of Internal Tertiary H-Transfers in Methyl substituted 1-Nonyl Radicals*.

H-shift	ΔH_{act} (kcal/mol)	d_1 (Å)	d_2 (Å)	α degree	charge
1-3	39.6	1.44	1.40	99.4	0.156
1-4	23.9	1.39	1.33	126.3	0.158
1-5	17.6	1.37	1.30	147.3	0.174
1-6	18.6	1.36	1.28	168.2	0.167
1-7	21.0	1.36	1.29	172.9	0.167
1-8	21.7	1.36	1.29	180.0	0.168

*structures of type c in Figure 4.3.

Table 4.4 AM1 Activation Enthalpies and Geometric Parameters for H-transfer between Methyl Radicals.

α (degree)	ΔH_{act} (kcal/mol)	d_1 (Å)	Charge
180.0	15.5	1.29	0.154
175.0	15.5	1.29	0.154
170.0	15.6	1.29	0.155
165.0	15.7	1.29	0.156
160.0	15.8	1.29	0.157
155.0	16.0	1.30	0.159
150.0	16.2	1.30	0.161
145.0	16.6	1.30	0.164
140.0	17.0	1.31	0.167
135.0	17.6	1.32	0.170
130.0	18.5	1.32	0.174
125.0	19.6	1.34	0.178
120.0	21.1	1.35	0.183
115.0	23.0	1.36	0.189
110.0	25.6	1.38	0.195
105.0	28.9	1.40	0.203
100.0	33.1	1.42	0.213

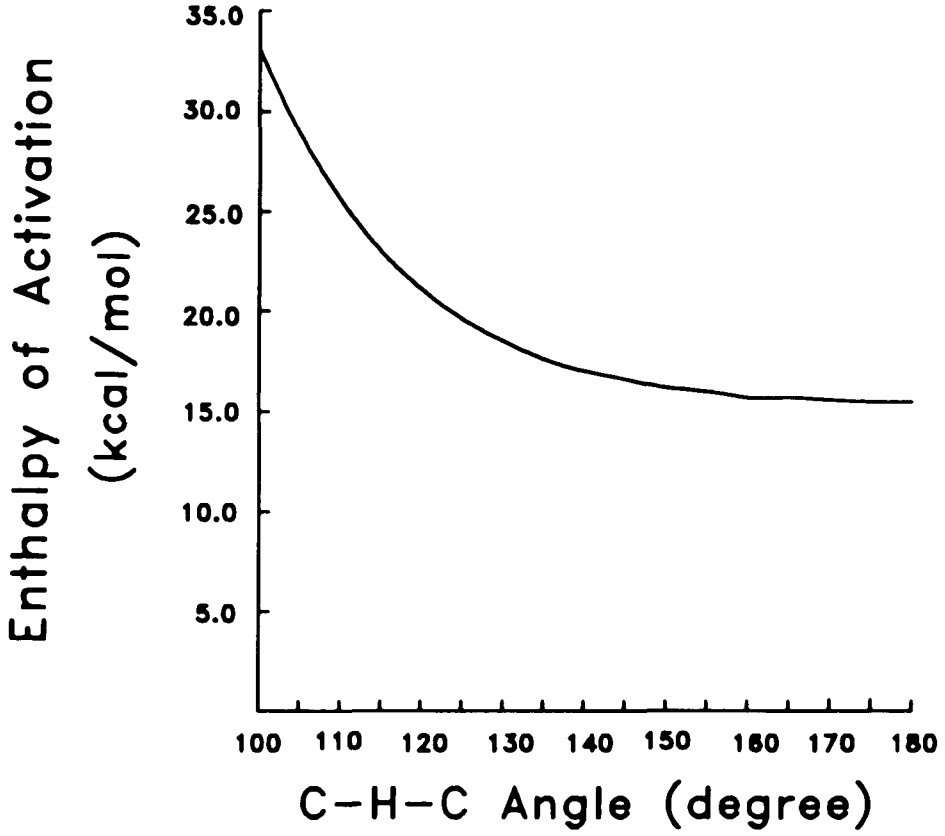

Figure 4.4 Variation of Enthalpy of Activation with C-H-C Angle in the Transition Atate for H-transfer from Methane to Methyl Radical.

The differences in ΔH_{act}'s for the 1-6 and 1-5 H-transfers are 0.1, -0.1 and 1.0 kcal/mol for transfer from primary, secondary and tertiary carbons. The C-H-C angle for 1-6 H-transfer varies from 158.0 to 168.2, corresponding to no more than 0.3 kcal/mol additional

activation due to C-H-C angle constraint. The results suggest that the 1-5 H-transfer has less ring strain than the 1-6 H-transfer (other than due to C-H-C angle). Furthermore, the difference increases from 0.2 to 1.4 kcal/mol as the transition state becomes increasingly early (changing from transfer of a primary to a tertiary hydrogen).

The 1-7 and 1-8 H-transfers are essentially without strain due to the C-H-C angle. Their differential ΔH_{act}'s are entirely due to conformational strain in the rings.

The data in Tables 4.1 - 4.3 indicate that the C-H partial bond length in the transition state and the charge on the migrating hydrogen both increase as the C-H-C angle increasingly deviates from 180 degrees. These phenomena are due to the changes in the orbitals 1, 7 and 8 (Figure 4.5). Orbital 1 involves interaction of the carbon 2S orbitals with the hydrogen orbital. This orbital becomes progressively more bonding (by 0.381 ev) as the angle changes from 180 to 100 degrees. The enhanced bonding is due to the increase in direct interaction between the carbon 2S orbitals (the interaction between the hydrogen orbital and the carbon orbitals decreases). Orbital 7 is primarily comprised of two carbon 2P orbitals and the hydrogen orbital. It becomes less bonding (by 0.601 ev) as the angle changes from 180 to 100 degrees. This effect is likely due to a decrease in sigma-overlap that is not

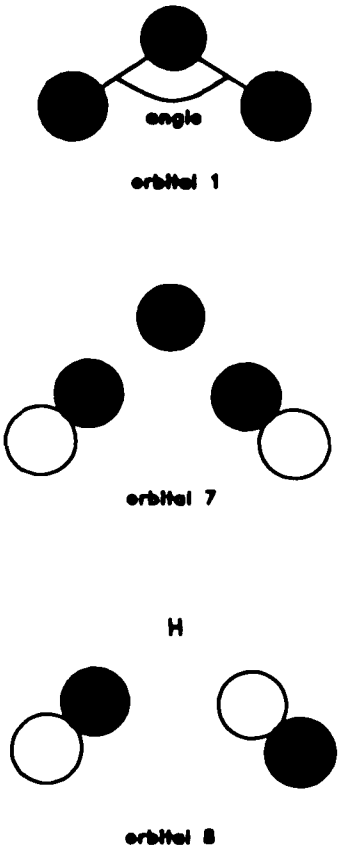

Figure 4.5 Orbitals 1,7 (highest doubly occupied), and 8 (singly occupied) for the Transition State for H-Transfer from Methane to Methyl Radical.

compensated for by an increase in pi-overlap between the carbon 2P orbitals. Orbital 8 (the SOMO) is comprised of the antibonding combination of carbon 2P orbitals with a node passing through the migrating hydrogen. It becomes less bonding by 0.727 ev as the angle changes from 180 to 100 degrees. Orbital 7 has the largest effect as it

contains two electrons compared to the one in orbital 8.

The enthalpies of activation for the reactions studied are not known quantitatively except the transfer of a H-atom between methyl radicals, whose ΔH_{act} (14.9 kcal/mol)[12] is in good agreement with the AM1 results previously reported with other similar results.[10b] Tunneling is generally considered to be part of the preexponential factor in the Arrhenius equation or incorporated into the transmission coefficient in transitin-state theory.[13] As such, it should have no effect upon the experimental enthalpies of activation that are (necessarily) measured over a range of temperatures.

Conclusion

We conclude from these calculations that H-atom transfer can easily occur with C-H-C angles moderately distorted from linearity, such as occurs in 1-5, 1-6, 1-7, and 1-8 transfers. For these cases, the differential ΔH_{act}'s are primarily due to other differences in the conformational requirements of the various cyclic transition states. For the cases of 1-3, and 1-4 H-transfers the necessary distortions of the C-H-C angle are sufficient to provide the major impediment to the reaction.

CHAPTER 5

5. POLARIZED π-FRONTIER MOLECULAR ORBITALS (PPFMO) - A METHOD FOR PREDICTING DIASTEREOFACIAL SELECTIVITIES

5.1 Introduction

The question of how electronic effects influence diastereofacial selectivity in organic chemistry has been the subject of much recent debate. Several earlier proposals have been made by Felkin,[1] Anh,[2] and Cieplak.[3] Felkin and Anh suggested that interaction between the bonding orbital being formed and the anti-bonding orbitals of adjacent bonds might be the controlling factor. Cieplak places more importance in the interaction between the anti-bonding orbital of the incipient bond and the bonding orbitals of the adjacent bonds. Much of the discussion of these models has centered on the selectivity of the reduction of cyclohexanone. These suggestions have been recently reviewed by le Noble, who also adds some interesting analyses.[4] These proposals have been criticized by Frenking,[5] Paddon-Row,[6] and Houk,[7,8] who have performed molecular orbital calculations on the reaction paths for carbonyl addition and other related reactions.

We have been interested in understanding similar selectivities in the reactions of free radicals and cycloadditions. While there has been much debate on the electronic causes of diastereofacial selectivity of the Diels-Alder reaction in the literature, most of the discussion involving free radicals is based upon steric arguments.[9]

Frontier molecular orbital theory (FMO)[10,11] has often been used with some success in predicting reactivity and regioselectivity of various reactions. Although Dannenberg and Franck[12,13] have suggested that this methodology be used with some caution as it considers only the reagents (not the transition state), the simplicity of its application argues for its use in appropriate situations. Dannenberg and Franck also have suggested that FMO theory might be best applied a) when the reaction is likely to have an early transition state, b) when the perturbational effect being considered is large, and c) when there is conformational correlation between the reagents and products.[12,13]

In this chapter, we shall present an extension of FMO theory, a new method of predicting π-diastereofacial selectivity. The theory is illustrated by application to acyclic π-systems containing from one to four π-centers. We critically evaluate the treatment of carbonyl reductions by this method in comparison with other theoretical and

experimental results in the following chapter.

5.2 Development of the Polarized π-Frontier Molecular Orbital Method

The atomic p-orbitals used in simple molecular orbital treatments are rigorously antisymmetric. Thus, one cannot use the coefficients of these orbitals to predict diastereofacial selectivity like that employed in FMO theory to predict regioselectivity. In this chapter we describe a simple construct that allows us to desymmetrize the p-orbitals for applying a simple FMO interpretation. We call this new application polarized-π frontier molecular orbital (PPFMO) theory.

The basic construct is the superposition of two new basis functions, one upon each lobe of an atomic p-function (Figure 5.1). The p-orbital would then be constructed from a linear combination of these three functions. The original antisymmetry of the p-function will be tempered by the two additional functions, which can differ in magnitude. The difference in magnitude between these functions will indicate the extent to which the π-orbital is polarized at each particular atomic site. This polarization, in turn, can be used to predict the diastereofacial selectivity according to approximations normally associated with FMO theory. The polarization, p, is given by Equation 5.1,

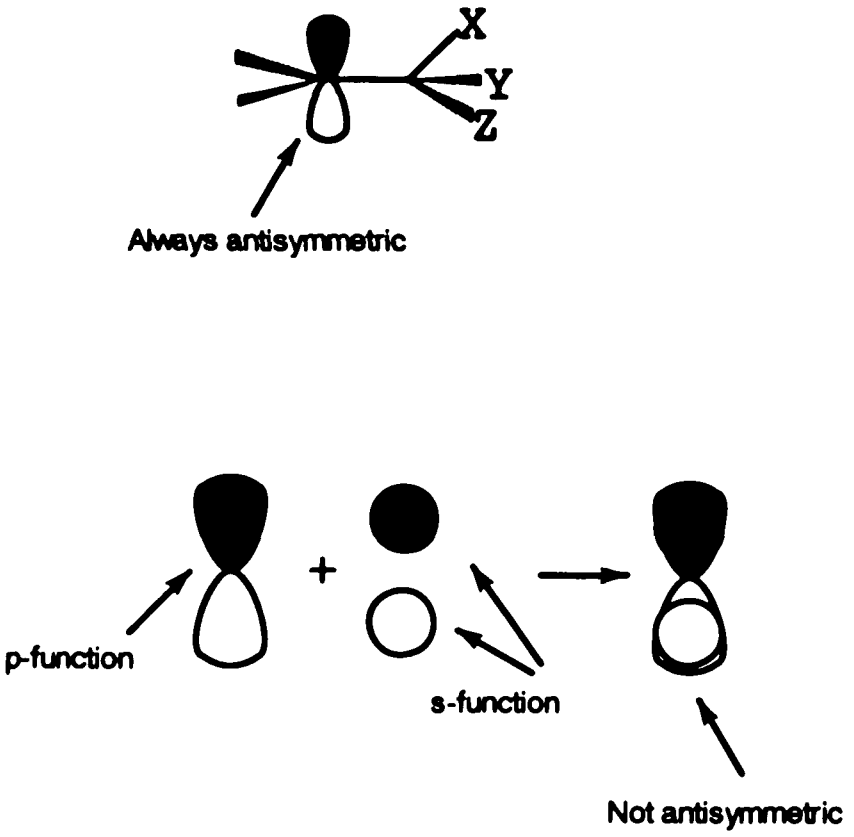

Figure 5.1 Schematic Representation of the Combination of P-orbital with Two S-functions.

where c_+ and c_- are the coefficients on the s-type basis functions χ_+ and χ_-, respectively. The +/- notations correspond to the sign of the lobe of the p-orbital on which the new basis function is superimposed. A positive value of p signifies polarization in the direction of the positive lobe of the p-orbital.

$$p = c_+ \chi_+ + c_- \chi_- \qquad (5.1)$$

Two initial observations will be extremely important: a) only small basis sets should be used, and b) the geometries must be optimized using another method. The use of only small basis sets is dictated first by the need to keep the method as simple as possible. However, one also must consider the fact that the larger the basis set, the less influence the added gaussians will have. At the extreme of the Hartree-Fock limit, the addition of the two new gaussians would have no effect whatever. The need to use another method for optimization comes from the destruction of the spherical symmetry of the atoms whose basis sets have been augmented by the added gaussians. Optimization with such a basis set would not give reasonable geometries.

For the reasons indicated above, we have chosen to use the simple STO-3G basis set for our studies. The p-orbitals whose polarizations we are trying to determine are augmented by two s-type gaussians. The exponents of these gaussians and their distances from the nuclei have been determined by analysis of the effects of these parameters upon the results in the manner indicated below. A model compound (allyl alcohol) was first optimized using the AM1[14] semiempirical method. Single point STO-3G calculations were performed using the Gaussian88 and Gaussian90 computer programs.[15] The s-functions were positioned along the axis of the π p-orbitals at varying

distances from the carbon nuclei. The exponents of the gaussians were also varied. A plot of the total energy as functions of both the distance from the carbon nucleus and the exponent of the gaussian is displayed in Figure 5.2. For this figure, allyl alcohol in the conformation having the C-OH bond co-planar with the π-system was used. Gaussian s-functions were superimposed over each of the two p-orbitals involved in the double bond. The total energy generally decreases with the distance from the nucleus (see Figure 5.2). This result is likely due to the difficulty that small gaussian basis sets have with adequately describing the cusp in the electron density at the nucleus. At virtually all distances from the nucleus, the minimum energy occurred with an orbital exponent of slightly greater than 0.1. Rather than simply using the energetically optimal distance and exponents, we tempered the relationships depicted in Figure 5.2 by our desire to maximize the magnitude of desymmetrization. We chose a distance from the nucleus of 1.3 Å, as the figure shows the energy to be a shallow function of this distance until about 1.3 Å above which it increases more rapidly. Similarly, we chose a value for the exponent of 0.1 (slightly less than the energy optimum) to keep the effect localized.

In the cases considered in this chapter, the π-systems were kept rigorously planar. In general, this may

not be the case. This problem is addressed in the following chapter on carbonyl reductions.[16]

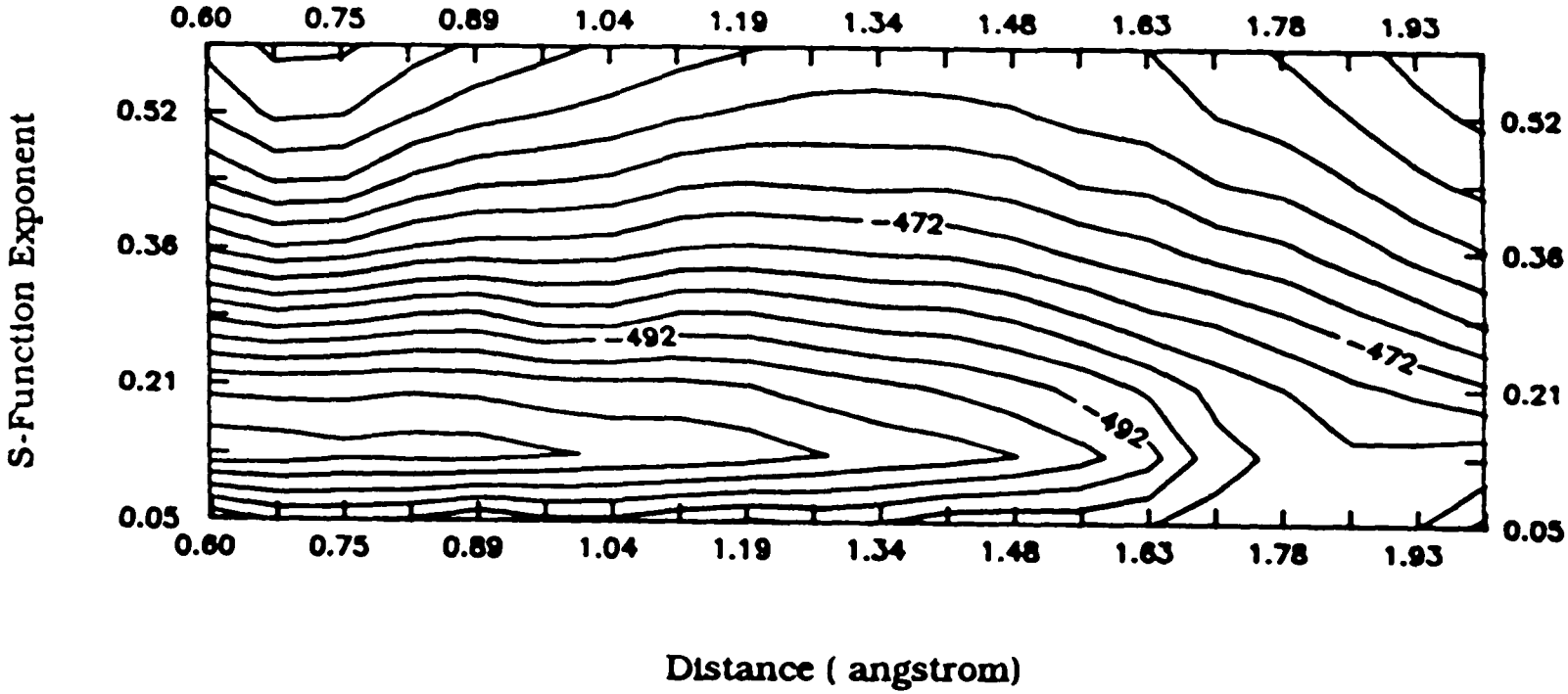

Figure 5.2 Contour Plot of the Total Energy (in hartrees) as a Function of the Distance from the Carbons and the Orbital Exponents of the S-functions for Allyl Alcohol.

A complete integration into the mathematical (second order perturbational) treatment that is used in FMO theory (Equation 5.2) is presented in Equation 5.3, where ΔE_{face} is the difference in the perturbational energies for the two faces of the π-system. The summation over i is for all of the two-center interactions between the HOMO and LUMO (e.g. one for carbonyl reductions or reactions of free radicals, but two for cycloadditions such as the Diels-Alder reaction). Equation 5.3 is illustrated for a polarized LUMO interacting with a nonpolarized HOMO. For a polarized HOMO interacting with a nonpolarized LUMO, p^{HOMO} and c^{LUMO} should be used in the summation.

$$\Delta E_{interaction} \propto \frac{\sum_i c_i^{HOMO} c_i^{LUMO}}{E^{LUMO} - E^{HOMO}} \qquad (5.2)$$

$$\Delta E_{face} \propto \frac{\sum_i p_i^{LUMO} c_i^{HOMO}}{E^{LUMO} - E^{HOMO}} \qquad (5.3)$$

For calculations on free radicals, UHF/STO-3G calculations have been performed. In these cases the singly occupied molecular orbital (SOMO), which is the HOMO of the α spin-orbitals, is used in place of HOMO. The LUMO is the lowest unoccupied ß spin orbital. FMO theory for free radical reactions can sometimes be more complicated than

for closed shells. Thus, a radical addition to an alkene would involve both the interactions between the radical SOMO and the alkene LUMO, and that of the radical LUMO with the alkene HOMO. The product of the addition would, itself, be a radical. Since the SOMO's of alkyl radicals (for example, ethyl radical) generally have a node between the α and ß carbons,[17] one might expect that the interaction of the SOMO of the original radical with the LUMO of the alkene leads to the SOMO of the new radical (see Figure 5.3a). For radical-radical couplings (Figure 5.3b) and disproportionation reactions, each radical contributes one electron. In these cases, the SOMO of one will interact with the LUMO of the other and vice versa. For atom-transfer (abstraction) reactions, one might expect the interaction of the radical SOMO with the highest energy filled orbital involving the C-H bond to be dominant (Figure 5.3c).

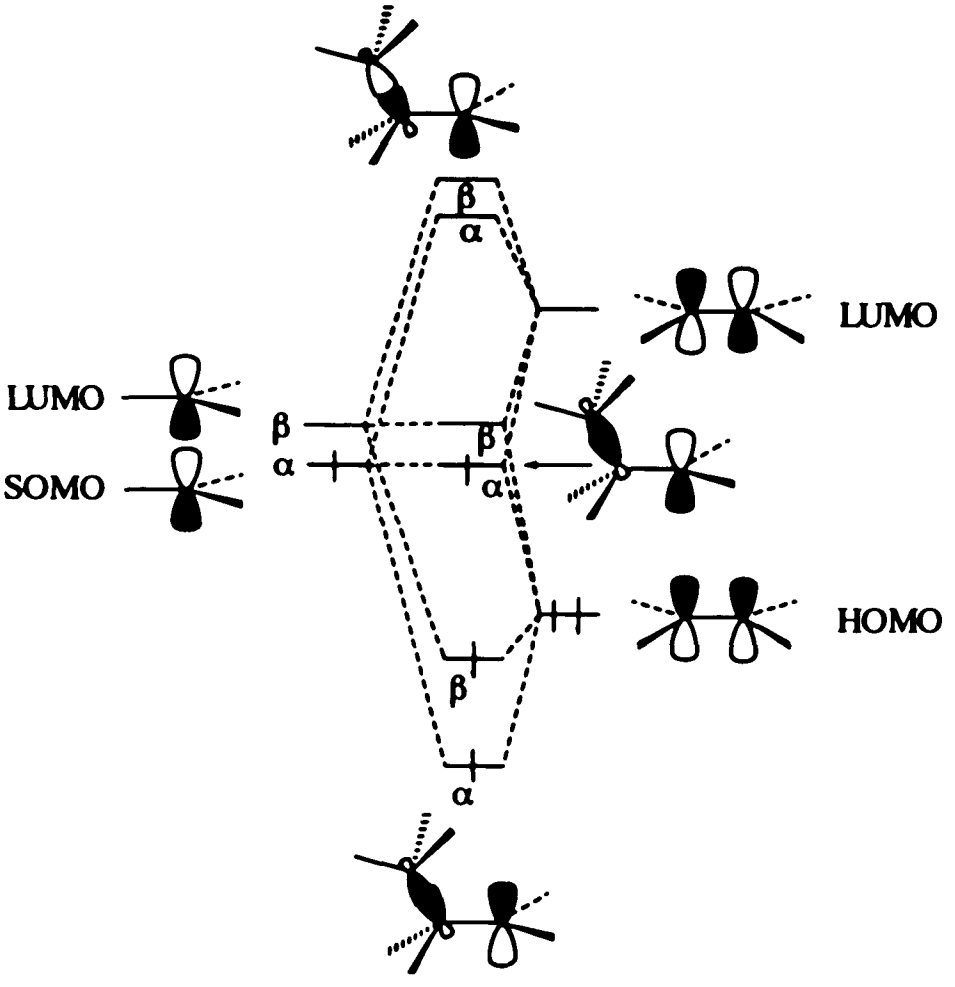

Figure 5.3a FMO Diagram of the Interactions for Radical Addition to an Alkene. (the center orbitals represent the product)

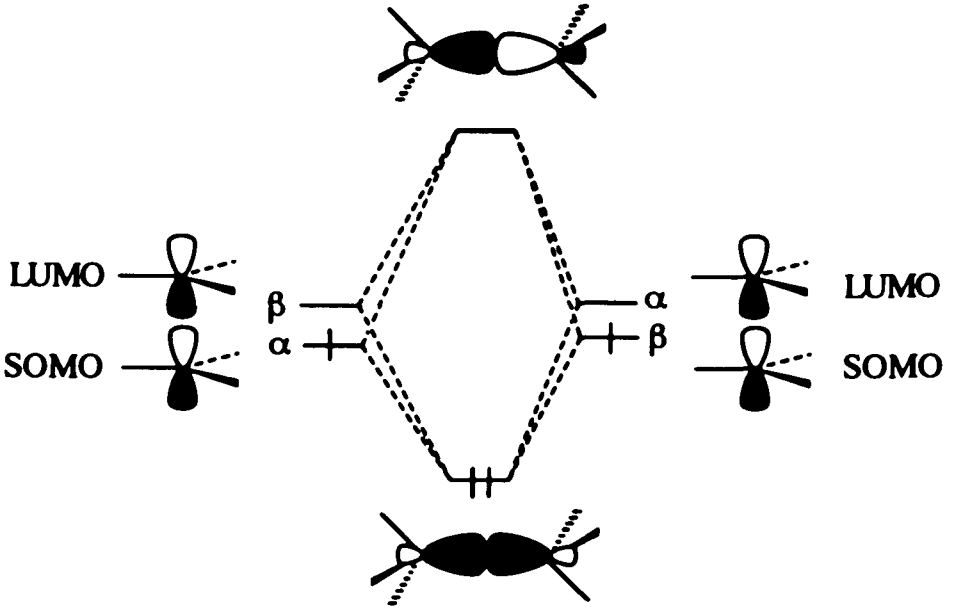

Figure 5.3b FMO Diagram of the Interactions for Radical-radical Combination. (the center orbitals represent the product)

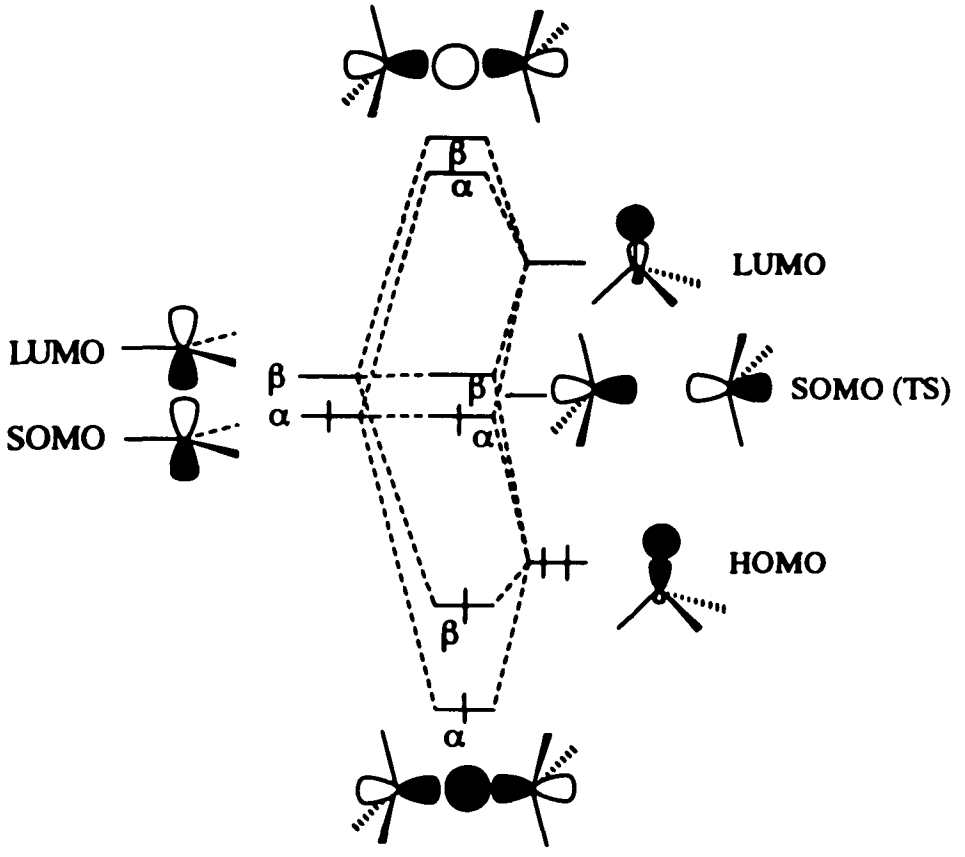

Figure 5.3c FMO Diagram of the Interactions for Atom Transfer. (the center orbitals represent the transition state)

5.3 Results

5.3.1 α-substituted Free Radicals

The results for substituted methyl radicals are collected in Table 5.1. Each of the calculations involves a methyl radical with a substituent that breaks the symmetry of the p-orbital's nodal plane. In the first three cases, the α carbon has two C-H bonds. The third bond, which is kept parallel with the axes of the π p-orbital, was varied. From examination of the table, one sees that although the polarization of both the SOMO and LUMO of the radical change with substituent, the changes are not what one would necessarily expect from simple arguments based upon the electron donating or withdrawing abilities of the substituents relative to hydrogen. Except for the SOMO of the methyl substituted case (where there is no polarization), all substituents lead to polarizations that predict attack at the face opposite to the substituent in both the SOMO and LUMO. A methyl substituent, generally thought to be electron-donating, has little effect upon the orbital energies of either the SOMO or LUMO (compared to H). However, the slight polarization of the SOMO disappears, while the more moderate polarization of the LUMO is significantly increased. Hydroxyl, the weaker of the two electron-withdrawing groups (as evidenced by the

Table 5.1 The PPFMO Results for α-substituted Methyl Radicals.

Compound	ΔH_f(AM1) (kcal/mol)	E^{SOMO} hartree	E^{LUMO} hartree	polarization, p		coefficient, p_z		coefficient, χ^a	
				p^{SOMO}	p^{LUMO}	C^{SOMO}	C^{LUMO}	C^{SOMO}	C^{LUMO}
	-26.11	-0.339	0.132	-37	-222	802	409	220	509
								-257	-731
	47.69	-0.352	0.120	-56	-100	806	418	181	586
								-237	-686
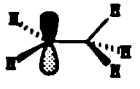	15.49	-0.313	0.146	-17	-44	798	396	225	641
								-242	-685
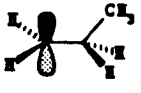	10.91	-0.312	0.147	0	-112	786	397	250	613
								-250	-725
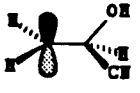	9.57	-0.365	0.112	-29	-202	792	420	197	498
								-226	-700

Table 5.1 Continued

Compound	ΔH_f(AM1) (kcal/mol)	E^{SOMO} hartree	E^{LUMO} hartree	polarization, p		coefficient, p_z		coefficient, χ^a	
				p^{SOMO}	p^{LUMO}	C^{SOMO}	C^{LUMO}	C^{SOMO}	C^{LUMO}
	8.37	-0.355	0.122	-20	-9	797	431	197	616
								-217	-625
	7.92	-0.354	0.120	-28	45	767	419	208	664
								-236	-619
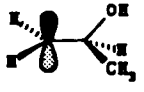	-30.25	-0.335	0.138	-42	-218	794	414	213	512
								-255	-730
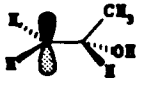	-31.80	-0.318	0.149	18	2	743	417	248	660
								-230	-658
	-31.89	-0.318	0.142	-50	40	725	404	205	676
								-255	-636

[a] The coefficient of χ are listed for χ_+ (upper value) and χ_- (lower value) for each entry.

lowering of the orbital energies) somewhat increases the polarization of the SOMO, while enormously increasing the polarization of the LUMO (from 0.044 to 0.222, compared to H). The cyano group, which is the most electron-withdrawing substituent, provides the greatest (yet, still moderate) increase in polarity of the SOMO, but the smallest increase in polarization of the LUMO (again, compared to H).

5.3.2 Two-center Systems (substituted alkenes)

As can be seen from Table 5.2, the effect upon the more proximal of the two π-centers is much greater the other. As in the case of the one π-center system, the general tendency of the polarization in both the HOMO and LUMO favors attack anti to the substituent. The only exception is the slight polarization towards syn attack predicted for the HOMO of the methyl substituted case. In the one π-centered case, methyl reduced the polarization of the SOMO to zero. Here, it reverses the polarization of the HOMO for the proximal center. The two electron-withdrawing groups both increase the polarization of the HOMO for the proximal center, but the order is reversed with hydroxyl having a larger effect than cyano. For the LUMO, only cyano increases the polarization of the proximal π-center, while both methyl and hydroxyl decrease it. The polarizations of the distal center are lower by almost an order of

Table 5.2 The PPFMO Results for Substituted Alkenes.

Compound	ΔH_f (AM1) (kcal/mol)	ε^{HOMO} hartree	ε^{LUMO} hartree	polarization, p				coefficient, P_π				coefficient, χ^α			
				HOMO		LUMO		HOMO		LUMO		HOMO		LUMO	
				P_β	P_α	P_β	P_α	C_β	C_α	C_β	C_α	C_β	C_α	C_β	C_α
	-38.01	-.348	.155	32	-98	-9	-104	477	451	384	447	162	4	795	703
												-130	-102	-804	-807
	38.56	-.365	.151	7	-42	-21	-132	520	507	376	480	151	60	789	667
												-144	-102	-810	-799
	6.84	-.339	.173	6	-12	7	-113	533	487	353	484	170	73	822	706
												-164	-85	-815	-819
	0.82	-.339	.171	-4	11	26	-90	529	481	357	474	156	100	836	731
												-160	-89	-810	-821
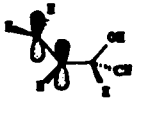	-1.84	-.371	.139	50	-76	12	-179	494	476	394	458	174	19	783	629
												-124	-95	-771	-808

Table 5.2 Continued

Compound	ΔH_f (AM1) (Kcal/mol)	E^{HOMO} hartree	E^{LUMO} hartree	polarization, p				coefficient, P_x				coefficient, χ^a			
				HOMO		LUMO		HOMO		LUMO		HOMO		LUMO	
				p_β	p_α	p_β	p_α	C_β	C_α	C_β	C_α	C_β	C_α	C_β	C_α
	-2.77	-.370	.147	1	-23	14	17	515	506	386	493	143	68	795	712
												-142	-91	-781	-695
	-2.91	-.372	.143	6	-14	5	-170	501	486	385	465	140	88	794	656
												-134	-102	-789	-826
	-43.18	-.343	.164	34	-112	-1	-51	471	442	378	476	167	-18	808	715
												-133	-94	-809	-766
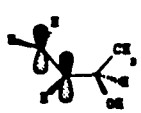	-43.62	-.345	.167	9	1	71	51	514	470	364	495	144	110	852	769
												-135	-109	-781	-718
	-43.81	-.342	.165	22	-24	13	-116	450	411	373	469	139	71	823	714
												-117	-95	-810	-830

[a] The coefficients of χ are listed for χ_+ (upper value) and χ_- (lower value) for each entry.

magnitude. For the HOMO, they are opposite to that of the proximal center in each case, but only that for hydroxyl is reasonably large. For the LUMO, the distal polarization is opposite to that at the proximal center for all cases except cyano. Two of the substituents (methyl and cyano) have reasonably large polarizations.

5.3.3 Three-center Systems (substituted allyl radicals)

Once again, the proximal carbon is polarized to suggest attack anti from the substituent in all cases except for the HOMO in the methyl substituted case (Table 5.3). The polarizations are generally smaller than in the previous cases. Both electron-withdrawing groups increase the polarization in both the SOMO and LUMO, while methyl reverse the polarization of the SOMO, but increases that of the LUMO. The effects upon the distal center are small without a clear trend.

Table 5.3 The PPFMO Results for Substituted Allyl Radicals.

Compound	ΔH_f (AM1) (kcal/mol)	ε^{SOMO} hartree	ε^{LUMO} hartree	polarization, p				coefficient, p_π				coefficient, χ^α			
				SOMO		LUMO		SOMO		LUMO		SOMO		LUMO	
				p_γ	p_α	p_γ	p_α	C_γ	C_α	C_γ	C_α	C_γ	C_α	C_γ	C_α
	-22.52	-.3056	.1213	-3	-32	4	-141	572	626	397	391	207	167	538	290
												-210	-199	-534	-431
	51.41	-.3181	.1116	-4	-38	-2	-69	573	634	401	400	202	149	533	332
												-206	-187	-535	-401
	19.18	-.2926	.1283	2	-21	12	-52	542	644	408	374	211	161	602	289
												-209	-182	-590	-341
	13.40	-.2920	.1273	0	12	6	-48	540	635	403	378	207	198	580	319
												-207	-186	-574	-367
	13.32	-.3180	.1107	-9	-131	3	-284	543	622	392	391	187	071	528	182
												-196	-202	-525	-466

Table 5.3 Continued

Compound	ΔH_f (AM1) (kcal/mol)	g^{SOMO} hartree	g^{LUMO} hartree	polarization, p				coefficient, p_π				coefficient, χ^α			
				SOMO		LUMO		SOMO		LUMO		SOMO		LUMO	
				p_γ	p_α	p_γ	p_α	c_γ	c_α	c_γ	c_α	c_γ	c_α	c_γ	c_α
	12.86	-.3146	.1104	5	57	14	186	516	610	398	399	191	172	540	432
												-186	-115	-526	-246
	12.45	-.3102	.1095	4	-22	10	-50	516	616	409	387	203	124	583	296
												-199	-146	-573	-346
	-27.81	-.3027	.1256	-2	-43	-2	-119	571	629	403	388	209	158	567	265
												-211	-201	-569	-384
	-28.26	-.2945	.1285	2	6	18	-27	541	620	402	389	206	196	574	333
												-204	-190	-556	-360
	-28.32	-.2961	.1275	3	-27	6	20	545	627	406	377	210	168	598	325
												-207	-195	-592	-305

[α] The coefficients of χ are listed for χ_+ (upper value) and χ_- (lower value) for each entry.

5.3.4 Four-center Systems (substituted butadienes)

These systems were considered in their s-cis conformations as these are significant for cycloadditions (Table 5.4). In these cases the effects are further attenuated, particularly for the HOMO. Nevertheless, for the proximal center the general trend is the same as that for the two-center systems. The effect on the LUMO is significant in all cases with the electron-withdrawing groups augmenting and the methyl group diminishing the polarization, in contrast with the two center cases.

Chiral substituents

When the substituent is made chiral by substituting the α carbon with one hydrogen and two different other substituents, the effect of the polarization upon acyclic systems will depend upon the polarization of each rotamer, the relative energies of the FMO's as well as those of the rotamers. As can be seen from Tables 5.1 - 5.4, the most polarized rotamer may not have the optimal FMO energy nor be the most stable. Thus, the complexity of the combined effects makes simple predictions of the face selectivities in these systems difficult.

Table 5.4 The PPFMO Results for Substituted Butadienes.

Compound	ΔH_f (AM1) (kcal/mol)	E^{HOMO} hartree	E^{LUMO} hartree	polarization, p				coefficient, p_x				coefficient, χ^a			
				HOMO		LUMO		HOMO		LUMO		HOMO		LUMO	
				p_δ	p_α	p_δ	p_α	C_δ	C_α	C_δ	C_α	C_δ	C_α	C_δ	C_α
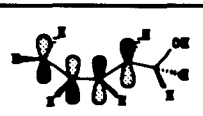	-21.43	-.302	.113	-3	-22	-8	-128	424	439	335	371	119	85	527	377
												-122	-107	-535	-505
	52.79	-.310	.098	-2	-25	-7	-76	434	440	341	390	122	74	507	411
												-124	-99	-514	-487
	20.83	-.291	.115	-2	-14	1	-50	430	428	333	387	127	70	544	415
												-129	-84	-543	-465
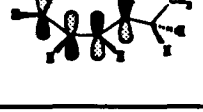	14.87	-.290	.114	1	8	-2	-33	428	424	333	383	130	96	537	439
												-129	-88	-539	-472
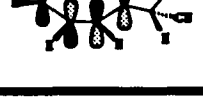	14.33	-.313	.096	0	-19	-3	-109	435	443	344	380	121	85	501	380
												-121	-104	-504	-489

Table 5.4 Continued

Compound	ΔH_f (AM1) (kcal/mol)	ε^{HOMO} hartree	ε^{LUMO} hartree	polarization, p				coefficient, p_x				coefficient, χ^{α}			
				HOMO		LUMO		HOMO		LUMO		HOMO		LUMO	
				p_δ	p_α	p_δ	p_α	c_δ	c_α	c_δ	c_α	c_δ	c_α	c_δ	c_α
	13.86	-.308	.100	-4	-24	-8	-49	431	449	343	384	121	78	510	414
												-125	-102	-518	-463
	13.73	-.310	.101	-3	-16	10	20	434	437	345	389	122	90	530	443
												-125	-106	-520	-423
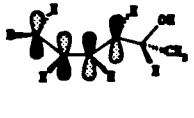	-26.73	-.295	.113	-2	-29	-10	-105	433	438	341	383	126	80	538	363
												-128	-109	-548	-468
	-27.01	-.290	.115	-2	4	-1	-11	424	431	337	379	127	102	542	437
												-129	-98	-543	-448
	-27.01	-.292	.115	-3	-17	3	34	429	423	338	386	125	82	550	444
												-128	-99	-547	-410

[α] The coefficients of χ are listed for χ_+ (upper value) and χ_- (lower value) for each entry.

5.4 Discussion

The results suggest that the perturbational effect upon the polarization of the π system may be very different from the effect upon the orbital energies. If this be the case, then some perturbational arguments made previously, based solely upon considerations involving orbital energies, may not be valid. For example, comparison of the results for substituted ethyl radicals shows that when a methyl substituent is exchanged for an electron withdrawing group, such as cyano, the LUMO is lowered in energy, as one would expect. Thus one would expect the incipient bonding orbital formed from this LUMO with another orbital to be stabilized when the cyano group is anti. However, the polarization of the LUMO is greater for the methyl substituted radical. If one compares the effects of cyano vs. hydroxyl, the orbital energy difference is smaller, and the polarization difference larger.

Perhaps the best means of evaluating the effects of substituents on face selectivities would be to combine the polarization effects with the energetic perturbation of the relevant FMO's. For the case of a reagent whose polarized LUMO is to react with a generalized non-polarized HOMO, the relative reactivities could be calculated from Equation 3, where c_i^{HOMO} and E^{HOMO} are both constants. This leads to Equation 4, where the constant, K, is the product of all

constants. In this equation, E^{HOMO} is also a constant. Since $E^{HOMO} \leq 0$ (as all bonding orbital must be more stable than a free electron, it can be replaced by another constant, -k, where $k \leq 0$ (Equation 5.5).

$$\Delta E_{face} = K \sum_{I} \frac{p_i}{E^{LUMO} - E^{HOMO}} \tag{5.4}$$

$$\Delta E_{face} = K \sum_{I} \frac{p_i}{E^{LUMO} + k} \tag{5.5}$$

$$\Delta E_{face} = K \sum_{I} \frac{p_i}{E^{LUMO}} \tag{5.6}$$

In many MO calculations, the LUMO is calculated to have a positive energy (although this need not always be true). The highest energy the HOMO of a nucleophile can have is 0. If we assume that $E^{HOMO}=-k=0$, then Equation 4 becomes Equation 5.6. The difference in the relative reactivities of competing reactions will decrease as the HOMO becomes more stable.

For cases where a polarized HOMO interacts with a generalized LUMO (as in electrophilic attack), a similar development yields Equations 5.7 and 5.8. Here, k represents the energy of the LUMO of the electrophile, which is arbitrarily set to zero in Equation 8. Analogous

$$\Delta E_{face} = K \frac{\sum_i p_i}{k - E^{SOMO}} \qquad (5.7)$$

$$\Delta E_{face} = -K \sum_i \frac{p_i}{E^{SOMO}} \qquad (5.8)$$

to the case for nucleophilic attack, the differences in relative reactivities decrease as the LUMO of the nucleophile increases in energy.

The largest polarizations calculated were for the one center π systems, the simple free radicals. For each of the individual substituents considered, the polarizations of the p-orbital were all in the anti direction for both SOMO and LUMO (except the SOMO of n-propyl radical, where p=0). In a recent review of the stereoselectivities of intermolecular free radical reactions, Giese has shown that addition reactions and atom transfer reactions generally occur anti to substituents on the ß carbon of the radical.[9] He attributed this observation to the differences in the steric requirements in the transition states for the reactions of interest. While the steric effect is certainly important (probably dominant in most if not all cases discussed by Giese), one should note that the electronic effects also favor attack in the same direction.

The diastereofacial selectivities of Diels-Alder reactions has been of interest for some time. We have previously indicated that these selectivities can be a

complicated mixture of steric and electronic factors that is difficult to understand in simple terms.[13] The present results do little to alter that assessment. The optimized transition states previously reported all have their shorter (i.e. stronger) bonds at the unsubstituted end of the diene. While the polarizations of the HOMO's are generally small for the dienes, they virtually vanish for the unsubstituted end.

Comparison of our results with the suggestions of Cieplak and Anh are informative. Replacing a hydrogen with a methyl group that is parallel to the axis of the π system has a negligible effect upon the energies of the HOMO's and LUMO's of all the π-systems studied (about 0.001 ev). On the other hand, the effect on the polarization varies significantly (from a change of 0.078 to .004) with the methyl substituted case more polarized in the cases with one π center, and less polarized in the other three cases for the adjacent p-orbital in the LUMO. As both the Anh and Cieplak models take only the orbital stabilization into account, they necessarily miss the polarization effect.

$$SE(\sigma_i, \sigma_r^*) \approx \frac{S^2\sigma_i, \sigma_r^*}{\Delta\epsilon(\sigma_i, \sigma_r^*)} \qquad (5.9)$$

The Cieplak model, originally proposed to explain the nucleophilic attack on cyclohexanone, assumes that the

principle stabilization can be approximated by Equation 5.9.[3] In this equation, ΔE is the stabilization energy, S, the overlap, σ_i, the doubly occupied orbital vicinal to the incipient bond, and σ_ϕ^*, the antibonding orbital of the incipient bond. He emphasizes that the incipient bond is intrinsically electron deficient, very stretched and very polarized. If one imagines the transition state to be very early (reactant-like), the σ_ϕ^* orbital will be the LUMO of the π-system. Thus, Cieplak's argument is one that focuses on lowering the LUMO under nucleophilic attack in a manner analogous to FMO theory.

Anh's model assumes that the antibonding orbital of the σ-bond, σ_i^*, antiperiplanar to the incipient bond will stabilize the latter's bonding orbital, σ_ϕ. As σ_ϕ can be thought as coming from the interaction of the LUMO of the π-system with the HOMO of the nucleophile, this analysis also resembles FMO theory. However, when the transition state is very early (as above) σ_ϕ will be the HOMO of the nucleophile, so that this interaction will initially be zero, but increase as the reaction proceeds. Thus, this effect should be more important for later transition states, while the Cieplak suggestion should be more important for early transition states.

Although the Cieplak and Anh models have been conceived for nucleophilic attacks (reductions of carbonyls), it is instructive to consider other

applications. For electrophilic attacks, the above analyses lead to the conclusions that the Cieplak and Anh models will be reversed in that the former will be important for a later, while the latter an earlier, transition state. The foregoing should be obvious in that an electrophilic attack is simply a nucleophilic attack where one is considering attack on the nucleophile (rather than the nucleophile as attacking).

For free radical reactions, one cannot assume that the incipient bonds are particularly polar in character. For both atom-transfers and additions to double bonds, the SOMO, of the radical should be the major contributor to the incipient bond. This will be true as conservation of spin requires that the SOMO of the product have an electron of the same spin as that of the reagent radical. However, in both cases the radical LUMO's also make significant contributions (see Figures 5.3a-b). For radical coupling reactions, the SOMO of one radical must interact with the LUMO of the other and vice versa (Figure 5.3c). Since the two models do not always make the same predictions, it is difficult to determine a clear preference based only on the polarizability.

The advantages of the PPFMO method over both the Anh and Cieplak formulations are a) an MO calculation for the reagent includes all substituent interactions that affect the reagent rather than focusing on only one, and b)

the interactions can be interpreted in terms of the π-polarizations, p, in combination with the effects upon the energies of the HOMO's and LUMO's.

In principle, one can calculate the frontier orbitals and integrate their densities to illustrate how they are polarized in one direction or another (for example see Frenking's calculation of cyclohexanone[5]). The calculations are generally much more difficult than PPFMO as a suitable basis set must be used. Graphical depiction is generally necessary. Comparisons between two different molecules are difficult to make. In principle, the difference in the electron densities for the orbitals of the two molecules under study can be obtained. However, since the bond lengths and other structural features will differ, making such a difference surface is not very convenient. Previous discussions of polarizations of π-systems have appeared. Klein has used perturbation arguments to suggest how the π-orbitals are polarized.[17,18] Comparison of his treatment of cyclohexanone with the PPFMO results and ab initio calculations are discussed in the following chapter. Paquette has related the polarization of π-orbitals to deviations from planarity.[19] As PPFMO theory requires no orbital tilting, Paquette's analysis is also somewhat different from what we propose in this chapter.

The PPFMO theory is simple and inexpensive to use. It is applicable to electrophilic, nucleophilic and free

radical reactions. The PPFMO results accord quite well with ab initio calculations and experimental results for the reduction of carbonyls, as presented in the following chapter. We have also found that the method also successfully predicts the facial selectivities for electrophilic attacks.[20]

CHAPTER 6

6. APPLICATION OF THE PPFMO METHOD WITH OTHER ANALYSES OF EXPERIMENTAL DATA

6.1 Introduction

In the previous chapter, we have described a method of predicting the electronic contributions to diastereofacial selectivity. In this chapter, we critically evaluate the PPFMO method by comparing its results with those of other theoretical techniques as well as with experimental results. In particular, we shall focus upon the facial selectivities of the reduction of carbonyl groups. This problem has been analyzed by several theoretical techniques including MO calculations of transition states, the Cieplak[1] and Anh[2] models for predicting the interactions.

At the outset, we emphasize that since the PPFMO method is based upon frontier orbital theory, it is subject to the limitations of a method that only treats electronic effects in the reagents. Thus, one should not expect perfect agreement with experimental results or with accurate transition state calculations. The method does

have the advantages of frontier orbital theory in that it is simple to apply.

We divide our comparisons into three categories. In the first, we compare our results with more sophisticated MO calculations on reagents. In the second, we compare the PPFMO results with MO transition state calculations. In the third, we compare the PPFMO results with experiment. We expect the method to agree well with ground state calculations. However, transition state calculations and experimental results add effects that the PPFMO method does not treat directly. Transition state calculations should introduce steric and other interactions that are important in gas phase reactions. Experimental results introduce a myriad of other problems such as solvent effects, experimental analysis, competing reactions, etc.

The specific cases that we shall consider are 1) the reduction of cyclohexanone and its equatorial 3-substituted derivatives; 2) reductions of propanal, fluoroethanal and 2-fluoropropanal; 3) reaction of grignard reagents with ortho esters; and 4) reactions of 2,6-disubstituted 1,3-dioxin-4-ones; 5) reductions of substituted norbornanones; and 6) reductions substituted adamantanones.

Methods

The PPFMO calculations were performed using the STO-3G basis with two s-type gaussians superimposed upon each atomic p-orbital of the π-systems studied. The same exponent (0.1) and distance from the nucleus (1.3 Å) used in the previous chapter were employed here. The polarization, p, is calculated using Equation 5.1, where c_+ and c_- refer to the coefficients of the s-functions placed along the positive and negative directions of the p-orbital axis. The direction of attack expected for $p > 0$ is indicated for each of the structures in the following discussion. The π-orbitals of the carbon and oxygen of the carbonyl were considered for ketones and aldehydes, the O-C-O fragment for the cationic intermediate in the reactions of grignard reagents with ortho esters, the three carbons and the oxygen for the dioxin-4-ones. The geometry of each species was initially optimized using the AM1 method.[3] The reference plane of the π-system was taken to be that of the carbonyl and an α-carbon. When the second α-carbon was out of this plane, each was used separately. When they differed, the average was taken.

6.2 Results and Discussion

6.2.1 Reductions of Cyclohexanones and Its Equatorial 3- and 4-Substituted Derivatives.

The reduction of cyclohexanone, Ia, has been widely discussed in the literature. Attack of hydride upon the

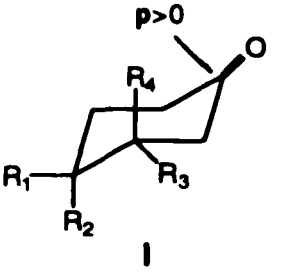

I

a: $R_1=R_2=R_3=R_4=H$
b: $R_1=F$, $R_2=R_3=R_4=H$
c: $R_2=F$, $R_1=R_3=R_4=H$
d: $R_1=Cl$, $R_2=R_3=R_4=H$
e: $R_2=Cl$, $R_1=R_3=R_4=H$
f: $R_1=OH$, $R_2=R_3=R_4=H$
g: $R_2=OH$, $R_1=R_3=R_4=H$
h: $R_1=NH_2$, $R_2=R_3=R_4=H$
i: $R_2=NH_2$, $R_1=R_3=R_4=H$
j: $R_3=F$, $R_1=R_2=R_4=H$
k: $R_4=F$, $R_1=R_2=R_3=H$
l: $R_3=Cl$, $R_1=R_2=R_4=H$
m: $R_3=CH_3$, $R_1=R_2=R_4=H$
n: $R_3=NH_2$, $R_1=R_2=R_4=H$

carbonyl comes from the most hindered face of the carbonyl, strongly suggesting that the selectivity operative here is

electronic (rather than steric) in origin. Application of PPFMO here results in a strong preference for attack at the correct face. The calculation was done both on cyclohexanone, itself, and upon protonated cyclohexanone. The latter was used to mimic reaction of a cyclohexanone that is pre-coordinated to a cation (i.e., Li or Na) during its reduction. For cyclohexanone, itself, the LUMO is highly polarized in the direction of the observed attack at the carbonyl carbon (0.166). Protonation at the carbonyl slightly increases the polarization to 0.171.

This calculation is in good agreement with the recent suggestion by Frenking[4] that the facial selectivity could be explained by a polarized LUMO. His ab initio calculations indicated both the LUMO and the HOMO to be polarized in the same (axial) direction, in agreement with the PPFMO results. Klein had previously suggested that the LUMO might be polarized in the axial direction, but the HOMO would be oppositely polarized.[5] Also, both Frenking[4] and Houk[6] have reported ab initio calculations (using MP2/6-31G(d)//HF/3-21G and HF/3-21G, respectively) that favor the axial transition state.

The results for substituted cyclohexanones are shown in Table 6.1 where we have used the convention that a positive polarization indicated a larger lobe in the direction of axial attack. The calculated polarizations for the substituted cyclohexanones, Ib-j are in agreement with

Table 6.1 The PPFMO Results for Substituted Cyclohexanones.

	c_+	c_-	p	$2p^{LUMO}$	E^{LUMO}	ΔE	p/E^{LUMO}
					hartrees	kcal	
Ia	0.798	-0.632	0.166	0.618	0.193	1.0[a]	0.861
Ib(eq)	0.798	-0.622	0.176	0.617	0.185	1.3[a]	0.952
Ic(ax)	0.837	-0.576	0.261	0.614	0.187	2.5[a]	1.390
Id(eq)	0.790	-0.631	0.159	0.617	0.179	1.3[a]	0.889
Ie(ax)	0.850	-0.555	0.295	0.611	0.182	2.9[a]	1.622
If(eq,in)	0.809	-0.604	0.205	0.618	0.188	0.9[a]	1.090
(eq,out)	0.820	-0.601	0.219	0.614	0.186	1.6[a]	1.179
Ig(ax,in)	0.836	-0.579	0.256	0.615	0.192	2.3[a]	1.338
(ax,out)	0.804	-0.622	0.181	0.615	0.184	1.0[a]	0.987
Ih(eq,in)	0.816	-0.586	0.230	0.619	0.191	0.6[a]	1.205
(eq,out)	0.828	-0.581	0.247	0.616	0.189	1.2[a]	1.303
Ii(ax,in)	0.887	-0.569	0.318	0.593	0.194	2.2[a]	1.640
(ax,out)	0.828	-0.581	0.247	0.615	0.187	1.0[a]	1.320
Ij(eq)	0.810	-0.607	0.203	0.615	0.184	2.7[b]	1.107
Ik(ax)	0.712	-0.642	0.070	0.634	0.190	-2.3[b]	0.366
Il(eq)	0.805	-0.615	0.191	0.610	0.176		1.084
Im(eq)	0.801	-0.623	0.178	0.619	0.194		0.919
In(eq)	0.802	-0.607	0.195	0.621	0.191		1.019

[a]reference 6; [b]reference 7.

the *ab initio* calculations for the addition of LiH to these compounds as reported by Houk and Frenking. In all cases the preferred attack was axial (see Table 6.1). For the cases of the 4-hydroxy and 4-amino cyclohexanones, If-i, the conformations with and without the lone pairs directed into the ring were considered, as calculated by Houk.[6] Examination of the ratio p/E^{LUMO} shows an approximate correlation with the reported ab initio activation energy differences for the axial and equatorial attacks. Three other cyclohexanones, the 3-chloro, 3-methyl and 3-amino-derivatives, Il-n, have also been calculated. However, no ab initio calculations have been performed on the corresponding transition states.

The only discrepancy between the PPFMO and *ab initio* results is for attack on axial 3-fluorocyclohexanone, Ik. In this case, while we calculate a polarization that is significantly lower than for the other cyclohexanones, we do not find a reversal of the polarization. Frenking's ab initio calculation on the transition state predicts that the attack will be preferred from the equatorial side of Ik. It is not clear whether this is a deficiency in the PPFMO method, a problem in the ab initio calculations (no BSSE corrections were made) or simply a reflection of the repulsion between the axial fluorine and the attacking hydride that is included in the ab initio calculation, put not in the PPFMO. This reaction

is not experimentally verifiable (without a 4-t-butyl group or other such substitution) due to the conformational mobility of Ik which is in equilibrium with Ij.

6.2.2 Reductions of Propanal, Fluoroethanal and 2-Fluoropropanal

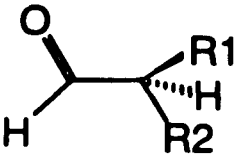

II

a: R_1=CH_3, R_2=H
b: R_1=F, R_2=H
c: R_1=F, R_2=CH_3

The π-polarization and the orbital energies of the three aldehydes, propanal (IIa), fluoroethanal (IIb), and 2-fluoropropanal (IIc), were calculated as a function of the torsional angle about the C-C bond adjacent to the carbonyl. They are collected in Table 6.2 and Figures 6.1-6.7. The orbital energies (ST0-3G) for the π and π* orbitals (stated in hartrees in the table) are plotted in kcals in the figures. The relative energies of the π and π*-orbitals of propanal as a function of torsional angle agree reasonably well with those of Frenking.[7] The

polarization of the π^*-orbital varies quite significantly with the torsional angle, changing signs several times within the unique 0-180 degree range, with the largest effect at about 90 degrees. However, the polarization of the π-orbital remains positive from 0 to 180 degrees (note that the positive side of the carbonyl is syn to the methyl from 0 to 180, but anti from 180 to 360 degrees). For purpose of comparison, in cyclohexanone, the torsional angles between each of the ring carbons and the C=O is about 130 degrees, which is in the range of positive polarization values for propanal. All three of the transition states found by Frenking[8] using MP2/6-31G(d)//HF/6-31G(d) ab initio calculations for the addition of LiH to propanol are polarized as predicted by the PPFMO results.

For fluoroethanal, the polarization of the π^*-orbital follows the qualitative pattern of that for propanal. However, the polarization of the π-orbital differs somewhat from that of propanal in that it is polarized in the opposite direction for most torsional angles. The polarization 2-fluoropropanal is shown in Figures 6.5, 6.6 and 6.7. In the last figure, we compare it with the sum of the polarizations for propanal and fluoroethanal. For this figure, zero torsional angle is defined as the C-F bond eclipsed with the carbonyl group. The polarization for propanal is added with the appropriate

Table 6.2 The PPFMO Results for Propanal, Fluoroethanal and 2-Fluoropropanal.

	LUMO			HOMO		
angle	p	E(hartrees)	p/E	p	E(hartrees)	-p/E
			Propanal			
0	0.000	0.164	0.000	0	-0.441	0.000
30	0.174	0.158	11.014	26	-0.440	0.591
60	0.006	0.152	0.394	32	-0.440	0.728
90	-0.140	0.156	-8.982	26	-0.443	0.587
120	-0.071	0.162	-4.390	39	-0.443	0.881
150	0.073	0.159	4.596	39	-0.437	0.892
180	0.000	0.155	0.000	0	-0.435	0.000
			Fluoroethanal			
0	0.000	0.151	0.000	0	-0.489	0.000
30	0.136	0.143	9.494	7	-0.487	0.144
60	-0.049	0.132	-3.707	-45	-0.482	-0.934
90	-0.213	0.132	-16.145	-25	-0.477	-0.524
120	-0.165	0.140	-11.819	-52	-0.483	-1.076
150	0.003	0.143	0.210	-60	-0.490	-1.224
180	0.000	0.141	0.000	0	-0.493	0.000

Table 6.2 Continued

	LUMO			HOMO		
angle	p	E(hartrees)	p/E	p	E(hartrees)	-p/E
			2-fluoropropanal			
0	0.062	0.154	4.024	0.023	-0.480	0.479
30	0.137	0.147	9.313	0.015	-0.475	0.316
60	-0.029	0.139	-2.081	-0.034	-0.469	-0.725
90	-0.223	0.137	-16.230	-0.036	-0.471	-0.764
120	-0.183	0.144	-12.748	-0.059	-0.477	-1.237
150	0.019	0.146	1.300	0.028	-0.479	0.584
180	0.003	0.144	0.209	-0.057	-0.482	-1.183
210	-0.106	0.144	-7.381	0.043	-0.469	0.916
240	0.069	0.148	4.656	0.041	-0.474	0.866
270	0.146	0.142	10.272	0.031	-0.471	0.658
300	0.058	0.139	4.177	0.035	-0.480	0.729
330	-0.056	0.147	-3.798	0.054	-0.479	1.126
0	0.062	0.154	4.024	0.023	-0.480	0.479

offset of 120 degrees for the dihedral angle. As can be seen, the polarization of the π^* orbital is qualitatively

additive, while that for the π-orbital is not. If we compare the PPFMO results with the calculated transition states reported by Frenking for the additions of LiH to chloroethanal and 2-chloropropanal,[8] all the selectivities agree with one exception. The exception is for a transition state for chloroethanal whose dihedral angle is -170 degrees. From Figure 5, the predicted polarization is close to zero, but opposite to that calculated by Frenking. Since the polarization is predicted to be small, and we are comparing fluoro- and chloro-derivatives, this difference does not seem to be important. In addition, our PPFMO calculations are in apparent excellent agreement with the HF/3-21G calculations of Paddon-Row on the transition states for cyanide addition to propanal, fluoroethanal, and 2-fluoropropanal.[9] Exact comparison is not possible, as Paddon-Row does not give the torsional angles for his transition states. He states that the best transition state for addition to propanal has the methyl in the 'inside' position. Frenking's TS for the addition of LiH to the same compound has a dihedral angle (OCCC) of 29 degrees. These results are consistent with each other and with Figure 6.1 which shows the LUMO to be very polarized in the syn direction and have a moderate energy at this angle.

For fluoroethanal Paddon-Row finds the lowest TS to have the C-F bond antiperiplanar to the incipient C-C bond. This puts the OCCF dihedral in the range of -120 to 0

degrees. Frenking's TS for LiH addition to chloroethanal (which is 0.3 kcal/mole less stable than the TS with a dihedral angle of 17 degrees) has a dihedral angle of 257 (-103) degrees. Figure 6.3 clearly shows this to be an optimal interaction as the LUMO is close to the maximum anti polarization while its energy is close to its minimum. For 2-fluoropropanal, Paddon-Row reports that the TS has the C-F bond antiperiplanar and the methyl group 'inside' (syn) to the incipient bond. The lowest TS for the addition of LiH to 2-chloropropanal by Frenking has an OCCCl dihedral of 84 degrees, similar to that for chloroethanal. Figure 5 indicates that the LUMO polarization is strongly anti while the LUMO energy is near its minimum at this dihedral angle. The best TS leading to the diastereomeric product also has the C-F bond antiperiplanar to the incipient bond. Again taking the dihedral from Frenking's results for the addition of LiH, the OCCCl dihedral is -104 (256) degrees, which figure 5 shows to correspond to a region of moderately high anti polarization and moderately low energy for the LUMO.[10]

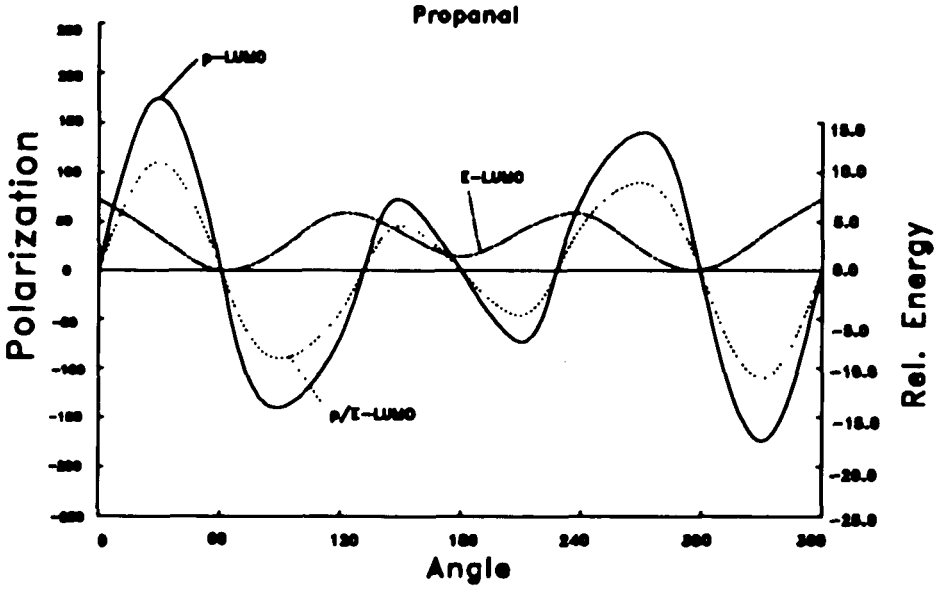

Figure 6.1 p, E^{LUMO}, and $10p/E^{LUMO}$ Plotted against OCCC Dihedral for Propanal.

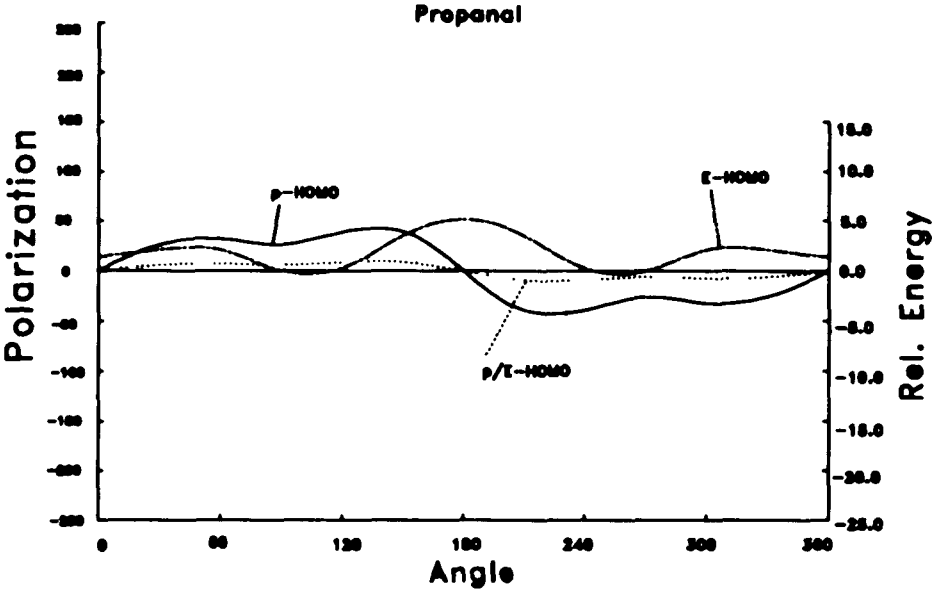

Figure 6.2 p, E^{HOMO}, and $10p/E^{HOMO}$ Plotted against OCCC Dihedral for Propanal.

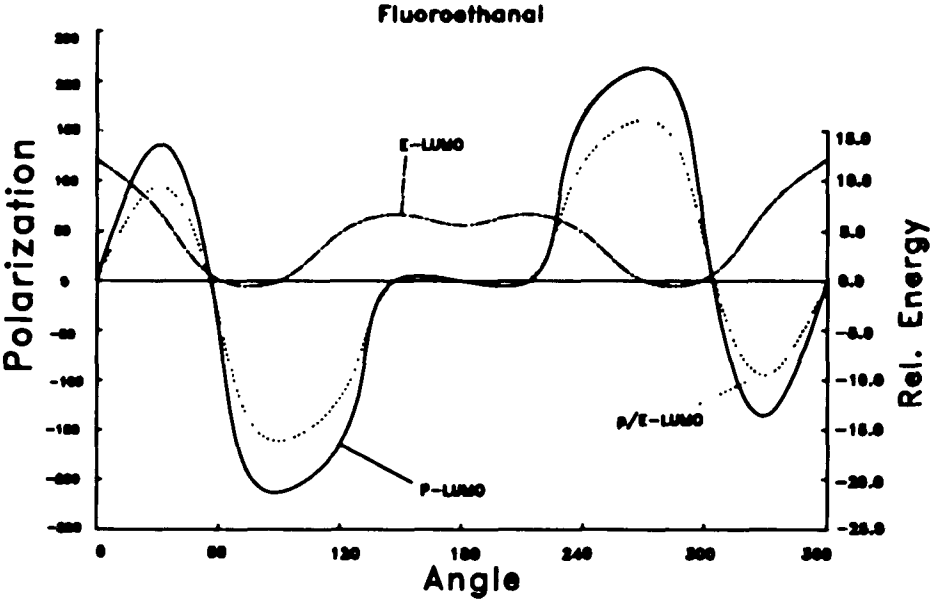

Figure 6.3 p, E^{LUMO}, and $10p/E^{LUMO}$ Plotted against OCCF Dihedral for Fluoroethanal.

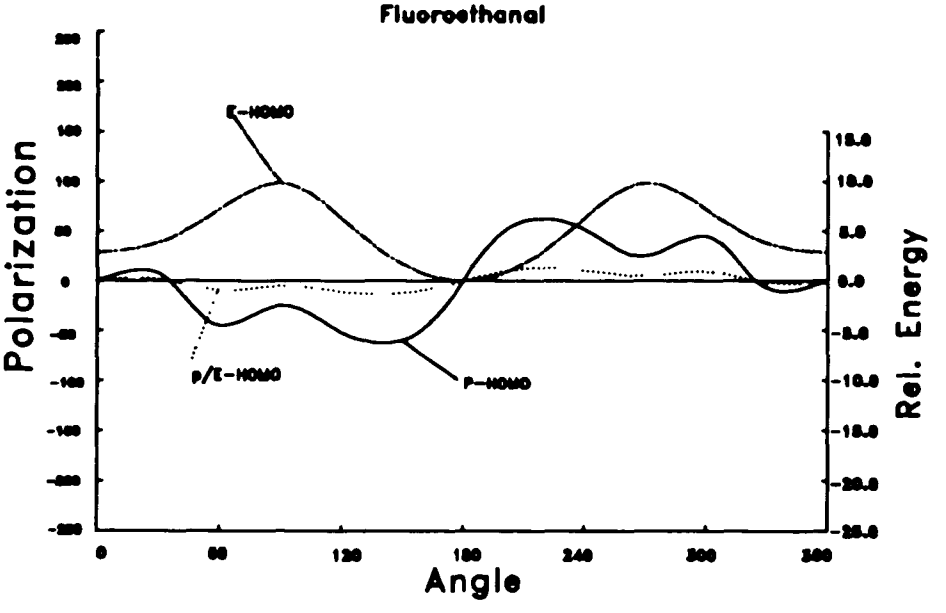

Figure 6.4 p, E^{HOMO}, and $10p/E^{HOMO}$ Plotted against OCCF Dihedral for Fluoroethanal.

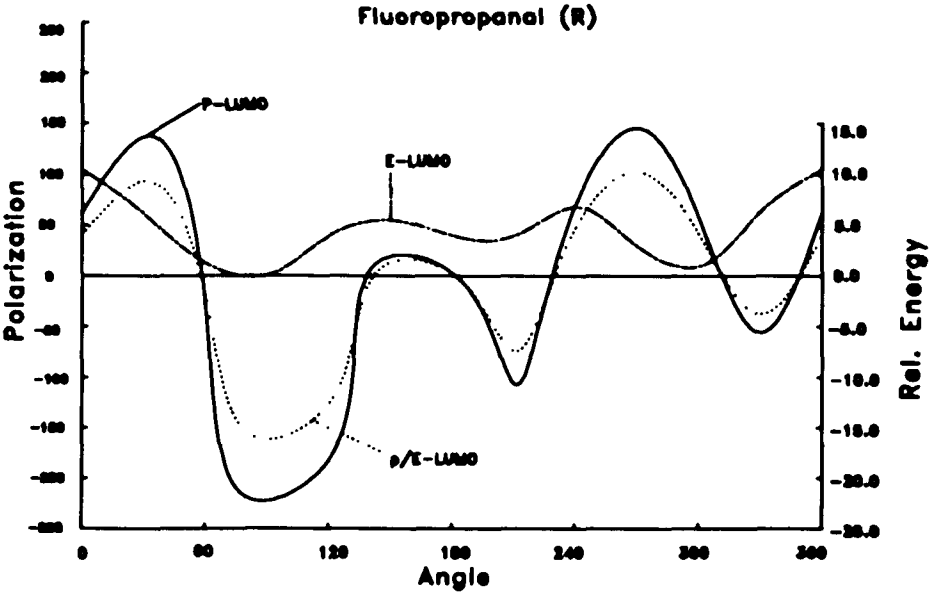

Figure 6.5 p, E^{LUMO}, and $10p/E^{LUMO}$ Plotted against OCCF Dihedral for R-fluoropropanal.

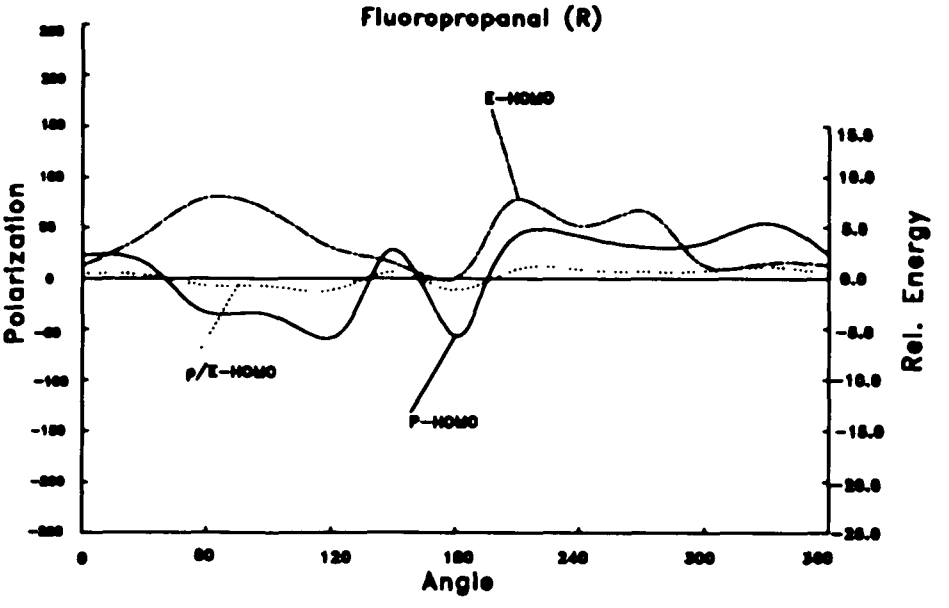

Figure 6.6 p, E^{HOMO}, and $10p/E^{HOMO}$ Plotted against OCCF Dihedral for R-fluoropropanal.

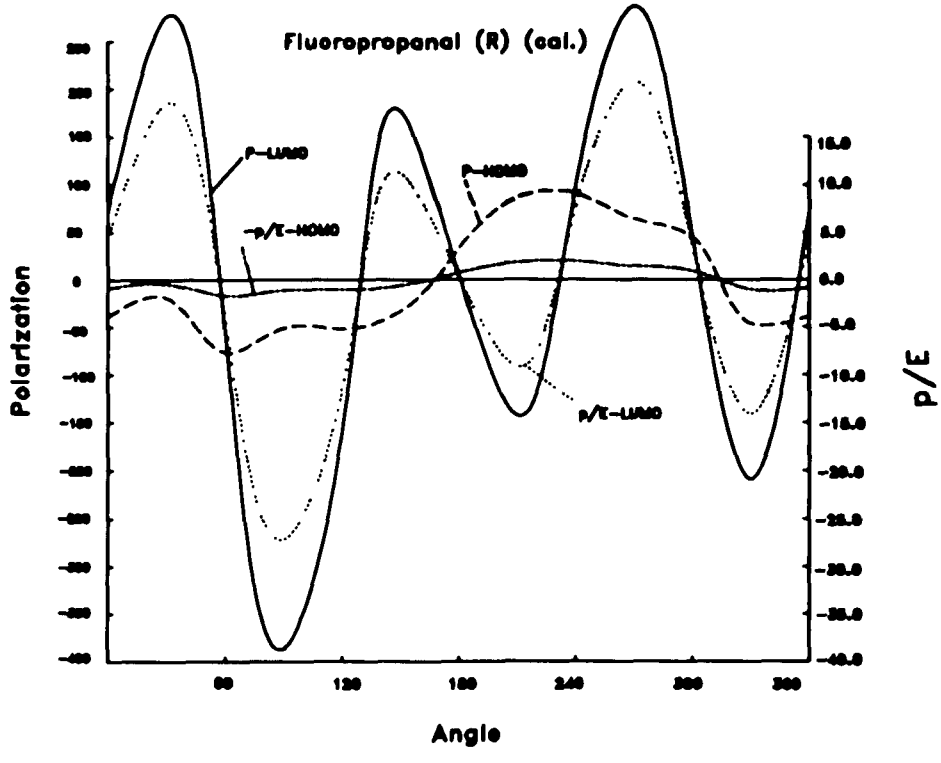

Figure 6.7 p(propanal) + p(fluoroethanal) Compared to p(R-fluoropropanal) as a Function of OCCF Dihedral for both LUMO and HOMO. The OCCC Angle for Propanal is Offset by 120 Degree for the Comparison.

6.2.3 Reaction of Grignard Reagents with Ortho Esters

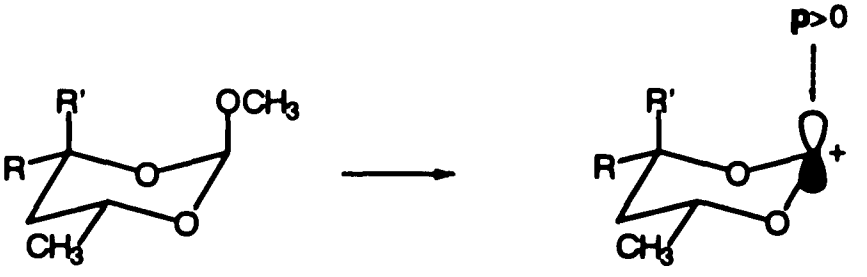

III IV

a: R=R'=H
b: R=CH_3, R'=H
c: R=R'=CH_3

In 1969, Eliel reported that the reaction of methoxydioxanes, IIIa-c, with Grignard reagents afforded primarily trans product, presumably via attack on the cationic intermediates, IVa-c.[11] Although this reaction is not a carbonyl reduction, we decided to include it in this study because of the evident similarities. PPFMO calculations on IVa-c indicate polarizations in the direction of axial attack leading to the observed product. We do not include p/E^{LUMO} in Table 6.3, since (due to its cationic character) $E^{LUMO} < 0$, making Equation 5.6 of the preceding chapter inappropriate. Eliel also noted that the isomeric methoxydioxanes which are epimerized at the methoxy-substituted carbon were much less reactive. If one

considers the loss of the methoxy group as a reaction equivalent to the reverse of attack on the cationic intermediate, IV, this observation is also consistent with the calculated polarizations.

Table 6.3 The PPFMO Results for Orthoesters

	c_+	c_-	p	$2p^{LUMO}$	E^{LUMO} hartrees	attack
IIIa	0.357	-0.299	0.058	0.654	-0.546	axial
IIIb	0.355	-0.315	0.040	0.647	-0.047	axial
IIIc	0.347	-0.321	0.027	0.648	-0.039	axial

6.2.4 Additions to 2,6-disubstituted 1,3-dioxin-4-ones

In 1988, Seebach reported that dialkyl, allyl and phenyllithium cuprates add to the 1,3-dioxin-4-ones, Va-c stereospecifically to give the ul (unlike) products, VIa-c.[12] He attributed the stereoselectivity to a small amount of pyrimidalization about the π-system. We thought this a useful test for the PPFMO method for two reasons. First, the rationale present for the observations is different from those presented for the reduction of ketones and aldehydes. Second, the reaction involves a conjugate

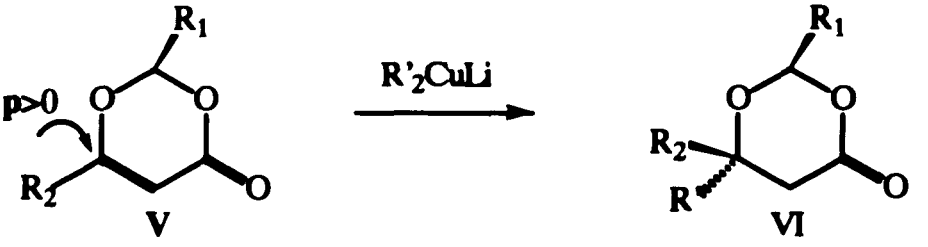

a: R_1=C$(CH_3)_3$; R_2=CH_3
b: R_1=C$(CH_3)_3$; R_2=CH_2CH_3
c: R_1=R_2=CH_3

addition to the π-system, rather than a simple addition to a carbonyl. The data in Table 6.4 show a clear polarization in the direction (negative) that gives the observed ul products (anti to R_1).

Table 6.4 The PPFMO Results for 2,6-Disubstituted 1,3-Dioxin-4-ones.

compound	C_+	C_-	p	$2p^{LUMO}$	E^{LUMO}	attack[12]	p/E^{LUMO}
Va	0.367	-0.600	-0.234	0.609	0.173	syn	-1.353
Vb	0.407	-0.598	-0.190	0.599	0.175	syn	-1.090
Vc	0.363	-0.606	-0.243	0.606	0.172	syn	-1.413

6.2.5 Reductions of Substituted Norbornanones

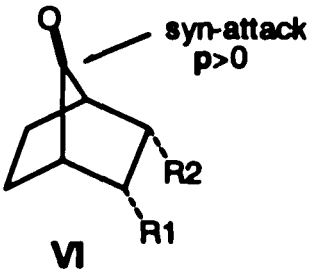

VI

a: R_1=R_2=$COOCH_3$
b: R_1=R_2=CH_2OCH_3
c: R_1=R_2=vinyl
d: R_1=vinyl, R_2=ethyl
e: R_1=R_2=ethyl

Several experiments have been designed to evaluate the effects of purely electronic influences on the diastereofacial selectivities by designing experimental systems where other (i.e, steric, solvation) influences should be minimal. One of these systems involves the substituted norbornanones, VIIa-e.[13] Table 6.5 compares the calculated polarizations with the experimentally observed selectivities. The PPFMO results agree with the experimental observations in that the correct direction of attack is predicted in each case. This is true even for VIIa, where attack comes from the syn side, while all

others undergo anti attack. In several cases, particularly Va and Vb, the polarizations are quite small. In fact, Va gives the opposite polarization for some higher energy rotomers.

Table 6.5 The PPFMO Results for Norbornanones.

compound	c_+	c^-	p	$2p^{LUMO}$	E^{LUMO} hartrees	attack[13]	p/E^{LUMO}
VIIa	0.745	-0.742	0.003	0.615	0.181	syn	0.018
VIIb	0.757	-0.761	-0.005	0.624	0.197	anti	-0.024
VIIc	0.722	-0.776	-0.054	0.619	0.196	anti	-0.275
VIId	0.740	-0.761	-0.021	0.620	0.198	anti	-0.106
VIIe	0.750	-0.770	-0.020	0.627	0.201	anti	-0.100

6.2.6 Reductions of Adamantanones

In a series of papers, le Noble has presented numerous results on the reductions of various substituted adamantanones,[14,15,16,17] and adamantyl radicals[18] in an attempt to separate the electronic and steric influences on diastereofacial selectivity. We have performed PPFMO calculations on virtually all of the relevant adamantanones

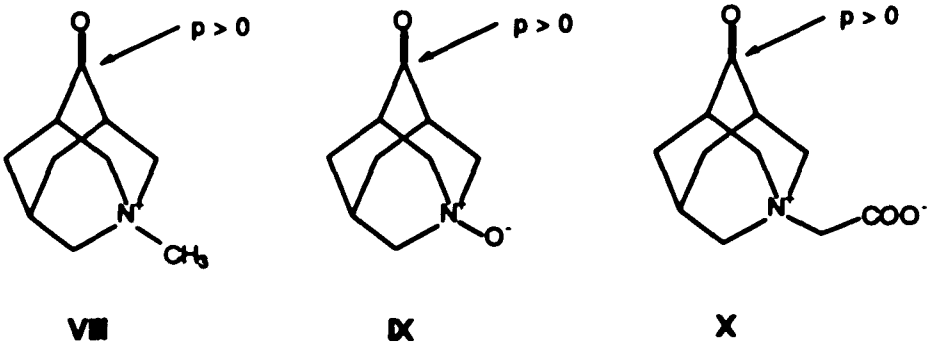

VIII IX X

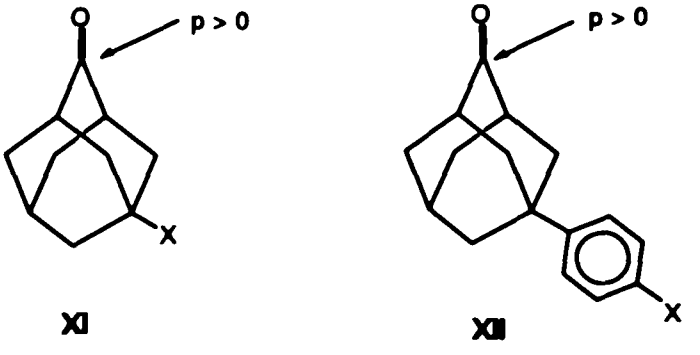

XI XII

a: X=F
b: X=CH_3
c: X =CF_3
d: X=Cl
e: X=t-butyl

a: X=H
b: X=NO_2
c: X =CN
d: X=OH
e: X=NH_2

that he has studied. The results are collected in Table 6.6. The PPFMO method successfully predicts the observed syn-attack for all cases involving the 5-azaadamantanones, VIII, IX, and X.[15] PPFMO, also, predicts polarizations that favor the observed syn-attack in the cases of 5-substituted adamantyl derivatives, XIa-e. For the series of p-substituted 5-phenyladamantanones, XIIa-e, le Noble reported

Table 6.6 The PPFMO Results for Adamantanones.

Compound	c_+	c_-	p	$2p^{LUMO}$	E^{LUMO}	attack[a]	p/E^{LUMO}
					hartrees		
VIII	0.784	-0.627	0.157	0.606	0.042	syn	3.701
IX	0.714	-0.703	0.011	0.633	0.175	syn	0.063
X	0.751	-0.666	0.085	0.624	0.146	syn	0.581
XIa	0.717	-0.711	0.006	0.635	0.190	syn	0.031
XIb	0.719	-0.718	0.001	0.636	0.197		0.007
XIc	0.719	-0.711	0.008	0.634	0.187	syn	0.042
XId	0.710	-0.712	-0.001	0.634	0.184	anti[b]	-0.008
XIe	0.717	-0.718	-0.001	0.637	0.198	anti[c]	-0.005
XIIa	0.723	-0.715	0.008	0.635	0.196	syn	0.041
XIIb	0.724	-0.714	0.010	0.633	0.187	syn	0.056
XIIc	0.723	-0.715	0.008	0.634	0.191	syn	0.043
XIId	0.721	-0.717	0.005	0.635	0.196	syn	0.023
XIIe	0.721	-0.718	0.003	0.635	0.198	syn	0.017

[a]references 14 and 17. [b]reference 14 (earlier work reports syn). [c]depending upon reaction conditions, either anti or no selectivity[14].

that the relative amount of syn attack could be related to the Hammett σ constant for the substituents. The comparison with the calculated polarities and p/E^{LUMO}'s are included in

Table 6.6. The p/E^{LUMO}'s for XIIa-e are plotted against the σ constants in Figure 6.8. The agreement is remarkably good for calculations made with so simple a theory as PPFMO. In the case of XId, the polarization is quite sensitive to dihedral angle the O-H makes with the phenyl ring. The values used are for the lowest energy rotomer, but p/E^{LUMO} varies between 0.012 to 0.046 as a function of the dihedral.

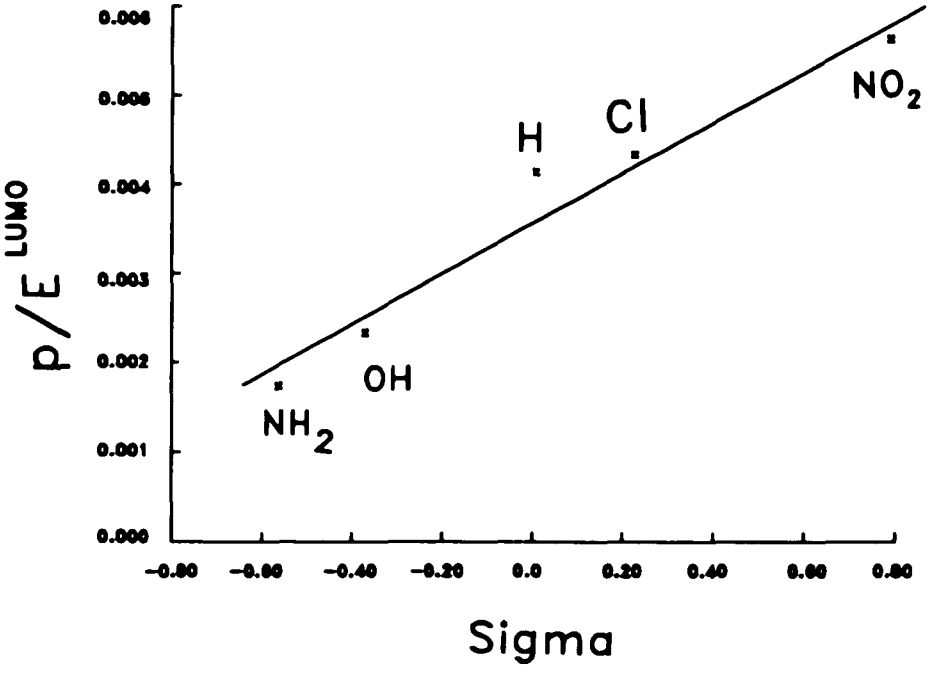

Figure 6.8 Plot of p/E^{LUMO} versus Hammett Constant σ for Compounds XIIa-e.

The correspondence of the PPFMO polarizations, p, with the experimental and theoretical results that have been reported on the same systems is qualitatively surprisingly good. Quantitative agreement is much more difficult to attain. In this case, comparison should be made not with p, but with either p/E^{LUMO} or $p/(E^{LUMO}+k)$,[19] as PPFMO theory relates the relative activation energies to $E^{LUMO-HOMO}$ as well as to p. Here, the agreement is not as good, although the trends are often reproduced within groups of similar reactions (such as XIIa-e). This is not surprising, since FMO theory takes neither the transition states nor the other reagent directly into account. Because of the simplicity of the approach, the good qualitative agreement is more remarkable.

We also have applied the PPFMO method to other kinds of reactions, such as electrophilic attacks.[20] Preliminary results show that the method is successful in predicting the experimentally observed facial selectivities in protonations of glycals.[21]

The results presented in this chapter invite comparison with the predictions of the perturbational models of Anh[2] and Cieplak.[1] These, as well as several other models for explaining the facial selectivities observed in the reduction of cyclohexanones have been critically discussed by le Noble in a recent review.[22] We have also discussed their relationships with FMO theory in the

preceding chapter. Several of the papers cited earlier have included discussions that are critical or supportive of one or the other of these models.

We have indicated in the preceding chapter that both models are based upon perturbation arguments that relate to a stabilization of a bonding orbital by interaction with an antibonding orbital. Anh holds that the incipient bonding orbital is stabilized by an antibonding orbital of an antiperiplanar bond, while Cieplak claims that the bonding orbital of the antiperiplanar bond is stabilized by the incipient antibonding orbital. Neither of these models takes polarization of the π-orbitals directly into account. Le Noble notes that the interactions involved in both models are potentially important. Their importance will vary in different directions as the transition state varies from early to late. We have come to similar conclusions using a different analysis than le Noble.

Since the PPFMO method involves MO calculations, it should include the perturbations to the frontier orbitals that are operative in both the Anh and Cieplak formulations. These should be manifest in the energy of the LUMO, which will be the orbital involved in the incipient bond. In addition, the PPFMO method includes the effect of π-orbital polarization, which is absent in the Anh and Cieplak models. It is tempting to try to extend the Anh and Cieplak models to π-polarizations. Such extensions would

require that the effects on the FMO's and p be qualitatively similar. However, examination of the data presented in this and the previous paper illustrate the lack of correlation of substituent effects on p with those on the HOMO or LUMO energies.

Conclusion

The PPFMO method is capable of predicting diastereofacial selectivities in a wide range of applications. It is particularly successful in predicting the polarizations of MO's that would arise from more complex analyses of the shapes of individual MO's, as well as, qualitatively predicting the relative energies of optimized transition states calculated by MO methods. It has qualitatively reproduced all of the experimental results discussed.

REFERENCES

CHAPTER 2

1. P. O. Löwdin, *Advan. Chem. Phys.*, 1959, **2**, 207.

2. C. C. J. Roothaan, *Rev. Mod. Phys.*, 1951, **23**, 69.

3. G. G. Hall, *Proc. Roy. Soc.*, 1951, **A205**, 541.

4. J. E. Lennard-Jones, *Proc. Roy. Soc.*, 1949, **A198**, 1, 14.

5. C. C. J. Roothaan, *Rev. Mod. Phys.*, 1951, **23**, 69.

6. R. Hoffmann, *J. Chem. Phys.*, 1963, **39**, 1397.

7. J. A. Pople and G. A. Segal, *J. Chem. Phys.*, 1965, **43**, S136; 1966, **44**, 3289.

8. J. A. Pople, D. L. Beveridge and P. A. Dobosh, *J. Chem. Phys.*, 1967, **47**, 2026.

9. J. A. Pople, D. P. Santry and G. A. Segal, *J. Chem. Phys.*, 1965, **43**, S129.

10. R. C. Bingham, M. J. S. Dewar and D. H. Lo, *J. Am. Chem. Soc.*, 1975, **97**, 1285, 1294, 1302, 1307.

11. M. J. S. Dewar and W. Thiel, *J. Am. Chem. Soc.*, 1977, **99**, 4899, 4907.

12. M. J. S. Dewar, E. G. Zoebisch, E. F. Healy and J. J. P. Stewart, *J. Am. Chem. Soc.*, 1985, **107**, 3902.

13. M. J. S. Dewar and D. H. Lo, *J. Am. Chem. Soc.*, 1972, **94**, 5296; L. Oleari, L. DiSipio and G. DeMichelis, *Mol. Phys.*, 1966, **10**, 97.

14. R. G. Parr, *J. Chem. Phys.*, 1960, **33**, 1184; B. Voigt, *Theo. Chim. Acta.*, 1973, **31**, 289.

15. R. Pariser, *J. Chem. Phys.*, 1953, **21**, 568.

16. R. G. Parr, D. P. Craig and I. G. Goss, *J. Chem. Phys.*, 1950, **A210**, 224.

17. M. J. S. Dewar and D. M. Storch, *J. Am. Chem. Soc.*, 1985, **107**,3898.

18. C. Møller and M. S. Plesset, *Phys. Rev.*, 1934, **46**, 618.

19. J. A. Pople, J. S. Binkly and R. Seeger, *Int. J. Quant. Chem.*, 1976, **S10**, 1; J. A. Pople, R. Seeger, and R. krishnan, *Int. J. Quant. Chem.*, 1977, **S11**, 165; R. Krishnan and J. A. Pople, *Int. J. Quant. Chem.*, 1978, **14**, 91.

20. S. D. Peyerimhoff and R. J. Buenker, *Chem. Phys.*, 1981, 279; K. Ishida, K. Kondo and T. Yonezawa, *J. Chem. Phys.*, 1977, **66**, 2883.

21. E. Gorin, *J. Chem. Phys.*, 1939, **7**, 263.

22. S. W. Benson, *Acc. Chem. Res.*, 1986, **19**, 335.

23. M. J. S. Dewar, J. A. Hashwall and C. G. Venier, *J. Am. Chem. Soc.*, 1968, **90**, 1953.

24. J. J. Dannenberg and D. Rocklin, *J. Org. Chem.*, 1982, **47**, 4529.

25. L. S. Miller, K. Grohmann and J. J. Dannenberg, *J. Am. Chem. Soc.*, 1983, **105**, 6862.

26. J. J. Dannenberg and K. Tanaka, *J. Am. Chem. Soc.*, 1985, **107**, 671.

27. J. J. Dannenberg, J. C. Rayez, M. T. Rayez-Meaume and P. Halvick, *J. Mol. Struct.* (Theochem), 1985, **123**, 343.

28. G. Klopman, P. Andreozzi, A. J. Hopfinger, O. Kikuchi, and M. J. S. Dewar, *J. Am. Chem. Soc.*, 1978, **100**, 6267.

29. T. J. Zielinski, D. L. Breen, and R. Rein, *J. Am. Chem. Soc.*, 1978, **100**, 6266.

CHAPTER 3

1. Lankamp, Nauta and MacLean, *Tetrahedon Lett.*, 1968, 249; Staab, Brettschneider; Brunner, *Chem. Ber.*, 1970, 103, 1101; Voltz; Lotsch, Schnell, *Tetrahedron*, 1970, 26, 5343; McBride, *Tetrahedron*, 1974, 30, 2009.

2. D. M. White and J. J. Sonnenberg, *J. Am. Chem. Soc.*, 1966, 88, 3825.

3. J. J. Dannenberg and K. Tanaka, *J. Am. Chem. Soc.*, 1985, 107, 671.

4. J. J. Dannenberg and D. Rocklin, *J. Org. Chem.*, 1982, 47, 4529.

5. a) G. Leroy, M. Sana, C. Wilante, D. Peeters and C. Dogimont, *J. Mol. Struct. (Theochem)*, 1987, 153, 249; b) M. Sana, G. Leroy, L. Vinson and J. J. Dannenberg, *J. Mol. Struct. (Theochem)*, 1990, 205, 89.

6. This could not be accomplished when the activation energy was close to zero, i. e., when there was no transition state.

7. J. J. Dannenberg and K. Tanaka, *J. Am. Chem. Soc.*, 1985, 107,671.

8. H. Lenghals and H. Fischer, *Berichte*, 1978, 111, 543.

9. R. A. Marcus, *J. Chem. Phys.*, 1956, 24, 966; *J. Chem. Phys.*, 1965, 43, 679.

10. J. E. Leffler and E. Grunwald, *Rates and Equilibria in Organic Reactions*, Wiley: New York, 1963; R. A. Marcus, *J. Chem. Phys.*, 1965, 43, 679; T. W. Newton, *J. Chem. Educ.*, 1968, 45, 571; D. J. Lenman, *J. Chem. Educ.*, 1976, 53, 348.

11. R. A. Marcus, *J. Chem. Phys.*, 1956, 24, 966.

12. R. A. Marcus, *J. Chem. Phys.*, 1968, 72, 891.

13. J. R. Murdoch and D. E. Magnoli, *J. Am. Chem. Soc.*, 1982, 104, 3792; J. R. Murdoch, *J. Am. Chem. Soc.*, 1972, 94, 4410; D. E. Magnoli and J. R. Murdoch, *J. Am. Chem. Soc.*, 1981, 103, 7465.

14. G. L. Closs, L. T. Calcaterra, N. J. Green, K. W. Penfield and J. R. Miller, *J. Chem. Phys.*, 1986, 90, 3673.

15. G. Leroy, *Advances in Quantum Chemistry*, 1985, 17, 1.

CHAPTER 4

1. a) R. C. Lamb, P. W. Ayers and M. K. Toney, *J. Am. Chem. Soc.*, 1963, **85**, 3483; b) C. Walling and M. S. Pearson, *J. Am. Chem. Soc.*, 1964, **86**, 2262; c) C. Walling and A. Cioffari, *J. Am. Chem. Soc.*, 1972, **94**, 6069; M. Julia, *Acc. Chem. Res.*, 1971, **4**, 386.

2. For some representative examples see a) E. J. Corey, K. Shimoji and C. Shih, *J. Am. Chem. Soc.*, 1984, **106**, 6425; b) D. Curran and D. M. Rakiewicz, *J. Am. Chem. Soc.*, 1985, **107**, 1448; c) G. Stork and N. H. Baine, *J. Am. Chem. Soc.*, 1982, **104**, 2321.

3. G. Stork and R. Mah, *Heterocycles*, 1989, **28**, 723.

4. For some examples, see: a) M. D. Bachi, F. Frolow and C. Hornaert, *J. Org. Chem.*, 1983, **48**, 1841; b) J.-K. Choi and D. J. Hart, *Tetrahedron*, 1985, **41**, 3959; c) A. Padwa, H. Nimmesgern and G. S. Wong, *J. Org. Chem.*, 1985, **50**, 5620; d) S. J. Danishefsky and J. S. Panek, *J. Am. Chem. Soc.*, 1987, **109**, 917.

5. For example see a) G. Stork and R. Mah, *Tetrahedron Lett.*, 1989, **30**, 3609; b) G. Stork, *Bull. Chem. Soc. Jpn.*, 1988, **61**, 149; c) A. Padwa, H. Nimmesgern and G. S. K. Wong, *Tetrahedron Lett.*, 1985, **26**, 957.

6. For the examples of intramolecular 1,5-hydrogen atom transfer in the presence of n-Bu3SnH see a) V. Snirckus, J.-C. Cuevas, C. P. Sloan, L. Liu and D. P. Curran, *J. Am. Chem. Soc.*, 1990, **112**, 896; b) D. P. Curran, A. C. Abraham and H. Liu, *J. Org. Chem.*, 1991, **56**, 4335.

7. G. Stork, R. Jr. Mook, S. A. Biller and S. D. Rychnovsky, *J. Am. Chem. Soc.*, 1983, **105**, 3741.

8. A. E. Dorigo, M. A. McCarrick, R. J. Loncharich and K. N. Houk, *J. Am. Chem. Soc.*, 1990, **112**, 7508.

9. M. J. S. Dewar, E. G. Zoebisch, E. F. Healy and J. J. P. Stewart, *J. Am. Chem. Soc.*, 1985, **107**, 3902.

10. M. J. S. Dewar, J. A. Hashwell and C. G. Venier, *J. Am. Chem. Soc.*, 1968, **90**, 1953.

11. a) J. J. Dannenberg, *Advances in Molecular Modeling*, D. Liotta, Ed. JAI Press: Greenwich, 1990, Vol. 2, p1; b) J. M. Lluch, J. Bertran and J. J. Dannenberg, *Tetrahedron*, 1988, 24, 7621.

12. G. A. Creak and F. S. Dainron, *Trans. Faraday Soc.*, 1962, 58, 326.

13. G. C. Schatz, *Chem. Rev.*, 1987, 87, 81.

CHAPTER 5

1. M. Cherest, H. Felkin and N. Prudent, *Trtrahedron Lett.*, 1968, 2201.

2. N. T. Anh and O. Eisenstein, *Nouv. J. Chim.*, 1977, 111, 199.

3. A. S. Cieplak, *J. Am. Chem Soc.*, 1981, 103, 4540.

4. H. Li and W. J. le Noble, *Recl. Trav. Chim.* Pays Bas, 1992, 111,199.

5. G. Frenking, K. F. Koehler and M. T. Reetz, *Angew, Chem.*, 1991, 103, 1167.

6. S. S. Wong and P.-R. M. N., *J. Chem. Soc. Chem. Commun.*, 1990, 456

7. Y.-D. Wu, K. N. Houk and B. M. Trost, *J. Am. Chem. Soc.*, 1987, 109, 5560.

8. Y. D. Wu, J. A. Tucker and K. N. Houk, *J. Am. Chem. Soc.*, 1991, 113, 5018.

9. B. Giese, *Angew. Chem. Int. Ed. Engl.*, 1989, 28, 969.

10. K. Fukui, *Acc. Chem. Res.*, 1971, 4, 57.

11. I. Fleming, *Frontier Orbitals and Organic Chemical Reactions*; Wiley: New York, 1976.

12. J. J. Dannenberg and R. W. Franck, J. Org. Chem., 1985, *50*, 2635.

13. N. Kaila, R. W. Franck and J. J. Dannenberg, *J. Org. Chem.*, 1989, 54, 4206.

14. M. J. S. Dewar, E. G. Zoebisch, E. F. Healy and J. J. P. Stewart, *J. Am. Chem. Soc.*, 1985, 107, 3902.

15. Gaussian Inc., Pitsburgh, PA.

16. J. J. Dannenberg and B. Baer, *J. Am. Chem. Soc.*, 1989, 109, 292.

17. J. Klein, *Tetrahedron Lett.*, 1973, 29, 4307.

18. O. Eisenstein, J. Klein and J. M. Lefour, *Tetrahedron* 1979, 35, 225.

19. L. A. Paquette, L.-Y. Hsu, J. C. Gallucci, J. D. Korp, I. Bernal, T. M. Kravetz and S. J. Hathaway, *J. Am. Chem. Soc.*, 1984, 106, 5743.

20. X. L. Huang, N. Kaila, R. W. Franck and J. J. Dannenberg, in preparation.

CHAPTER 6

1. A. S. Cieplak, *J. Am. Chem. Soc.*, 1981, 103, 4540.

2. N. T. Anh and O. Nouv. Eisenstein, *J. Chem.*, 1977, 1, 62.

3. M. J. S. Dewar, E. G. Zoebisch, E. F. Healy and J. J. P. Stewart, *J. Am. Chem. Soc.*, 1985, 107, 3902.

4. G. Frenking, K. F. Koehler and M. T. Reetz, *Angew. Chew.*, 1991, 103, 1167.

5. J. Klein, *Tetrahedron Lett.*, 1973, 29, 4307.

6. Y. D. Wu, J. A. Tucker and K. N. Houk, *J. Am. Chem. Soc.*, 1991, 113, 5018.

7. G. Frenking, K. F. Koehler and K. N. Houk, *Tetrahedron* 1991, 47, 8991.

8. G. Frenking, K. F. Koehler and M. T. Reetz, *Tetrahedron* 1991, 47, 9005.

9. S. S. Wong and P.-R. M. N. *J. Am. Chem. Soc. Chem. Commun.*, 1990, 456.

10. Comparisons to the literature are complicated by notational differences. Both Frenking and Paddon-Row inverted the chiral center in the halopropanal, rather than the side of attack. Furthermore, each attacked from a different side, so that (assuming F=Cl) they calculated enantiomeric transition states. We worked with the R-enantiomer, with anti attack in the dihedral range of 0-180 yielding one diastereomer, while anti attack in the range 180-360 yields the other (syn attack would yield the opposite diastereomer in each range). Frenking's reported dihedrals of -84 and -104 degrees must be modified to +84 and -104 (256) degrees for comparison with our results.

11. E. L. Eliel and F. Nader, *J. Am. Chem. Soc.*, 1969, 91, 536.

12. D. Seebach, J. Zimmermann, U. Gysel, R. Ziegler and T. K. Ha, *J. Am. Chem. Soc.*, 1988, 110, 4763.

13. G. Mehta and F. A. Khan, *J. Am. Chem. Soc.*, 1990. 112, 6140.

14. C. K. Cheung, L. T. Tsend, M. H. Lin, S. Srivastava and W. J. le Noble, *J. Am. Chem. Soc.*, 1986, 108, 1598.

15. M. J. Hahn and L. W. J. *J. Am. Chem. Soc.*, 1991, 114, 1916.

16. M. H. Lin, J. E. Silver and W. J. le Noble, *J. Org. Chem.*, 1988, 53, 5155.

17. H. Li and W. J. le Noble, *Tetrahedron Lett.*, 1990, 31, 4391.

18. V. R. Bodepudi and l. W. J., *J. Org. Chem.*, 1991, 56, 2001.

19. X. L. Huang, J. J. Dannenberg, M. Duran and J. Bertran, submitted.

20. X. L. Huang, N. Kaila, R. W. Frank and J. J. Dannenberg, in preparation.

21. N. Kaila, M. Blumenstein, H. Bielawaka and R. W. Franck, *J. Org. Chem.*, 1992, 57, 4576.

22. H. Li and W. J. le Noble, *J. Recl. Trav. Chim.* Pays Bas, 1992, 111, 199.